EXCESSIVE DYNEIN FORCE IN *she1* MUTANTS REVEALS DIFFERENCES IN MICROTUBULE ANCHORAGE IN BUDDING YEAST

A Dissertation

Presented to the Faculty of the Graduate School

of Cornell University

In Partial Fulfillment of the Requirements for the Degree of

Doctor of Philosophy

By

Zane J Bergman

January 2012

EXCESSIVE DYNEIN FORCE IN *she1* MUTANTS REVEALS DIFFERENCES IN MICROTUBULE ANCHORAGE IN BUDDING YEAST

Zane J Bergman, Ph.D.

Cornell University 2012

Many microtubule functions, such as chromosome segregation and spindle orientation, depend on a stable anchor point in the cell. In the budding yeast, *Saccharomyces cerevisiae*, cytoplasmic microtubules (cMTs) are anchored at the spindle pole body (SPB), the equivalent of the microtubule organizing center. In ***she1Δ*** mutants, I observed cMTs detach from the SPB and trace the periphery of the cell before depolymerizing. Disabling the dynein pathway rescued this phenotype, suggesting that this defect stems from She1's function in regulating dynein as opposed to a weakened SPB. It was observed that cMTs in ***she1Δ*** mutants detach more readily early in the cell cycle, when the cMTS are anchored at the half-bridge, as opposed to after SPB duplication when cMTs are anchored at the outer plaque. This was confirmed by utilizing *kar1-Δ15* mutants that ablate cMT anchorage at the half-bridge. By visualizing GFP-tagged γ-tubulin complex proteins I determined that cMTs are pulled intact from the SBP and are subsequently depolymerized from their plus-ends. Similarly, the detachment phenotype could be rescued by expressing *SPC72-KAR1* or *SPC72-CNM67* fusion proteins that anchor cMTs solely at the half-bridge or outer

plaque, respectively. Over-expressing *SHE1* prevented the loading of dynactin components onto the plus-ends of cMTs, preventing proper spindle positioning by dynein. I found that She1 binds directly to MTs and that this binding may be the mechanism by which She1 controls dynein function.

BIOGRAPHICAL SKETCH

Zane Joseph Bergman was born on February 22nd, 1982 in Kokomo, IN, "The City of Firsts." As a young boy, Zane joined the Cub Scouts and eventually the Boy Scouts of America. On his way to achieving the highest rank of Eagle Scout, he enjoyed learning about the outdoors, civics, knot tying, and how to survive in the wilderness. This experience in nature and exploration was fostered and complemented by his science classes throughout grade school. In high school his instructors in biology, such as Rick Davis and Dennis Pogue, and chemistry, David Hole, were role-models that displayed a passion and understanding of scientific knowledge that influenced Zane into completing all the available science classes at Western High School. After graduating in 2000, Zane went on to attend Purdue University in West Lafayette, IN where he enrolled in the School of Science to pursue a Bachelor's degree in General Biology. Zane's thirst for knowledge pushed him into attaining minor degrees in chemistry and anthropology while attending Purdue before graduating in May of 2004. While at Purdue, Zane worked as a technician and part-time researcher in the lab of Dr. Jonathon LeBowitz, under the supervision of Tim Holzer, a graduate student in the lab. Here Zane learned about how labs were run and how basic scientific research was performed while studying the para-flagellar rod in the trypanosome, *Leishmania mexicana*. Zane also had the opportunity to participate in a summer research internship at Roswell Park Cancer Institute in Buffalo, NY during the summer of 2003. Zane worked in the lab of Dr. Andre Bakin and his project included looking at

the transcriptional response of Transforming Growth Factor β in murine cells to identify genes that are involved in the epidermal-to-mesenchymal transition that these cells undergo upon exposure to the peptide.

These research experiences led Zane to apply to graduate school. He was accepted into the Biochemistry, Cell, and Molecular Biology program in the Molecular Biology and Genetics Department of Cornell University starting in the fall of 2004. Here, Zane joined the lab of Dr. Tim Huffaker in the spring of 2005. While performing research, Zane had ample opportunity to be a teaching assistant in several classes in the department, most notably BioBM3340 with Jim Blankenship. He enjoyed the interaction with undergraduates and the opportunity to practice lecturing and instructing. Zane also participated in the Howard Hughes Medical Institute's summer program as a mentor by leading discussion groups on current scientific literature and aiding interns with presenting their work at the end of the program.

While at Cornell, Zane met Jennifer Page, a graduate student in the Genetics and Development program in the MBG department. The two were married in August of 2010. Upon completion of his Ph.D., Zane plans on moving to the San Francisco Bay Area.

ACKNOWLEDGEMENTS

The road to a Ph.D. is not traveled alone and there are numerous people to thank who have helped along the way with a great deal of support, either tangible or intangible. First off, I would like to thank my advisor, Tim Huffaker who not only is readily available to discuss anything with, but who has allowed me to pursue experiments and hypotheses even if they were either long-shots or dead-ends, but would ultimately paid off in one fashion or another. Tim has been supportive and has taught me to work independently and to develop my rational thinking skills. His guidance has truly shaped me into the scientist I am today. My committee members, Dr. Anthony Bretscher and Dr. Volker Vogt, have been incredibly helpful. Tony always has terrific ideas for experiments that get to the heart of the questions being asked. Volker has always been encouraging and has taught me the value of being thorough with my experiments. Life in the lab has been a terrific experience thanks to fellow lab members Beth Lalonde, Alex Amaro, and Kristy Blake. Alex and Kristy offered lots of advice on how to survive and complete graduate school and were always there to troubleshoot experiments and to chat while experiments were running. I would also like to acknowledge the undergraduates that have gone through the lab recently, Ryan Clagg, Tim Hannah, Demitri Dedousis, and Christine McIntosh. I am very grateful to Patrick Wu who shared a bay with me for 3.5 years and helped me on some projects that unfortunately did not yield positive results. I appreciate all the hard work he did with me and the time we spent in lab together.

I would also like to extend gratitude to the faculty that I have had a chance to be a teaching assistant with, especially Jim Blankenship. Teaching has not only helped me learn material better, but it has provided an outlet for interacting with future scientists and help them develop their skills. I would also like to thank Laurel Southard and Pam Davis in the Office of Undergraduate Biology for hiring me on as a Howard Hughes Medical Institute Summer Internship Mentor for two summers.

Completion of this thesis would not have been possible without help from others. The SGA screen was performed in the lab of Dr. Charlie Boone at the University of Toronto. Early work characterizing She1 was performed by a previous student in the lab, Xue Xia. Many thanks go to the labs of Elmar Shiebel, Tricia Davis, Mark Rose, Dean Dawson, and John Cooper for providing yeast strains and bacterial plasmids. I would like to thank graduate students Marie Bechler and Damien Garbett for their technical advice on using the spinning-disc confocal microscope. The tubulin QPCR project was made possible by collaborating with the lab of Jeff Pleiss and I had a great deal of help and math tutoring from Mohan Gudipati and Laura Bud. I also appreciate the protocols and reagents I received from several labs in the Biotech building, most notably the other yeast labs that would literally have a cup of sugar whenever I needed it.

Lastly, I would like to thank my friends and family for all their support throughout my graduate career at Cornell. My parents have been unconditional and unwavering in their support which I will be eternally grateful for. The graduate program here has fostered a great community for the students and most anyone is willing to share time,

protocols, and reagents which has been very appreciated. I am deeply indebted to my wife and fellow grad student, Jennifer Page, who has been helpful in every facet of my time here in Ithaca and has taught me to work hard while I've tried to teach her how to relax.

TABLE OF CONTENTS

LIST OF FIGURES

LIST OF TABLES

LIST OF ABBREVIATIONS

+TIP	Plus-end tracking protein
3-AT	3-amino, 1, 2, 4-triazole
γ-TuRC	Gamma-tubulin ring complex
γ-TuSC	Gamma-tubulin small complex
ADP	Adenosine diphosphate
ATP	Adenosine triphosphate
CCD	Charge-coupled device
cMT	Cytoplasmic microtubule
ChIP	Chromatin immunoprecipitation
CoIP	Co-immunoprecipitation
Cryo EM	Cryogenic electron microscopy
CSM	Complete synthetic media, yeast minimal media
DNA	Deoxyribonucleic acid
DTT	Dithiothreitol
ECL	Enhanced chemiluminescence
EDTA	Ethylenediaminetetraacetic acid
EGTA	Ethylene glycol tetraacetic acid
EM	Electron microscopy
Endo H	Endoglycosidase H
GDP	Guanosine diphosphate
GFP	Green fluorescent protein
GMPCPP	Guanosine-5'-[(alpha, beta) methyleno] triphosphate
GST	Glutathione S-Transferase
GTBP	Gamma tubulin small complex binding protein
GTP	Guanosine triphosphate
HEPES	4-(2-hydroxyethyl)-1-piperazineethanesulfonic acid

HRP	Horseradish peroxidase
kMT	Kinetochore microtubule
ipMT	Inter-polar microtubule
MAP	Microtubule associated protein
MAPK	Mitogen activated protein kinase
mRNA	Messenger ribonucleic acid
mRFP	Monomeric red fluorescent protein
MT	Microtubule
MTOC	Microtubule organizing center
LB	Lysogeny broth
NA	Numerical aperture
NaDOC	Sodium deoxycholate
NEM	N-ethylmaleimide
NFDM	Non-fat dry milk
OD_{xxx}	Optical density at XXXnm wavelength
ORF	Open reading frame
PCR	Polymerase chain reaction
P_i	Inorganic phosphate
PIPES	Piperazine-N,N′-bis(2-ethanesulfonic acid)
PMSF	Phenylmethanesulfonylfluoride
SDS	Sodium dodecyl sulfate
SDS-PAGE	Sodium dodecyl sulfate polyacrylamide gel electrophoresis
SGA	Synthetic genetic array
SPB	Spindle pole body
VALAP	Vaseline, Lanolin, Paraffin wax
YPD	Yeast extract peptone dextrose, rich yeast media

CHAPTER ONE

Introduction

General Introduction

The earliest form of biological chemistry most likely occurred in a soup of organic chemicals that gave rise to the precursors of modern biological molecules. At some point, these molecules became enveloped by a lipid membrane and cellular life began. As long as cells remained very small, no further organization was needed. The rise of filamentous polymers allowed cells to grow larger by organizing their contents and directing growth. Recent evidence suggests that this occurred very early in the history of cells, as both eubacteria and archeabacteria utilize protein filaments to partition plasmids and possibly entire genomes (Egelman et al., 2007; Erickson et al., 2010). Eukaryotic cells are much larger and much more diverse than bacterial cells and thus have utilized three classes of polymeric proteins to achieve these advantages. The actin network is assembled from actin monomers. A number of different subunits, including keratin and lamin, make up intermediate filament networks (Iwatsuki and Suda, 2010). The dynamic microtubules are assembled from tubulin.

Microtubules are an integral part of the cell's cytoskeleton providing structure, pathways for intracellular transport, and a means for segregating chromosomes during mitosis and meiosis. With so many functions, MTs must be organized into an array that is useful for the cell. This is accomplished by having the minus-ends of MTs anchored at microtubule organizing centers and the plus-ends extending into the cytoplasm,

giving an overall directionality to the MT network. This leaves the more dynamic plus-ends free to probe the interior of the cell so as to reach their points of action and to create new and remove old pathways quickly. Anchoring of MTs is important for organizing the MTs into useful arrays that must endure bending, pulling, and pushing forces.

Due to its simplified cytoskeleton and genetic tractability, the budding yeast *Saccharomyces cerevisiae* is a useful tool in finding the functions of the cytoskeleton and determining how it is regulated. This thesis presents work on a small, cytoskeletal regulatory protein named She1 and its unique phenotype that has led to the understanding of the importance of regulating microtubule motor-protein activity and the differences in the site of anchorage for cytoplasmic microtubules in *S. cerevisiae*.

Microtubule Structure and Dynamics

The basic building blocks of MTs are tubulin monomers. MTs are made of α- and β-tubulin heterodimers. These two tubulin proteins are very similar, sharing a molecular weight of approximately 55kDa and a primary sequence identity of 50%. Both subunits are capable of binding one molecule of GTP, but only β-tubulin is known to exhibit GTPase activity, slowly hydrolyzing its bound nucleotide (Burns, 1991). Heterodimer subunits arrange in a head-to-tail fashion to form a protofilament, as shown in Figure 1.1A. MTs formed *in vivo* contain 13 protofilaments associated laterally to

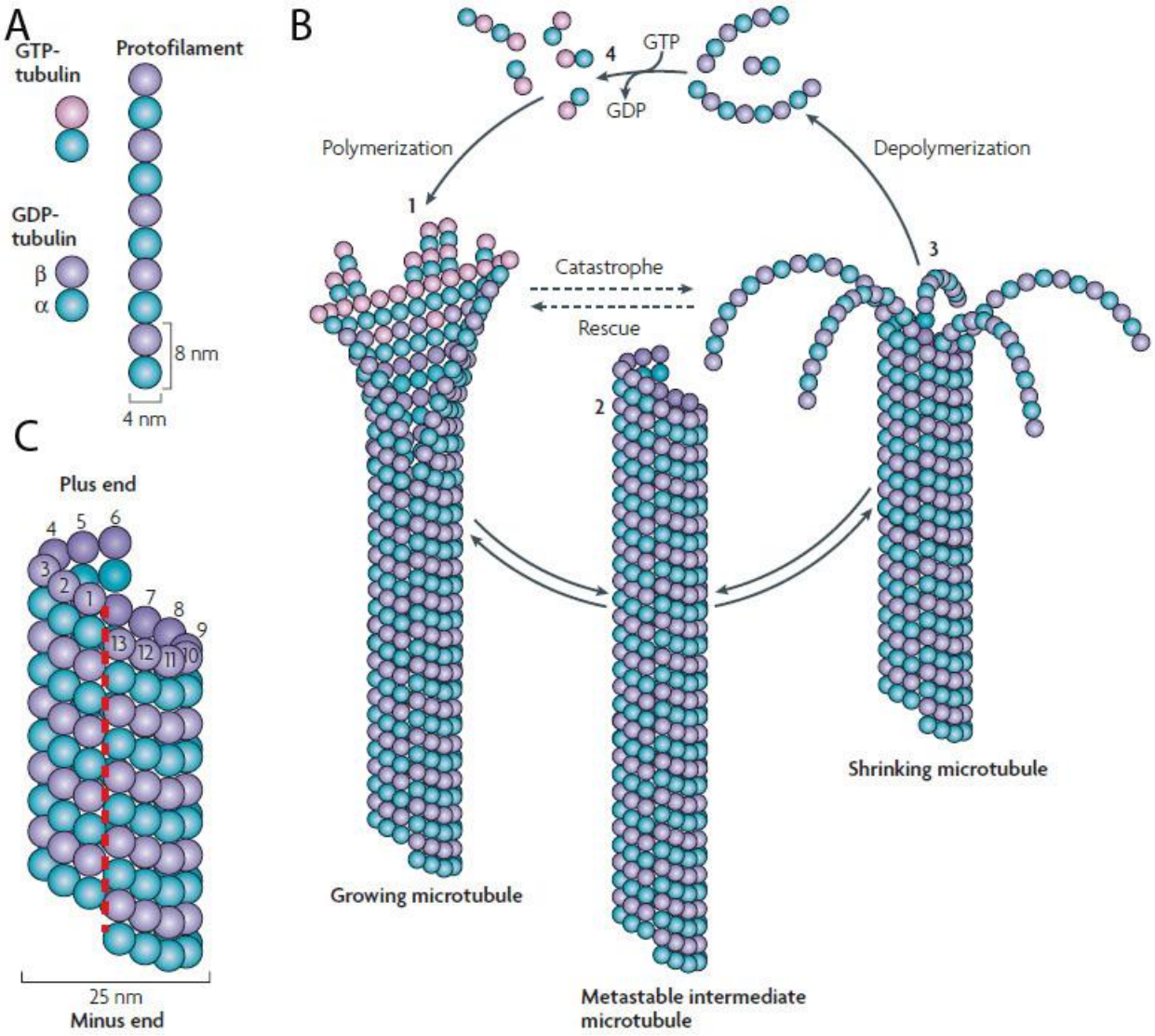

Figure 1.1 Overview of Microtubule Dynamic Instability. (A) GTP is bound by the β subunit of α/β tubulin dimers and hydrolyzed into GDP. Protofilaments arrange with the α subunit interacting with β subunits along the length of the polymer. (B) GTP-bound dimers are incorporated into the growing plus-end of MTs as a flat sheet which closes over time to form the hollow tube. MTs can switch between growing and shrinking through catastrophes or shrinking to growing through rescues. MTs not in either phase are paused. (C) 13 protofilaments make up a MT. Subunits are aligned in a B-type helix with a seam (red dashed line) where α subunits laterally contact β subunits. Figure adapted from (Akhmanova and Yap, 2008).

form a hollow, cylindrical tube with an approximate diameter of 25nm (reviewed in (Desai and Mitchison, 1997)) . There are exceptions to this model such as in *C. elegans* touch cells that have 11 protofilaments, and MTs created *in vitro* in the presence of GMPCPP typically have 14 (Wade, 2009). The protofilaments are arranged so that the lateral associations are mostly α-to-α or β-to-β. However, since the helical structure of the MT is known as a B-type helix, a seam runs down the length of the MT where lateral associations between α- and β-tubulin occurs, giving rise to a unique structural site of the MT (Figure 1.1C) (Kikkawa et al., 1994).

The organized lateral association of tubulin subunits ensures that all the heterodimers associate in the same direction. This gives the microtubule an inherent polarity with a ring of α-subunits at the minus-end of the MT and row of β-subunits at the plus-end. A heterodimer with GTP bound in the β-subunit will add on to the plus-end of a protofilament. The polarity of the MT also contributes to the rate of addition or subtraction of heterodimer subunits from the different ends. The rate of addition or subtraction is called dynamicity. When made *in vitro*, the dynamicity of the plus-ends of MTs is much higher than minus-ends. The switching between growing and shrinking is called catastrophe, where the change from shrinking to growth is called rescue. These changes occur more often at the plus-end than the minus-end (Mitchison and Kirschner, 1984). These dynamics can change *in vivo* depending upon the proteins associated with MTs and their ends and on the stage of the cell cycle. These events of polymerization and depolymerization, shown in Figure 1.1B, are what enable MTs to serve their functions, allowing them to probe the cytoplasmic space looking for contacts and substrates.

The conformation of the GTP-bound tubulin dimer is very rigid and straight, leading to the plus-ends of MTs looking more like a flat sheet where the seam has not yet formed (Wang and Nogales, 2005). The ends of MTs are then "zipped up" and the sheet closes into the cylindrical tube observed by EM. It is not known if this is triggered by GTP hydrolysis or vice-versa, but the conversion of GTP to GDP is important for the dynamic instability of MTs. MTs formed in the presence of a non-hydrolyzable analog of GTP, GMPCPP, are much longer and more stable at colder temperatures (Hyman et al., 1992). The majority of the length of assembled MTs is tubulin dimers bound to GDP. Upon catastrophe, the laterally associated protofilaments begin to peel away from the end of the MT and each other, forming a ram's head structure that retreats toward the minus-end, concurrently with tubulin subunits dissociating from the peeling ends. This is thought to be a function of the change in curvature of the tubulin dimer after it has hydrolyzed its GTP, a conclusion that is bolstered by the observance of 34nm diameter circular tubulin rings near the ends of depolymerizing MTs by cryo-EM (Thompson et al., 1981). Interesting work involving a recombinant antibody directed toward the GTP-bound state of tubulin dimers suggests that tubulin in the MT lattice that is still bound to GTP may aid in or lead to rescue events (Dimitrov et al., 2008).

MTs assembled *in vitro* exhibit dynamics inherent in the physical properties of the heterodimer subunits and the concentration of GTP present (Walker et al., 1988). However, MTs *in vivo* display dynamics much faster than those found *in vitro* (Cassimeris, 1993). For controlled and directed use of the MT network, a class of MT associated proteins (MAPs) has evolved that directly affect the dynamics of MTs by changing the rates of polymerization and depolymerization or the frequency of

catastrophes and rescues. This class of proteins gives shape and function to the MT network. The first MAPs identified were isolated from mammalian brains , where tubulin can make up as much as 20% of the protein content (Kuznetsov et al., 1978). These MAPs include MAP1, MAP2, and tau, and bind along the length of MTs directing their growth and association with other proteins. These proteins are especially important for stabilizing MTs in neurons where plus-ends are located quite a distance from and organizing center. Other MAPs include katanin (McNally and Vale, 1993) and spastin (Errico et al., 2002) which bind to the MT lattice and sever the MT along its length.

An entire class of MAPs tracks the tips of MTs and controls the dynamics at the plus-end. These +TIPS (plus-end tracking proteins) make a complex network at MT plus-ends. End Binding Protein 1 (EB1) binds to the plus-ends of MTs and promotes the addition of tubulin subunits (Komarova et al., 2009; Su et al., 1995). Its homolog in fission yeast, Mal3, has also been shown to bind along the seams of MTs to prevent catastrophes (Sandblad et al., 2006). The budding yeast homolog, Bim1 tracks MT plus-ends and helps target a number of other proteins to the plus-ends of MTs (Blake-Hodek et al., 2010; Wolyniak et al., 2006). XMAP215-family proteins bind to MTs and increase polymerization in a processive manner (Tournebize et al., 2000). The yeast homolog, Stu2, seems to have different effects depending on its binding partner and can act as a promoter of catastrophe or a MT stabilizer (Severin et al., 2001; Wang and Huffaker, 1997; Wolyniak et al., 2006). MAPs in the CLIP-170 family also bind to the plus-ends of MTs acting as a catastrophe suppressor (Schuyler and Pellman, 2001). Bik1, the *S. cerevisiae* CLIP-170 homolog increases overall MT dynamics (Blake-Hodek et al., 2010; Wolyniak et al., 2006). There are MAPs that facilitate depolymerization of

MTs, such as MCAK, by binding to the ends of MTs (Wordeman and Mitchison, 1995). In a general sense, members of the CLASP family are MT stabilizers. Beyond this, CLASP proteins play significant roles in maintaining MT connections to other structures such as kinetochores and for stabilizing mitotic spindle mid-zones (Lansbergen and Akhmanova, 2006). Entire families of MAPs that act as motors influence MT dynamics and use them as tracks to move around the cell. Examples of these proteins will be discussed later. As evidenced by this short list of MAPs, the inherent dynamic instability of MTs is not enough to account for and direct the many functions of MTs seen in cells.

MT Seeding and Anchorage

MTs can assemble *in vitro* with only purified α- and β-tubulin, magnesium ions, and GTP present. In a purified system a kinetic barrier of forming a MT seed, with which other dimer subunits can associate, must first be overcome. Even then, MTs only grow or shrink depending on the concentration of heterodimer subunits and GTP (Walker et al., 1988). Cells use other means to seed MTs that are directly linked to their organization. Assembling MTs *in vivo* involves a third tubulin gene, γ-tubulin, which is closely related to the α- and β-tubulin proteins in that it is ~55kDa and shares sequence identity of ~30% with α-tubulin (Oakely, 1989). For MTs found in most cell types, the minus-end of MTs is capped with γ-tubulin. This cap is thought to help overcome the kinetic barrier of assembling a MT seed by providing a platform or scaffold on which the first set of α/β tubulin dimers can assemble, starting the MT.

In most animal cells γ-tubulin localization comes to a point where the minus-ends of the interphase MTs coalesce. The structure at this terminus was first identified as a MT Organizing Center (MTOC) (Stearns et al., 1991). In animal cells the MTOC is the centrosome which contains two orthogonally placed centrioles. These centrioles are nine sets of MT triplets arranged in a ring (Azimzadeh and Marshall, 2010). Surrounding the two centrioles is layer of electron-dense, proteinacious material called pericentrin, whose function is to bind to a class of proteins that binds and organizes γ-tubulin (Doxsey et al., 1994). This structure gives rise to the seeding of MTs with γ-tubulin and to the organization of MTs at a single focus during interphase.

Saccharomyces cerevisae and some other fungi undergo a closed mitosis, where the nuclear envelope does not break down. Since the centrosomes' functions in mitosis require nuclear envelope breakdown, budding yeast has had to adapt its MTOC into the Spindle Pole Body (SPB). The SPB, diagrammed in Figure 1.2A, differs from the centrosome in that it is embedded in the nuclear membrane and does not have an amorphous structure, like the pericentrin surrounding centrosomes. In its place is a well-defined structure that spans the nuclear membrane and organizes and anchors MTs on both sides of this membrane. The SPB is a >1GDa structure that is mainly composed of a large amount of a few proteins along with several low-copy number periphery or satellite proteins. Electron micrographs of the SPB show three darkly-staining sections termed the inner plaque, central plaque, and outer plaque, with the inner plaque facing the nucleus, the outer plaque facing the cytoplasm, and the central plaque embedded in the nuclear membrane. Cryo-EM and electron tomography reveal

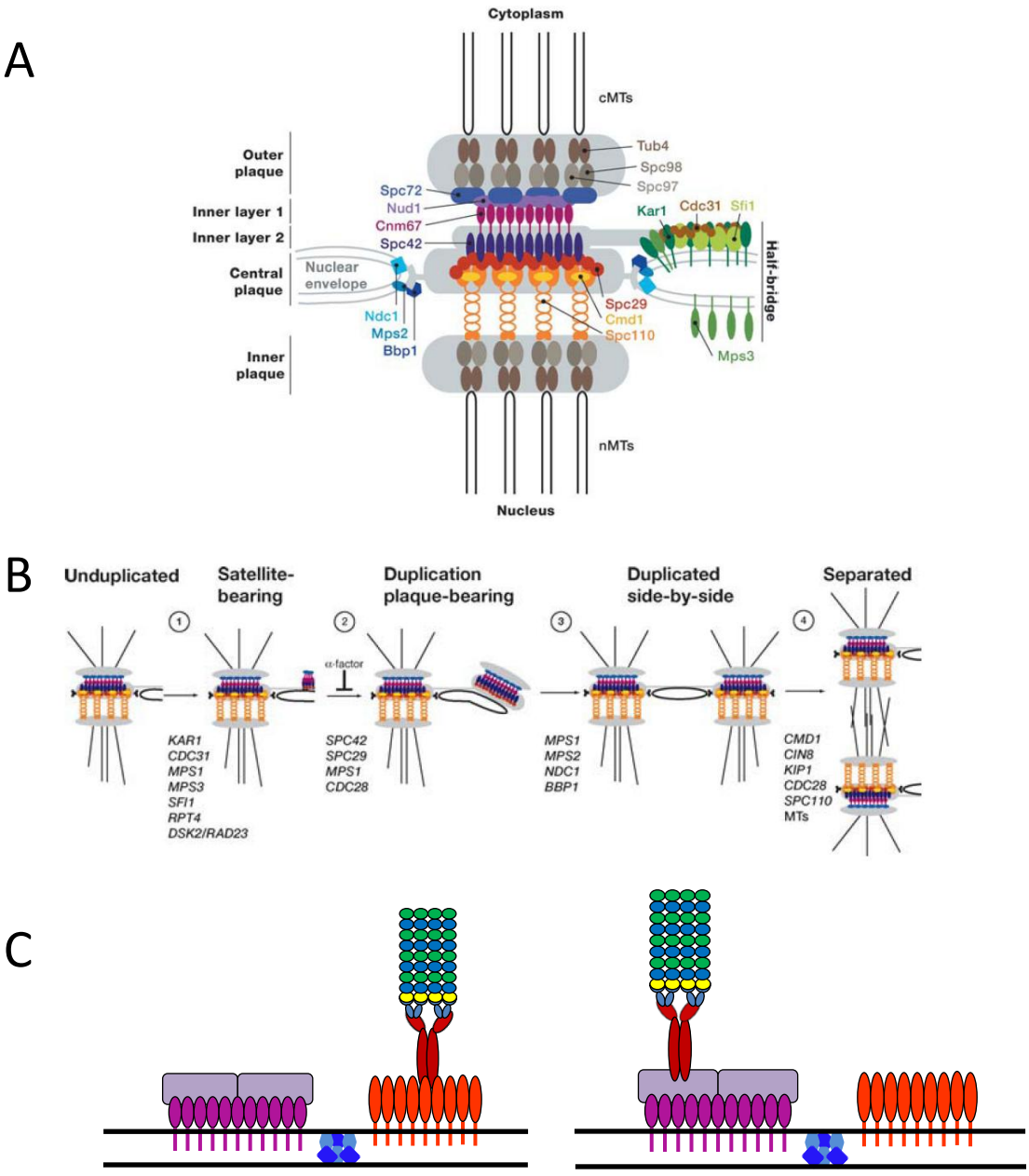

Figure 1.2 The Budding Yeast Spindle Pole Body. (A) Longitudinal cross-section of the SPB through the nuclear membrane. The electron-dense plaques are highlighted with a grey background. (B) Proposed model of SPB duplication and insertion into the nuclear membrane. Adapted from Jaspersen and Winey(2004). (C) Diagram of cMT organization through the cell cycle. During G1 and in the mating phase, cMTs (α/β heterodimers-blue and green, γ-tubulin-yellow) are organized at the half-bridge (Kar1 in orange) by the γ-TuSC (Spc72-red, Spc97/98-grey). After SPB duplication, Spc72 interacts with Nud1 (lavender) which interacts with the outer plaque (Cnm67-purple).

two additional layers between the central plaque and outer plaque, inner layer 1 and 2 (Jaspersen and Winey, 2004).

The main body of the SPB is composed of >1000 molecules of Spc42 trimers forming a hexagonal lattice. Spc42's coiled-coil structure determines the spacing of this hexagonal lattice and over-expression of the protein increases the diameter of the SPB into what has been termed a "super lattice" (Muller et al., 2005). Spc42 forms inner layer 2 and extends into the central plaque where its N-terminus interacts with Spc29. The central plaque is composed of Spc29 and Cmd1, calmodulin. Their interaction with Spc42 forms a dock for Spc110 which reinforces the hexagonal lattice and provides an organizational scaffold for the inner plaque (Sundberg et al., 1996).

The C-terminal portion of Spc42 interacts with another coiled-coil protein Cnm67, the main component of inner layer 1 (Schaerer et al., 2001). Through its coiled-coil domain, Cnm67 dimerizes and acts as a spacer between inner layer 1 and the outer plaque, which faces the cytoplasm. Cnm67 binds to Nud1, which forms the base layer of the outer plaque. In addition to its function of binding Spc72 and ultimately anchoring cytoplasmic MTs, Nud1 is involved with the mitotic exit network and plays a role in correctly localizing Cdc14 to the SPB (Gruneberg et al., 2000).

Off to the side of the central plaque is an electron-dense structure termed the half-bridge. The main components of this substructure are two single-pass membrane proteins, Cdc31 and Kar1 (Spang et al., 1993; Spang et al., 1995). These two proteins are aided by Sfi1 and Mps3 to form a small, dense satellite at the end of the half-bridge. The satellite is composed of a few core SPB proteins, such as Spc42, Spc29, Cnm67,

and Nud1 and is the site of SPB duplication, outlined in Figure 1.2B. Here, SPB component proteins are embedded in the nuclear membrane, giving rise to a daughter SPB which is connected to the mother SPB through the bridge (Schramm et al., 2000). Upon completion of SPB duplication prior to S-phase, the bridge is severed, making two structurally identical SPBs (Jaspersen and Winey, 2004).

The inner and outer plaques of the SPB are the sites of MT nucleation. The proteins that comprise these plaques are γ-tubulin (*TUB4*), and its adapter proteins, Spc97 and Spc98, each bound to one molecule of γ-tubulin (Figure 1.3A and B) (Knop et al., 1997; Knop and Schiebel, 1997; Spang et al., 1996). The prevailing model for MT nucleation shows that Spc97 and Spc98 form a repeating circular structure that is slightly offset at one side. This structure, elucidated through EM, matches the 13 protofilament B-helix structure of MTs (Figure 1.3C and D) (Kollman et al., 2010; Kollman et al., 2008). In budding yeast, these three proteins form the γ-Tubulin Small Complex (γ-TuSC), which seems to be the necessary feature for seeding MTs in both the cytoplasm and the nucleus. However, the γ-TuSC does not bind directly to the outer or inner plaques; it relies on separate binding proteins to attach to either the nuclear or cytoplasmic face of the SPB. In the nucleus, the γ-TuSC Binding Protein (GTBP) is Spc110 (Nguyen et al., 1998); the cytoplasmic counter-part GTBP is Spc72 (Chen et al., 1998; Knop and Schiebel, 1998).

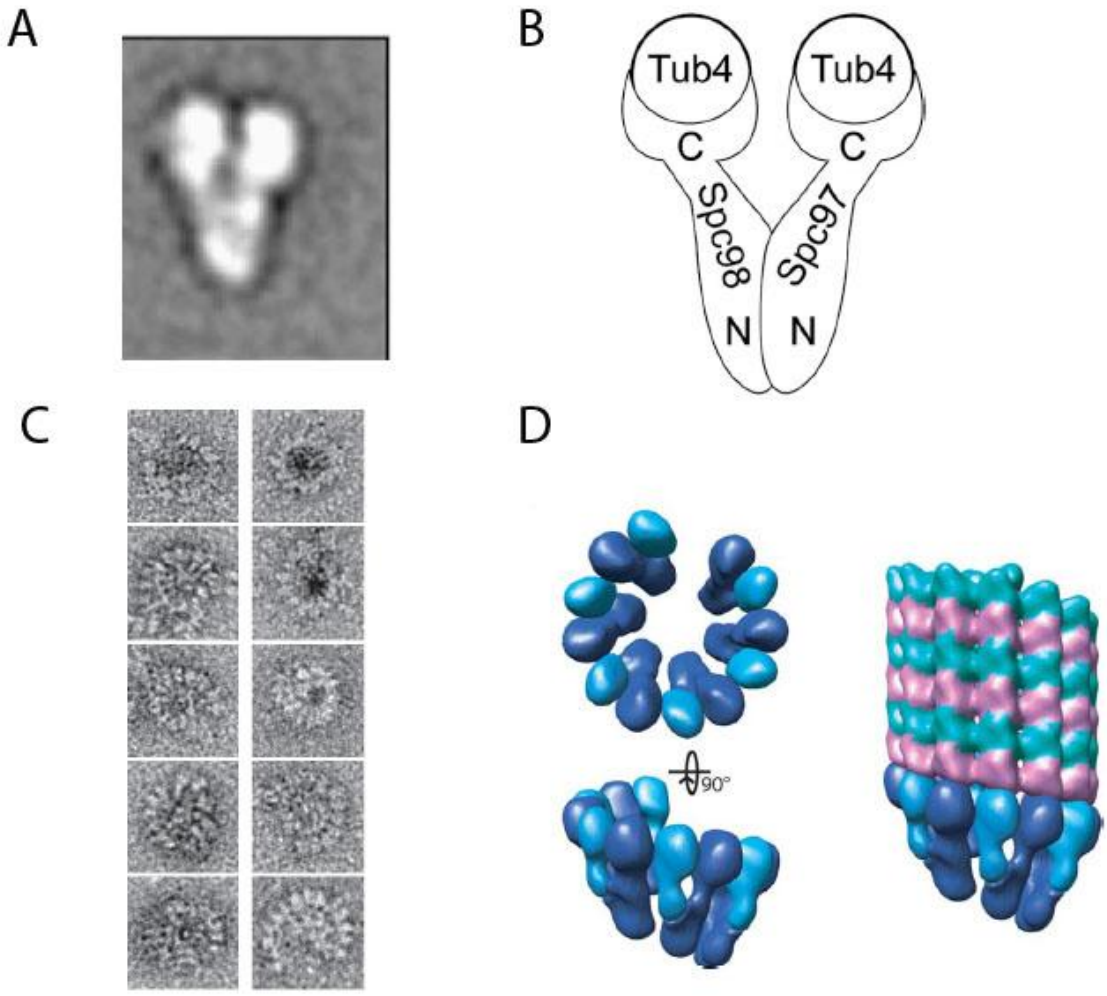

Figure 1.3 γ-Tubulin Small Complex. (A) Average of 68 negative stain EM structures of purified yeast γ-TuSC (Spc97, Spc98, Tub4). (B) Cartoon representation of structures obtained from A. (C) Negative EM stain of γ-TuSC assembled into ring structures from yeast (left) and *Drosophila* (right). (D) Model of ring structures that exhibit a 13-fold repeating structure (left). This forms a scaffold for seeding 13 protofilament MTs found *in vivo*. Adapted from Kollman and colleagues (2008 and 2010).

Anchoring and organization of cMTs change throughout the cell cycle (diagrammed in Figure 1.2C). Before SPB duplication, cMTs are anchored at the half-bridge, whereas afterwards, they are anchored at the outer plaque (Byers and Goetsch, 1975). The mechanism behind this change is the binding affinity for Spc72 to two different proteins, Kar1 on the half-bridge, and Nud1 at the outer plaque (Gruneberg et al., 2000; Pereira et al., 1999). Current evidence suggests that the hypophosphorylated form of Spc72 binds to Kar1p. Once Spc72 is phosphorylated by Cdc5p during the S-to-metaphase transition, it partners with Nud1. Co-immunoprecipitations have suggested that the strength of Spc72's association with Kar1 is weaker than that with Nud1 (Pereira et al., 1999). The purpose behind switching organizing sites or the difference in affinity has not been uncovered. In fact, one of these sites can be eliminated and the cells will survive. Though deletion of *NUD1* are lethal due to Nud1's role in the cell cycle (Gruneberg et al., 2000), its location there is not necessary and the outer plaque can be ablated by a ***cnm67Δ*** mutation (Schaerer et al., 2001), displacing Nud1 and ultimately, Spc72. Cells remain viable due to cMTs anchoring at the half-bridge. Conversely, Kar1 is essential for SPB duplication and is necessary for viability, but a partial deletion of *KAR1* that removes the Spc72 binding portion of the protein prevents cMTs from nucleating at the half-bridge, allows cells to survive by nucleating cMTs at the outer plaque (Vallen et al., 1992). Some yeast strain backgrounds are viable with the ***spc72Δ*** mutation and survive with only having short-lived cMTs that are <1µm (Hoepfner et al., 2002). How these cMTs form is not understood at this time.

Motor Proteins and Forces Acting on Cytoplasmic Microtubules

One group of MAPs is the motor proteins, which bind MTs and use the chemical energy of ATP hydrolysis to switch the protein between at least two structural states. The changing of states is converted into mechanical motion when one part of the protein stays bound to the MT and pushes the rest of the protein in front of it. In a series of steps that depend on the motor, the hydrolyzed ADP and P_i are released and the part of the protein that binds the substrate MT switches from the back "foot" to the leading "foot." This cycle is repeated and the protein transits along the length of the MT (Yildiz et al., 2004). A measure of how many steps a motor protein proceeds on a MT before dissociating is called processivity, which can differ from a few steps to many microns. Locomotion on MTs would not be useful in and of itself and motor proteins have differing tail or cargo domains to transport a number of molecules throughout the cell. Motor proteins have many functions in the cell including transport of various cargoes, such as organelles, mRNAs, chromosomes, and lipids; organization of MTs at the MTOC; and regulation of MT dynamics.

Directed movement of organelles and large molecules through the cytoplasm at rates faster than diffusion was eventually attributed to motor proteins that walk along MTs. Vale and colleagues used extracts from squid axons to show that a protein factor was responsible for the movement of MTs on glass or for the translocation of latex beads along stationary MTs (Vale et al., 1985). This protein factor was named kinesin and was the founding member of the super-family of MT motor proteins called kinesins or kinesin-like proteins.

Conventional kinesin contains two heavy chains that contain the motor domain and two light chains that interact with various targets. Kinesins share homology in their motor domains, and a large number of kinesin-like proteins have been identified through homology in this region. The light chains of kinesin differ in their binding regions and direct the types of cargo the motor carries. Though most classes of kinesins have the motor domain on their N-terminus and move toward the plus-end of MTs, the Kinesin-14's, like *Drosophila melanogaster* Ncd and *Homo sapiens* KIFC3, translocate towards the minus-end with motor domains on the C-terminus. Other kinesins, such as the kinesin-13 family members, only have a homologous motor domain, but do not travel along the MT. Instead, these kinesins bind to MT ends and destabilize them, leading to catastrophes (Dagenbach and Endow, 2004).

Figure 1.4A shows that in budding yeast, there are only 6 kinesin-related proteins (Hildebrandt and Hoyt, 2000). The motors Kip1 and Cin8 are in the Kinesin-5 family of homotetramers with plus-end directed motor activity on both ends of the molecule. Having motor domains on either side of these molecules allows them to cross-bridge and either organize parallel MTs or push apart anti-parallel MTs. (Cottingham et al., 1999; Saunders and Hoyt, 1992). To that effect, these proteins are necessary for initially forming the mitotic spindle by pushing apart the SPBs once they have duplicated. Since these proteins are in the same family of kinesins, they are mostly functionally redundant and cells can survive with a deletion of either locus, but not both. Cin8 may have MT disassembly properties as well (Gardner et al., 2008a).

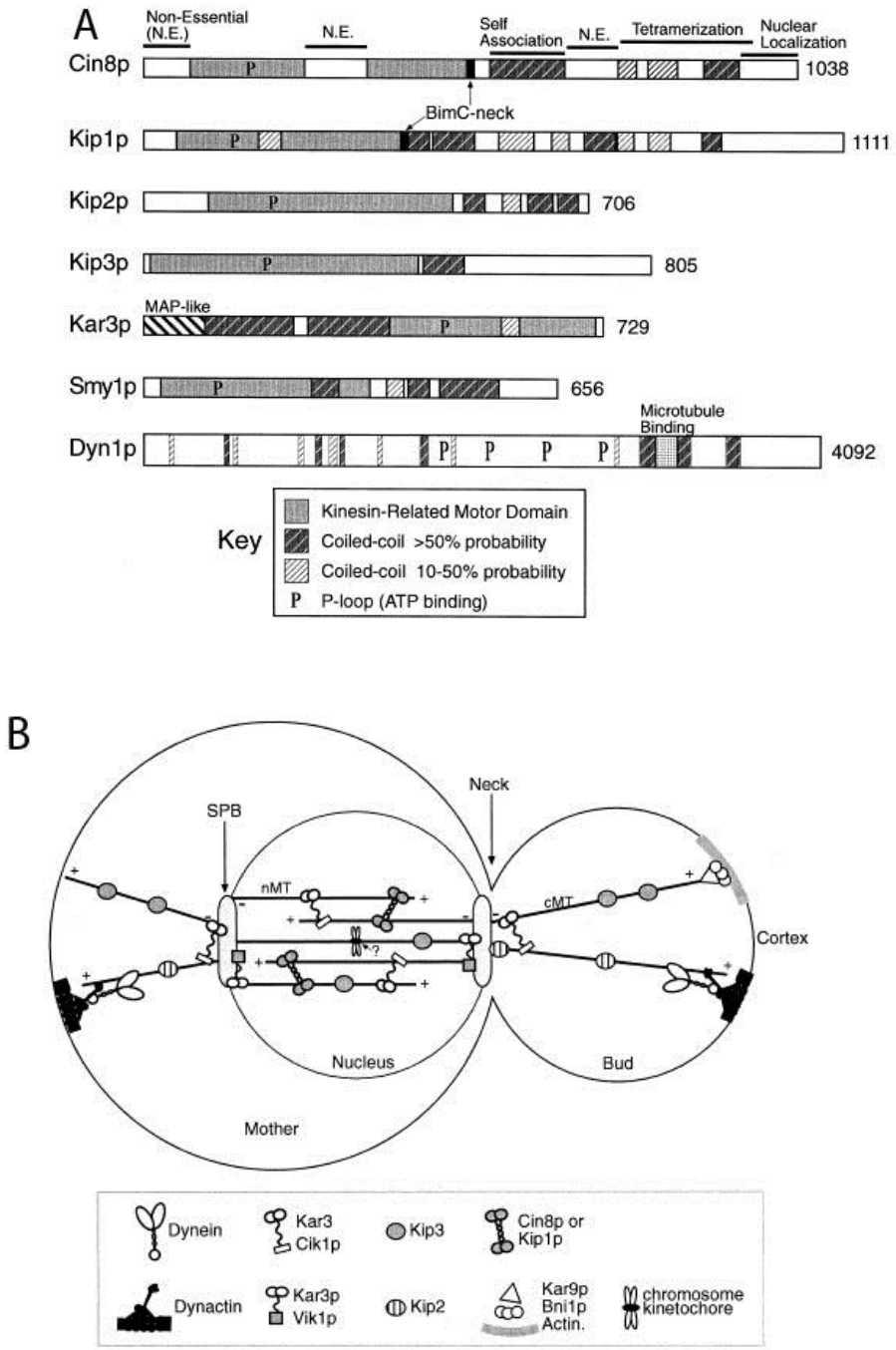

Figure 1.4 Motor Proteins in Budding Yeast. (A) Domain mapping of the 6 kinesin and dynein heavy chains that are found in *S. cerevisiae*. Kar3's motor is found on the C-terminus. Smy1 has a motor domain that is rendered non-functional. (B) Map of the location of these motors during mitosis. Adapted from Hildebrandt and Hoyt (2000)

Kip3, a member of the Kinesin-8 family, has been shown to have great processivity in walking to the plus-ends of MTs and removing tubulin subunits (Gupta et al., 2006; Varga et al., 2009). The cargo binding domain of Kip3 binds to free tubulin dimers, preventing their interaction with MTs. These features impart a length-dependent depolymerizing property to Kip3 (Varga et al., 2006). Kip3 controls the length of cMTs, as demonstrated in *kip3Δ* mutants that have longer than normal cMTs (Miller et al., 1998).

Kar3 is a heterodimer that binds to two different proteins that direct its function and perhaps its localization (Manning et al., 1999; Page et al., 1994). In the nucleus, Kar3 pairs with Cik1 through coiled-coil interactions (Chu et al., 2005). Kar3 is in the Kinesin-14 family which has minus-end directed motor activity and can depolymerize MTs as it walks along them (Sproul et al., 2005). During vegetative growth, Kar3 interacts with its other partner, Vik1, and possibly regulates the length and organization of the cMTs (Allingham et al., 2007).

There are only two exclusively cytoplasmic kinesin-related proteins. Smy1 is only included as a kinesin-like protein because it has a high degree of homology to kinesins, but its motor domain is non-functional and it has been shown to interact with the actin network (Lillie and Brown, 1994). Originally, Kip2 was thought to control the length of cMTs in opposition to Kip3 since *kip2Δ* mutants have average shorter cMTs (Huyett et al., 1998). However, it has been shown that this is an indirect effect of Kip2's real function to transport a number of +TIP proteins to the ends of cMTs, presumably protecting the ends from depolymerizing factors, such as Kip3 and Kar3, or by supplying

MAPs that contribute to the net growth of cMTs (Carvalho et al., 2004; Caudron et al., 2008).

Though the six kinesins in budding yeast exhibit a variety of functions and are coordinated through many mechanisms to ensure these processes occur correctly, cells can survive with only two of these motors intact. Work from the Hoyt lab has shown that a combination of Cin8 with either Kip3 or Kar3 is sufficient for viability (Hildebrandt and Hoyt, 2000).

In juxtaposition to kinesin is the MT motor dynein, a minus-end directed motor. There are a few classes of dyneins that have different functions in the cell. Dynein motors are responsible for the beating of cilia and flagella and are confined to these structures and compartments by independent targeting mechanisms (Gibbons, 1966; King et al., 1995). A distinct isoform of dynein performs functions only in the cytoplasm and is targeted to sites of action by an associate protein complex, dynactin(Vallee et al., 1995). Cytoplasmic dyneins carry out a number of different functions in the cell, including intracellular vesicular transport, centrosome positioning, and organization of MT arrays. Due to budding yeasts' small size and lack of higher-order MT structures, only one cytoplasmic dynein is necessary (Hildebrandt and Hoyt, 2000). Cytoplasmic dynein is a much larger molecule than kinesin (Figure 1.5A). It is composed of at least 4 subunits paired into a dimer of over 1.2MDa. A dynein molecule consists of a heavy chain (Dyn1), a light chain (Dyn2), an intermediate chain (Pac11), and an intermediate-light chain (Dyn3). The motor domain of dynein is at the carboxy terminus of the heavy chain. This region of the protein is highly conserved across eukaryotes, forming a ring

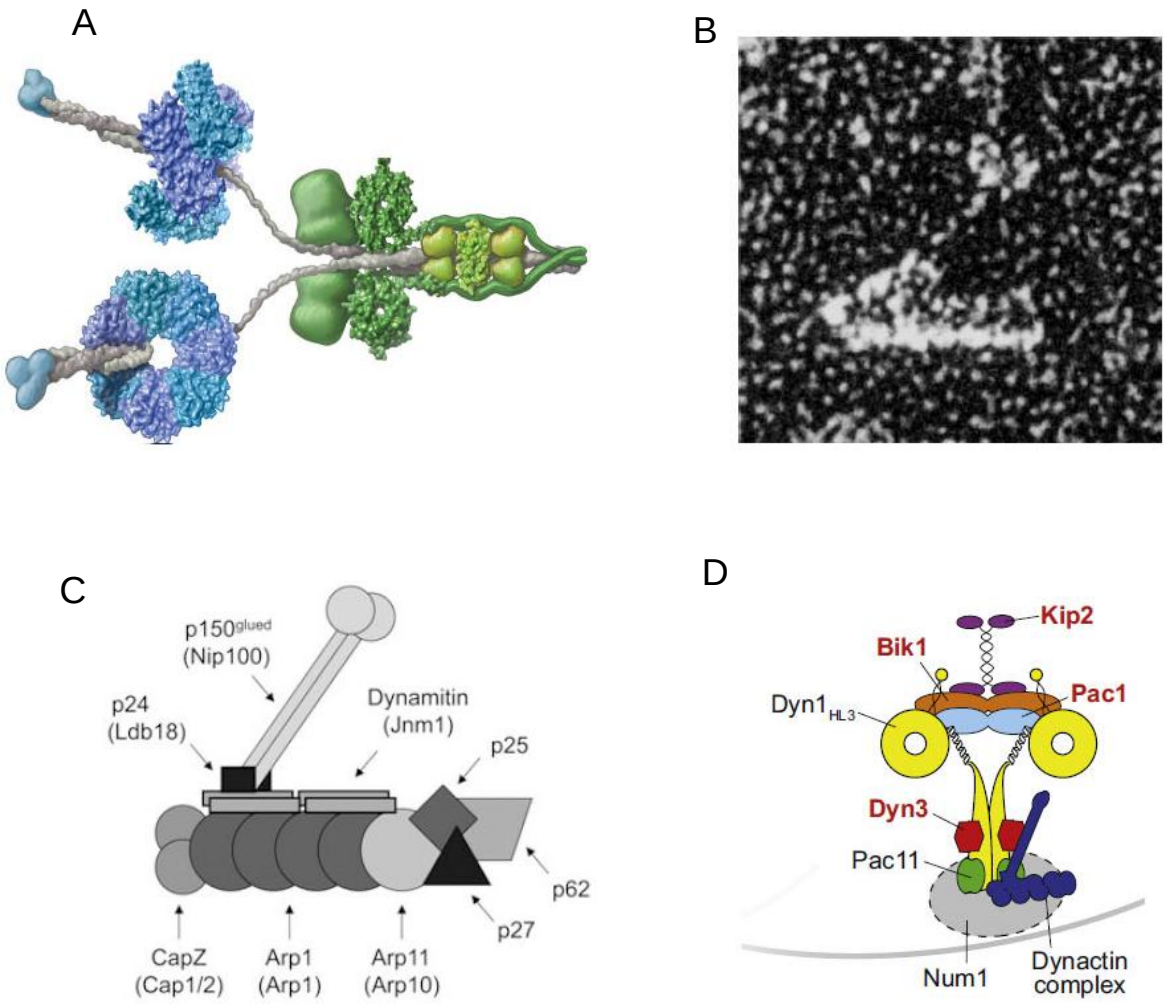

Figure 1.5 Structures of Dynactin and Dynein. (A) Cartoon representation of the dynein holoprotein. The 6 P-loops are represented by the teal, blue, and purple rings with the MT binding stalk domains pointed to the left. (Yildiz lab website) (B) Purified Dynactin prepared from quick-freeze, deep-etch, rotary shadow EM. (Schroer 2004) (C) Schematic of dynactin displaying mammalian gene names and yeast homologs in parantheses. (Amaro et al. 2009) (D) Proposed model of dynein loading onto cortical sites. Pac1/Bik1/Kip2 would be bound to the cMT that has made contact with Num1 (Markus et al. 2011).

of 6 AAA+ ATPase motifs and, along with a stalk region responsible for binding MTs, (Moore et al., 2009).

Cytoplasmic dynein depends upon its activator complex, dynactin, for activity (Muhua et al., 1994). This complex is well conserved between budding yeast and higher eukaryotes in both composition and protein sequence. Dynactin forms a rod-and-shoulder-sidearm complex (Figure 1.5B) where the 40nm rod is composed of actin-related proteins, Arp1, capped at the barbed-end by CapZ and at the pointed-end by Arp11. A group of small proteins, p25, p27, and p62, are also located at the pointed-end. The shoulder-sidearm projection contains $p150^{Glued}$, p24, and dynamitin, which binds to the rod portion (Schroer, 2004). Dynactin's activity depends upon $p150^{Glued}$ since it has both a CAP-Gly domain that binds to MTs and a separate domain responsible for activating dynein (Holzbaur et al., 1991). Known yeast homologs of these proteins include Nip100 ($p150^{Glued}$), Jnm1 (dynamitin), Ldb18 (p24), Arp1 (Arp1), and Arp10 (Arp11) (Figure 1.5C) (Amaro et al., 2008; Clark and Rose, 2006; Kahana et al., 1998; McMillan and Tatchell, 1994; Muhua et al., 1994). The complex is rendered inactive if any of these proteins are missing or mutated leading to mislocalization of the complex, failure to assemble, or an inability to activate dynein. Homologs of the pointed-end capping proteins seem to be missing in budding yeast as their role in other organisms of vesicular transport is absent (Moore et al., 2009).

Dynein's function in budding yeast is to bring the spindle through the bud neck during anaphase so that after the spindle elongates one SPB is located in the daughter cell and one in the mother, equally segregating the nuclear material in preparation for

cytokinesis (Li et al., 1993). In order for dynein's minus-end directed locomotion to achieve this, it must first make its way to the plus-end of a cMT that extends into the daughter cell that then makes contact with a cortical site of Num1 protein, as diagrammed in Figure 1.5D. Current models suggest that Pac1, with help from Ndl1, binds to dynein in the cytoplasm and inhibits its motor activity (Markus et al., 2009). The +TIP Bik1 binds to Pac1 and the entire complex is transported to the plus-end by the kinesin Kip2, and tracks the growing cMT plus-end (Markus et al., 2011). At this point, the dynein molecule is thought to be "masked" in a form of auto-inhibition preventing motor function. The "unmasking" of dynein may be controlled by its interaction with the dynactin complex at the plus-ends of cMTs (Markus and Lee, 2011). Once a loaded cMT makes contact with a cortical site of Num1, dynein and dynactin are off-loaded from the plus-end and remain stationary at the cortex. Num1 anchors itself into the plasma membrane via a pleckstrin homology motif and binds to dynein once it comes into contact with it (Yu et al., 2004). Once dynein is active and binds the plus-end of a cMT, the minus-end directed locomotion of dynein is translated into a pulling force, reeling in the daughter-bound SPB through the bud neck.

In addition to the spatial regulatory mechanisms for controlling dynein activity mentioned above, there is a level of temporal regulation. Cortical Num1 sites are found in the mother cell as well, so nuclear migration must take place prior to dynein activation so that the SPB is directed into the daughter cell (Heil-Chapdelaine et al., 2000). Dynein is considered to be inactive during the early phases of the cell cycle despite the fact it is localized to cMT plus-ends during all phases of the cell cycle. Dynein activity must also halt at the end of spindle orientation so that the spindle elongates correctly

and the daughter-bound SPB does not re-enter the mother cell. It is becoming apparent that the loading of the dynactin complex onto cMTs is temporally restricted by She1 (Woodruff et al., 2009).

Interactions between the MT array and the actin network have been found in lamellipodia during cell migration (Waterman-Storer and Salmon, 1997) and in neuronal growth cone guidance (Gordon-Weeks, 2004). In budding yeast, the actin network is responsible for delivering vesicles to the plasma membrane, endocytosis, the delivery of organelles into the daughter cell during cell division, and contraction of the cleavage furrow during cytokinesis (Pruyne et al., 2004). The actin and MT networks intersect in budding yeast for spindle migration, discussed later. These functions all rely upon actin's own family of motor proteins, the myosins. Actin filaments are similar to microtubules in that they polymerize from asymmetrical subunits that give rise to polarity within the polymer. Myosin motors walk down actin filaments in a directed motion (Yildiz et al., 2003). *Saccharomyces cerevisiae* uses 5 different myosins that fall into 3 different classes. The Class-V Myo2 motor is responsible for pulling cMTs as cargo towards the daughter cell (Yin et al., 2000).

Functions of Microtubules in Budding Yeast

Microtubules were first described as cellular fibers that are involved in the segregation of the chromosomes during mitosis. This is the most prominent role for MTs and disturbing MT function typically arrests cells in the mitotic phase. The mechanism for this action of MTs pulling DNA to the MTOC has seen an incredible amount of work

in the last century and it has gradually become clear how a dynamic, MTs coordinate the movement of condensed nucleic acid through the cell. One of the first steps in preparing the chromosome for segregation is to replace typical histones with a specialized histone analog at the site of MT attachment, forming the centromere (Pauleau and Erhardt, 2011). Assembled here is the kinetochore (modeled in Figure 1.6A), which bridges the centromeric DNA of chromatids to kinetochore MTs (kMTs) from the spindle (Kline-Smith et al., 2005). The basic architecture of the kinetochore is well conserved in eukaryotes with an inner layer that interacts with the specialized histones (CSE4), a spacer complex (COMA), a complex of proteins involved with binding the MT (KNL), and a long linker complex that binds the MT lattice as it depolymerizes (NDC80) (Cheeseman and Desai, 2005; Joglekar et al., 2006; Westermann et al., 2007). During mitosis, kMTs extend from the MTOC and eventually make contact with the kinetochore. At anaphase, the kMTs begin to depolymerize, the kinetochore maintains its connection to the kMTs and couples the poleward movement to the centromeric DNA, dragging the chromatid along.

This process differs in *S. cerevisiae*'s closed mitosis system in that this kMT-centromere connection is thought to persist throughout the cell cycle, except during S-phase when the centromeres are being duplicated, whereas in higher eukaryotes, this connection happens once the nuclear envelope breaks down and the spindle begins to form. The kMTs are then responsible for aligning the chromatids at the metaphase plate where spindle assembly checkpoint proteins check for tension across the chromatids to ensure that only one kMT attaches to the centromere and that its sister is attached to the opposite SPB. During chromosome capture in budding yeast (Figure

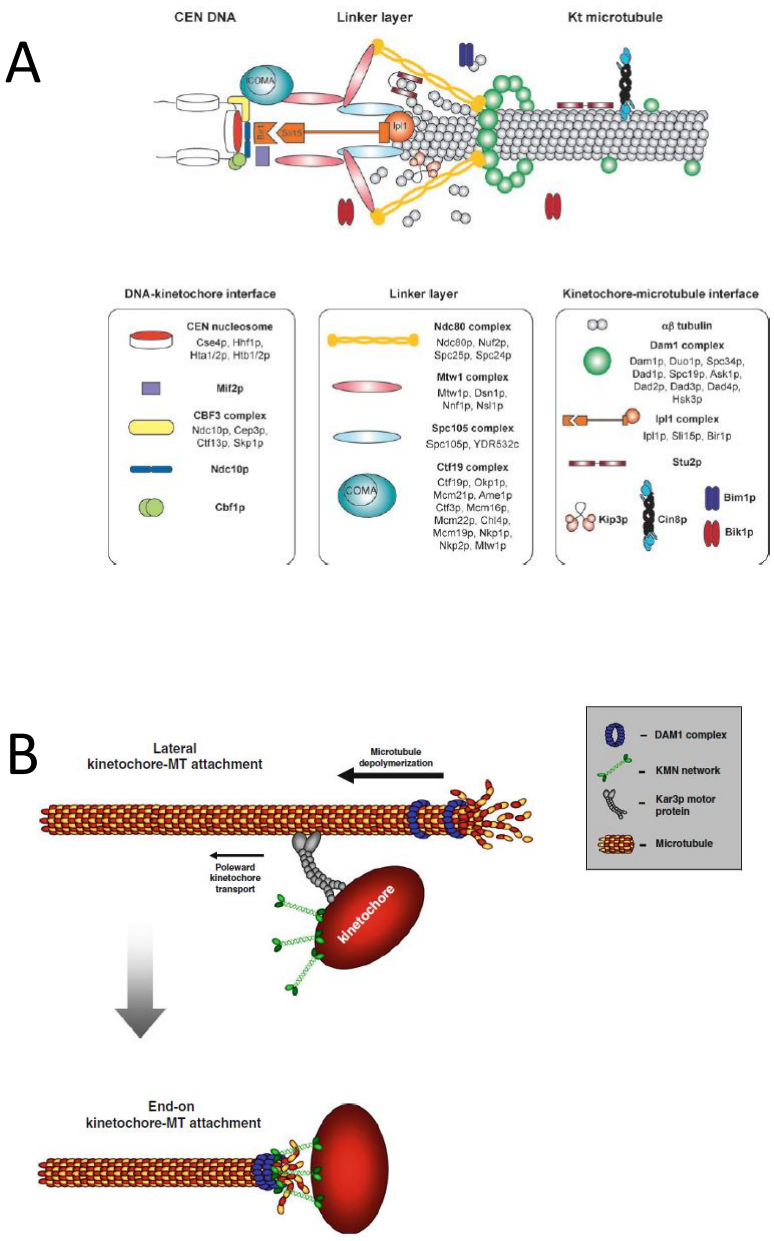

Figure 1.6 Kinetochore Architecture and Capture. (A) The yeast kinetochore is made of several sub-complexes that bind the centromeric DNA and attach it to a kMT. Adapted from (Westermann et al., 2007). (B) Capture of the kinetochore can happen laterally or end-on. If the kMT catches the kinetochore laterally, Kar3 attaches the kinetochore until the kMT depolymerizes and forms an end-on attachment. The DAM complex couples the force of the depolymerizing MT to propel the kinetochore towards the SPB. Adapted from (Kops et al., 2010).

1.6B), a single MT will try to make an end-on connection to the centromere. If the centromere is close enough to the MT to laterally associate with the side of a kMT, Kar3 moves down the kMT, depolymerizing it, until the end-on connection is made (Tanaka et al., 2007; Tanaka et al., 2005). Once anaphase begins, MT depolymerization is coupled to chromatid movement to the SPB by the kinetochore, the protein interface between kMT and the centromere. Though the nuclear kinesins are involved in organizing kMTs, the motor activity of Kar3 aids in kinetochore capture (Tytell and Sorger, 2006). The current model for kinetochore capture in *S. cerevisiae* has the DAM complex forming a ring, or cuff, around the plus-end of the kMT which is then connected to the centromere through the long, bridging Ndc80 complex (Cheeseman et al., 2001; Wang et al., 2007; Westermann et al., 2006). There is sufficient room for the ram's head structure of the depolymerizing kMT to fit in between, and the peeling of the MT lattice acts as a motor to push the DAM complex towards the minus-end (Wang et al., 2008).

In addition to the kMTs, the mitotic spindle is made of interpolar MTs (ipMTs) that extend from the inner plaque of one SPB to the opposing SPB, forming a network of anti-parallel MTs. These ipMTs are responsible for pushing apart the SPBs after cleavage of the bridge and for establishing the short spindle in pre-anaphase cells. Kip1 and Cin8 bind to anti-parallel ipMTs and push them apart by walking to the plus-ends (Hoyt et al., 1992). Simultaneously, ipMTs polymerization is promoted and stabilized so that the final length of the spindle is >7μm (Roof et al., 1992; Severin et al., 2001). Kar3's depolymerase activity is thought to oppose the pushing force of the Kinesin-5 proteins on the mitotic spindle by either rigidly cross-bridging the ipMTs or by

shortening them as they extend (Gardner et al., 2008b; Hoyt et al., 1993). At the end of mitosis, the spindle breaks down and the ipMTs rapidly depolymerize, retreating to the SPBs. This rapid depolmerization is thought to be partially controlled by Kip3, since mutants of *KIP3* show defects in the initiation of spindle breakdown and the site of breakage is offset from the middle of the spindle (Woodruff et al., 2010).

Budding yeast can grow vegetatively as either haploids or diploids. Upon stimulation by the opposite mating-type pheromone, a cascade of events begins through a G-protein coupled receptor and MAPK signaling pathway (Dohlman and Slessareva, 2006). This includes the formation of a shmoo, which is a projection of the plasma membrane and is the site of cell fusion. During mating, cMTs are responsible for positioning the haploid nucleus into the shmoo. The Bim1-Kar9 complex on the plus-ends of cMTs in conjunction with Myo2 and the actin network are responsible for orienting the cMTs to the shmoo tip, similar to positioning the nucleus during mitosis. The nuclei must then migrate into the shmoo tip (Molk and Bloom, 2006). The mechanism for this is not entirely understood, but the current paradigm holds that Bik1 maintains cMTs at the shmoo tip while Kar3/Cik1 processively depolymerizes them, bringing the nucleus with the approaching SPB (Maddox et al., 2003). After the cells fuse their membranes, the opposing cMTs from the haploid nuclei must cross-bridge and shorten in order to bring the nuclei into close enough proximity to fuse membranes and combine their genetic material. This mechanism too is not completely understood, but it is known that Bim1, Bik1, and Kar3 are all required for nuclear congression (Molk et al., 2006). The Kar3/Cik1 heterodimer is most likely responsible for only cross-linking the cMTs and not for depolymerizing them. Bim1 and Bik1 may control the dynamics of

these MTs and coordinate the state of persistent depolymerization that drives the two nuclei together (Maddox et al., 1999).

Since the plane of division in budding yeast is pre-determined by bud site selection following the previous round of cytokinesis, the nucleus must migrate to this area. Once here, the nucleus must also be oriented properly so that when the spindle elongates during anaphase, one SPB makes it through the bud neck and into the daughter cell. Nuclear migration and spindle orientation depend upon cMTs and their MAPs in order to occur sequentially after S-phase and in the daughter-bound direction. These two processes are divided into early and late pathways that are controlled by separate mechanisms and are partially redundant in that one of the pathways may be compromised without affecting the overall viability of the strain (Bloom, 2001).

Migration of the nucleus to the bud neck involves both the microtubule network and the actin network (Figure 1.7A). Cytoplasmic MTs from the SPB closer to the daughter cell are decorated at their plus-ends by a complex of Kar9 and Bim1 (Korinek et al., 2000). These cMTs will dynamically probe the cytoplasmic space until it comes into contact with the actin network and a class-V myosin motor, Myo2 (Miller et al., 2000). Kar9 bridges Bim1 on the plus-end of the microtubule to Myo2, which then takes the cMT, with the nucleus in tow, towards the bud neck (Hwang et al., 2003; Yin et al., 2000). This movement is aided by depolymerization of the leading cMT by Kip3 (DeZwaan et al., 1997; Yeh et al., 2000). There are several mechanisms in place to ensure that the movement of the nucleus is directed toward the new bud. Most

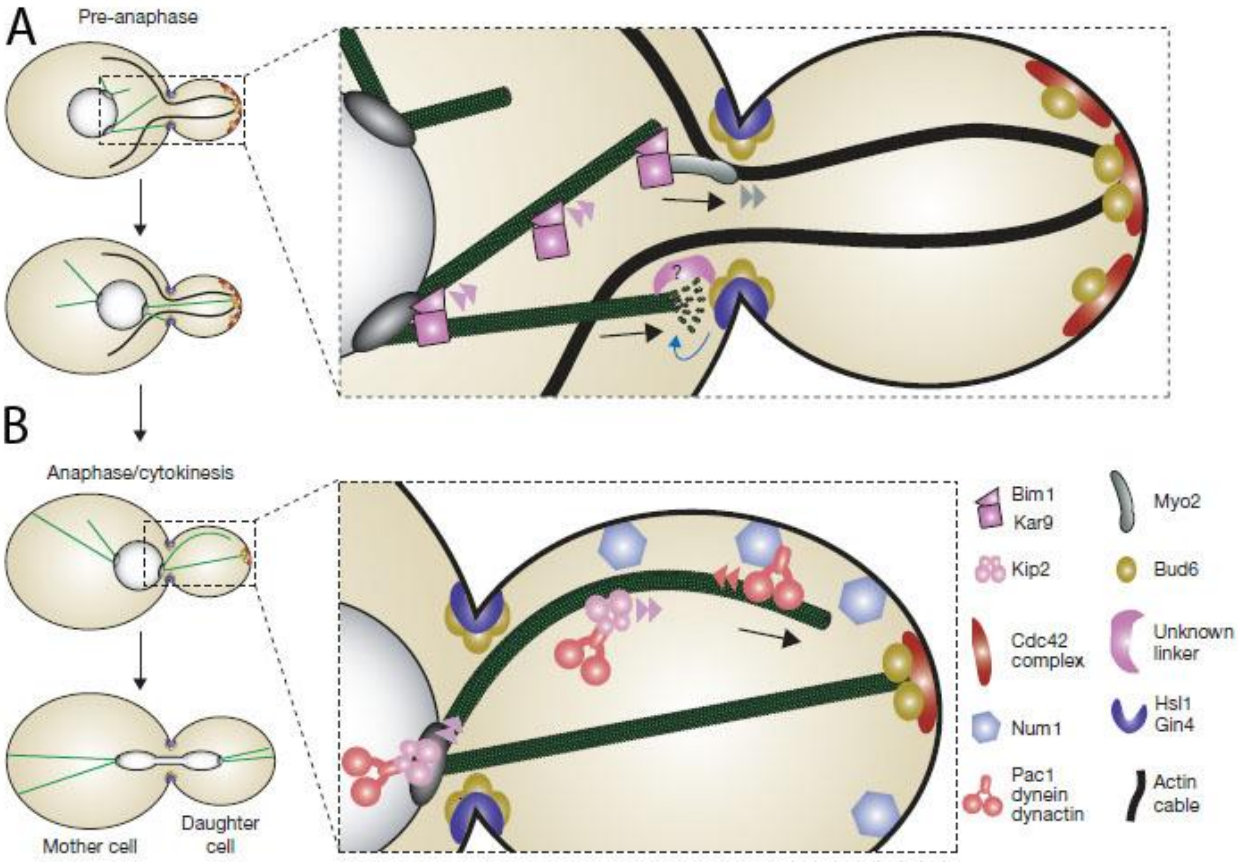

Figure 1.7 Nuclear Movements in Budding Yeast. (A) Nuclear migration to the bud neck is accomplished by Myo2 bringing a cMT as cargo along the actin network into the bud. (B) Spindle orientation requires dynein to become anchored in the cortex and pulling the SPB into the bud. (Siller and Doe, 2009)

prominent is the asymmetric loading of Kar9 onto the daughter-bound SPB (Liakopoulos et al., 2003). This is achieved through the loading of the B-type cyclin, Clb4, and the cyclin dependent kinase, Cdc28, onto the motherward SPB, which phosphorylates Kar9, inhibiting Kar9 activity at that SPB (Moore et al., 2006; Moore and Miller, 2007).

Once the nucleus has reached the bud neck, the spindle must be correctly oriented orthogonally to the bud neck so that a SPB will pass through upon anaphase onset (Figure 1.7B). This process requires the loading of dynein onto the plus-ends of cMTs which will again, dynamically probe the daughter cell (Yeh et al., 2000). Once the pre-loaded cMT makes contact with a cortical site of Num1, dynein is off-loaded onto the cortex (Markus et al., 2011). Here, dynein becomes anchored and activated. The minus-end directed locomotion of dynein is then converted into a pulling-force bringing the SPB through the bud neck and into the daughter cell, again with the nucleus in tow. The nuclear face of the SPB has the daughter chromatids attached to kMTs, effectively and equally segregating the genetic material. Dynein activity must then be turned off so that further spindle movements do not occur. Temporal regulation of dynein activity is thought to be controlled by She1 (Woodruff et al., 2009).

She1 Is a Relatively Unknown Protein

SHE1 was first named in a screen looking for cellular growth defects when single ORFS were highly over-expressed from an inducible *GAL1* promoter on a high-copy plasmid vector (Espinet et al., 1995). When cells over-expressed *SHE1*, they arrested in a large, un-budded state. This phenotype was confirmed in a second over-

expression screen that utilized a more automated approach to systematically characterize the over-expression profile of >5,000 genes and used the *GAL1/10* promoter (Sopko et al., 2006). This phenotype has not been further investigated.

She1-GFP is localized along lengths of cMTs and at the SPBs (Xue Xia, personal communication; and (Wong et al., 2007; Woodruff et al., 2009). Cells that have had the *SHE1* ORF deleted show increased and early localization of dynactin components to cMT plus-ends (Woodruff et al., 2009). This in turn prematurely activates dynein, leading to numerous phenotypes. Woodruff and colleagues (2009) reported that the motility of SPBs in G1 and pre-anaphase spindles is greatly increased in *she1Δ* mutants leading, in some cases, to spindle mis-orientation. Also, once the spindle enters the daughter cell and begins to elongate, the daughter-bound SPB is randomly pulled around the cortex of the cell, sometimes bending the spindle into loops and breaking it prematurely. Some of these events are so extreme that the daughter SPB re-enters the mother cell, leading to the inheritance of both SPBs by the mother cell and, thus, aneuploidy. These phenotypes can be rescued by deleting *DYN1*, abolishing the dynein pathway.

She1 has another role inside the nucleus as well. She1-GFP also localizes to ipMTs and She1 has been found to associate with the kinetochore proteins Dam1, Duo1, Spc34, and Sli15 through yeast two-hybrid screens and chromatin immunoprecipitation (Shang et al., 2003; Wong et al., 2007). Though these interactions suggest a role in kinetochore capture, it is not clear if She1 is involved in this process. It

has been shown that spindle breakdown in *she1Δ* cells is disrupted and occurs offset from the spindle mid-zone (Woodruff et al., 2010).

Though some of She1's roles in the cell have been described, very little is known about its structure and exact function. One reason for this is that She1 may be unique to budding yeasts. Nucleotide and amino acid sequence BLAST searches have returned no significant homologs in higher eukaryotes or even the fission yeast, *Schizosachharomyces pombe*. She1 does not have any predicted secondary structures or recognizable binding motifs nor does it have any canonical modification sites.

Experimental Overview and Significance

In this thesis, I explore the role of She1 in regulating dynein through dynactin and the mechanism behind it. In addition to the mutant *she1Δ* phenotypes discussed in the introduction, we have observed the detachment of cytoplasmic MTs from the SPB. This phenotype is also dependent upon dynein activity and is a function of excess dynein pulling forces in the cell. Further study into this phenotype has revealed that cMTs detach more readily when they are anchored at the half-bridge during G1 and mating than when they are anchored at the outer plaque.

The anchorage of cMTs is crucial for their function. In the case of budding yeast, the nucleus is moved through the cytoplasm from pulling forces exerted on a single cMT. If the attachment of the cMT to the SPB is compromised, nuclear migration and spindle orientation cannot occur properly. It is of interest to find out why cMTs detach

from the SPB in *she1Δ* cells so that an understanding of proper attachment can be gained. As mentioned previously, the site of cMT attachment changes through the cell cycle. This process has not been well characterized and the rationale behind it is not understood. The cMT detachment phenotype could give insight into why the process occurs. Thirdly, the activity of dynein is restricted to a very small portion of the budding yeast cell cycle, yet dynein is found at cMT ends at all points of the vegetative cell cycle. The mechanism to restricting dynein activity to a very small window is not well understood and it seems that She1 is a part of this pathway. The data presented here helps refine the models for both dynein regulation and anchorage of cMTs while perhaps providing insight into why cMT anchorage sites change during the cell cycle.

CHAPTER TWO

Materials and Methods

Strains, plasmids, and media

Yeast strains and DNA plasmids used in this study are listed in Tables 2.1 and 2.2, respectively. Yeast rich media (YPD) and amino-acid depleted, selective media (CSM) are prepared as previously described (Sherman, 2002), the carbon source in the media was 2% glucose unless otherwise noted as either 2% raffinose or 2% galactose. Bacterial strains were cultured in LB-Miller media and were selected for presence of plasmid with either 100µg/mL ampicillin or 50µg/mL kanamycin. Yeast strains were transformed by lithium acetate.

Where noted, growth conditions for strains were changed as follows. To arrest cells in the mating phase, cells were grown in YPD to mid- to late-log phase. Cells were then diluted to $OD_{600} \approx 0.1$ in a final volume of 3mL YPD and allowed to recover for 1hr. Cells were then arrested by addition of 3.75µL of 10mM α-factor to a final concentration of 12.5µM for 3hrs. Cells over-expressing She1 from plasmids were grown to late log-phase in drop-out CSM with glucose were then spun down, washed with distilled H_2O, and resuspended in drop-out CSM made with raffinose and grown to log phase. The media of these cultures was then replaced by drop-out CSM containing galactose for 4-6hrs. Cells with pKN109 integrated were grown in CSM lacking methionine overnight. They were then diluted back to early-log phase to recover in similar media. Cells were

Table 2.1 Yeast Strains

CUY Strain	Genotype
943	*MAT*a, *ade2-101, his3, leu2-3, 112, trp1-901, ura3-52, gal4, gal80, cyh^R, URA3::GAL-LacZ, LYS2::GAL(UAS)-HIS3*
1288	*MAT*a, *ade2-101, his3-111, can1-100, trp1-1, ura3-1, leu2-3,112, DAM1::TRP1::DAM1-9MYC*
1386	*MAT*a, *ade2-101, his3-Δ200, leu2-3,112, ura3-52, STU1-13MYC::HIS5$^+$*
1865	*MAT*a, *ade2-101, his3-Δ200, leu2-3, 112, ura3-52, SHE1-13MYC::HIS3MX6*
1909	*MATα, ade2Δ, ade3Δ, his3-Δ200, leu2-Δ1, lys2-801, trp1-Δ63::FUR1-TRP1, ura3-52, ARP10-3HA::kanMX, NIP100-13MYC::kanMX*
1923	*MAT*a, *ade2, leu2, trp1, his3, ura3, ndc10-1, STU1-13MYC::kanMX*
1926	*MAT*α, *his3-Δ200, lue2-3,112, lys2-801, trp1-1, ura3-52, NDC10-13MYC::kanMX*
1927	*MAT*a, *ade2, leu2, trp1, his3, ura3, ndc10-1-13MYC::kanMX*
1930	*MAT*a, *his3Δ0, leu2Δ0, met15Δ0, ura3Δ0, dyn1Δ::kanMX, P_{TUB1}-GFP-TUB1::LEU2*
1933	*MAT*α, *ade2Δ, his3-Δ200, leu2Δ, ura3-52, LDB18-13MYC::HIS5+, NIP100-3HA::kanMX*
1936	*MAT*a, *ade2Δ, his3, leu2, lys2-801, met15Δ0, JNM1-3HA::kanMX, ARP1-13MYC::kanMX*
1938	*MAT*α, *his3, leu2, lys2-801, met15Δ0, ura3, JNM1-3HA::kanMX, NIP100-13MYC::kanMX*
1972	*MAT*a, *his3-Δ200, leu2-3, 112, lys2-801, ura3-52, P_{HIS3}-mCherry-TUB1::URA3*
1990	*MAT*a, *his3Δ1, leu2Δ0, ura3Δ0, met15Δ0, arp1Δ::kanMX, P_{TUB1}-GFP-TUB1::URA3*
1991	*MAT*a, *his3Δ1, leu2Δ0, ura3Δ0, met15Δ0, nip100Δ::kanMX, P_{TUB1}-GFP-TUB1::URA3*
1994	*MAT*a, *his3Δ1, leu2Δ0, ura3Δ0, met15Δ0, urm1Δ::kanMX*
1995	*MAT*a, *his3Δ1, leu2Δ0, ura3Δ0, met15Δ0, uba4Δ::kanMX*
1996	*MAT*α, *ade2-101, his3-Δ200, leu2-3,112, ura3-52, trp1-Δ63, SHE1-13MYC::HIS5$^+$, SPC97-3HA::TRP1*
1999	*MAT*a, *ade2-101, his3-Δ200, leu2-3,112, ura3-52, SHE1-13MYC::HIS5$^+$, TUB4-3HA::kanMX*

2008	*MAT*a, *kar1-Δ15, ade2-101, his3-Δ200, leu2Δ1, lys2-801, trp1-Δ63, ura3-52, P_{TUB1}-GFP-TUB1::URA3*
2009	*MAT*a, *kar1-Δ15, ade2-101, his3-Δ200, leu2Δ1, lys2-801, trp1-Δ63, ura3-52, P_{TUB1}-GFP-TUB1::URA3, she1Δ::HIS5+*
2010	*MAT*a, *ade2-101, his3-Δ200, leu2Δ1, lys2-801, trp1-Δ63, ura3-52, $SPC72^{1-276}$-$KAR1^{192-433}$::LEU2, kar1Δ::HIS3, spc72Δ::kanMX, P_{TUB1}-GFP-TUB1::URA3*
2011	*MAT*a, *ade2-101, his3-Δ200, leu2Δ1, lys2-801, trp1-Δ63, ura3-52, $SPC72^{1-276}$-$KAR1^{192-433}$::LEU2, kar1Δ::HIS3, spc72Δ::kanMX, she1Δ::TRP1, P_{TUB1}-GFP-TUB1::URA3*
2015	*MAT*a, *his3-Δ200, leu2-3, 112, lys2-801, trp1-1, ura3-52, P_{TUB1}-GFP-TUB1::URA3*
2016	*MAT*a, *his3-Δ200, leu2-3, 112, lys2-801, trp1-1, ura3-52, P_{TUB1}-GFP-TUB1::URA3, she1Δ::$HIS5^{+}$*
2017	*MAT*a, *his3Δ1, leu2Δ0, ura3Δ0, met15Δ0, nip100Δ::kanMX, P_{TUB1}-GFP-TUB1::URA3, she1 Δ::$HIS5^{+}$*
2018	*MAT*α, *his3- Δ200, leu2-3, 112, lys2-801, trp1-1, ura3-52, P_{TUB1}-GFP-TUB1::URA3, P_{MET3}-3HA-CDC20::TRP1*
2019	*MAT*α, *his3- Δ200, leu2-3, 112, lys2-801, trp1-1, ura3-52, P_{TUB1}-GFP-TUB1::URA3, P_{MET3}-3HA-CDC20::TRP1, she1Δ::HIS5+*
2020	*MAT*a, *kar1-Δ15, ade2-101, his3-Δ200, leu2Δ1, lys2-801, trp1-Δ63, ura3-52, P_{TUB1}-GFP-TUB1::URA3, P_{MET3}-3HA-CDC20::TRP1*
2021	*MAT*a, *kar1-Δ15, ade2-101, his3-Δ200, leu2Δ1, lys2-801, trp1-Δ63, ura3-52, P_{TUB1}-GFP-TUB1::URA3, she1Δ::HIS5+, P_{MET3}-3HA-CDC20::TRP1*
2022	*MAT*a, *ade2-101, his3-Δ200, leu2Δ1, lys2-801, trp1-Δ63, ura3-52, P_{SPC72}-$SPC72^{1-276}$-$CNM67^{1-581}$::URA3, spc72Δ::HIS5+, P_{TUB1}-GFP-TUB1::LEU2*
2023	*MAT*a, *ade2-101, his3-Δ200, leu2Δ1, lys2-801, trp1-Δ63, ura3-52, P_{SPC72}-$SPC72^{1-276}$-$CNM67^{1-581}$::URA3, spc72Δ::HIS5+, P_{TUB1}-GFP-TUB1::LEU2, she1Δ::kanMX*
2024	*MAT*a, *ade2-101, his3-Δ200, leu2Δ1, lys2-801, trp1-Δ63, ura3-52, P_{SPC72}-$SPC72^{1-276}$-$CNM67^{1-581}$::URA3, spc72Δ::HIS5+, P_{TUB1}-GFP-TUB1::LEU2, P_{MET3}-3HA-CDC20::TRP1*
2025	*MAT*a, *ade2-101, his3-Δ200, leu2Δ1, lys2-801, trp1-Δ63, ura3-52, $SPC72^{1-276}$-$KAR1^{192-433}$::LEU2, kar1Δ::HIS3, spc72Δ::kanMX, P_{TUB1}-GFP-TUB1::URA3, P_{MET3}-3HA-CDC20::TRP1*
2027	*MAT*a, *his3-Δ200, leu2-3, 112, lys2-801, trp1-1, ura3-52, P_{TUB1}-GFP-*

	TUB1::URA3, she1Δ::HIS5^{+}*, kar3Δ::TRP1*
2028	*MAT*a, *ade2-101, his3-Δ200, lys2-801, ura3-52, she1Δ::kanMX, GFP-TUB4::HISMX6,* P_{HIS3}*-mCherry-TUB1::URA3*
2030	*MAT*a, *ade2-101, his3-Δ200, leu2Δ1, lys2-801, trp1-Δ63, ura3-52,*P_{SPC72}*-SPC72*$^{1-276}$*-CNM67*$^{1-581}$*::URA3, spc72Δ::HIS5+, she1Δ::kanMX,* P_{TUB1}*-GFP-TUB1::LEU2,* P_{MET3}*-3HA-CDC20::TRP1*
2033	*MAT*a, *his3-Δ200, leu2-3, 112, trp1-1, ura3-52, nip100Δ::kanMX,* P_{TUB1}*-GFP-TUB1::URA3,* P_{MET3}*-3HA-CDC20::TRP1*
2034	*MAT*a, *his3-Δ200, leu2-3, 112, trp1-1, ura3-52, nip100Δ::kanMX, she1Δ::HIS5*$^{+}$*,* P_{TUB1}*-GFP-TUB1::URA3,* P_{MET3}*-3HA-CDC20::TRP1*
2035	*MAT*a, *ade2-101, his3-Δ200, leu2Δ1, lys2-801, trp1-Δ63, ura3-52, SPC72*$^{1-276}$*-KAR1*$^{192-433}$*::LEU2, kar1Δ::HIS3, spc72Δ::NAT*^{R}*, she1Δ::kanMX,* P_{TUB1}*-GFP-TUB1::URA3,* P_{MET3}*-3HA-CDC20::TRP1*
2037	*MAT*a*, his3-Δ200, leu2-3, 112, lys2-801, ura3-52, she1Δ::HIS5*$^{+}$*, SPC72-GFP::kanMX,* P_{HIS3}*-mCherry-TUB1::URA3*
2039	*MAT*a*, his3-Δ200, leu2-3, 112, lys2-801, ura3-52, she1Δ::kanMX, SPC97-GFP:: HIS5*$^{+}$*,* P_{HIS3}*-mCherry-TUB1::URA3*
2040	*MAT*α, *his3-Δ200, leu2-3, 112, lys2-801, trp1-Δ63, ura3-52, DYN1-3GFP::TRP1,* P_{HIS3}*-mCherry-TUB1::URA3*
2041	*MAT*a, *ade2-101, his3-Δ200, leu2-3, 112, trp1-1, ura3-52, STU2-3GFP::TRP1,* P_{HIS3}*-mCherry-TUB1::URA3*
2045	*MAT*a, *his3Δ1, leu2Δ0, ura3Δ0, met15Δ0, cnm67Δ::kanMX,* P_{TUB1}*-GFP-TUB1::LEU2*
2046	*MAT*a, *his3Δ1, leu2Δ0, ura3Δ0, met15Δ0, cnm67Δ::kanMX, she1Δ::HIS5*$^{+}$*,* P_{TUB1}*-GFP-TUB1::URA3*
2055	*MAT*α, *his3-Δ200, leu2-3, 112, lys2-801, ura3-52, NIP100-GFP::HIS5*$^{+}$*,* P_{HIS3}*-mCherry-TUB1::URA3*
2056	*MAT*α, *his3-Δ200, leu2-3, 112, lys2-801, ura3-52, ARP1-GFP::HIS5*$^{+}$*,* P_{HIS3}*-mCherry-TUB1::URA3*
2057	*MAT*α, *his3-Δ200, leu2-3, 112, lys2-801, ura3-52, JNM1-GFP::HIS5*$^{+}$*,* P_{HIS3}*-mCherry-TUB1::URA3*
2062	*MAT*a, *kar1-Δ15, ade2-101, his3-Δ200, leu2Δ1, lys2-801, trp1-Δ63, ura3-52, nip100Δ::kanMX,* P_{TUB1}*-GFP-TUB1::URA3*
2063	*MAT*a, *kar1-Δ15, ade2-101, his3-Δ200, leu2Δ1, lys2-801, trp1-Δ63, ura3-52, nip100Δ::kanMX, she1Δ::HIS5+,* P_{TUB1}*-GFP-TUB1::URA3*
2064	*MAT*a, *kar1-Δ15, ade2-101, his3-Δ200, leu2Δ1, lys2-801, trp1-Δ63, ura3-52, nip100Δ::kanMX,* P_{TUB1}*-GFP-TUB1::URA3,* P_{MET3}*-3HA-CDC20::TRP1*
2065	*MAT*a, *kar1-Δ15, ade2-101, his3-Δ200, leu2Δ1, lys2-801, trp1-Δ63, ura3-52, nip100Δ::kanMX, she1Δ::HIS5+,* P_{TUB1}*-GFP-TUB1::URA3,* P_{MET3}*-3HA-CDC20::TRP1*

Table 2.2 Plasmids

CUB Plasmid	Markers
369	Amp^R, 2µ, TRP1, P_{ADH}-GAL4BD
370	Amp^R, 2µ, LEU2, P_{ADH}-GAL4AD
371	Amp^R, 2µ, LEU2, P_{ADH}-GAL4AD-SNF4
372	Amp^R, 2µ, TRP1, P_{ADH}-GAL4BD-SNF1
657	Amp^R, URA3, P_{TUB1}-GFP-TUB1
1210	Amp^R, HIS3, P_{TUB1}-GFP-TUB1
1213	Amp^R, URA3, GAL1/10-SHE1-GFP
1214	Amp^R, 2µ, LEU2, P_{ADH}-GAL4AD-SHE1
1215	Kan^R, GST-TEV-SHE1
1226	Amp^R, URA3, GAL1/10-SHE1
1227	Amp^R, LEU2, P_{TUB1}-GFP-TUB1
1255	Amp^R, URA3, P_{HIS3}-mCherry-TUB1
1263	Amp^R, HIS3, GAL1/10-SHE1-GFP
1264	Amp^R, 2µ, LEU2, P_{ADH}-GAL4AD-SPC98
1265	Amp^R, 2µ, LEU2, P_{ADH}-GAL4AD-SPC98 (1-361)
1266	Amp^R, 2µ, TRP1, P_{ADH}-GAL4BD-TUB4
1267	Amp^R, 2µ, LEU2, P_{ADH}-GAL4AD-TUB4
1268	Amp^R, 2µ, LEU2, P_{ADH}-GAL4AD-SPC97
1269	Amp^R, 2µ, TRP1, P_{ADH}-GAL4BD-SPC98
1270	Amp^R, 2µ, LEU2, P_{ADH}-GAL4AD-SPC97 (1-548)
1271	Amp^R, 2µ, TRP1, P_{ADH}-GAL4BD-SPC98
1272	Amp^R, P_{MET3}-3HA-CDC20-TRP1
1288	Amp^R, URA3, GAL1/10-SHE1-13MYC
1293	Amp^R, LEU2, GAL1/10-SHE1
1299	Amp^R, HIS3, GAL1/10-SHE1-13MYC
1305	Amp^R, 2µ, TRP1, P_{ADH}-GAL4BD-SHE1

then arrested in metaphase by adding methionine to a final concentration of 20µg/mL for 3hrs.

Synthetic Genetic Array

The SGA analysis was performed in the lab of Dr. Charlie Boone at the University of Toronto as previously described by Tong and colleagues (Tong et al., 2001). In summary, the query strain containing the temperature-sensitive allele *stu2-12* (CUY 1570) was mated to the yeast genome deletion collection. Diploids were sporulated on plates selecting for haploids containing both *stu2-12* and a deletion of a non-essential ORF. Growth at permissive temperature indicated no genetic interaction. Strains that exhibited slow or no growth were presumed to have a synthetic lethal interaction. These strains were confirmed by manual tetrad analysis of individual matings by Xue Xia.

Fluorescence Microscopy

Strains to be analyzed with fluorescent light microscopy were first screened for the presence of tagged proteins using wide-field fluorescence. Cells were grown to mid-log phase in CSM, concentrated by centrifugation, and 5µL were spotted onto a glass slide. Cells were visualized using a Zeiss Axioplan2 imaging microscope with a 100× 1.40NA Plan-APOCHROMAT objective and a Photometrics Cool SNAPfx CCD camera controlled by Micromanager software (ImageJ).

For time-lapse and static imaging of live cells a spinning-disc confocal imaging system was used. Cells were grown as specified, concentrated, and placed onto a 1.7% agarose-CSM pad slides and sealed under a cover slip with VALAP. Pads were made by mixing equal volumes 3.4% agarose with 2× synthetic, non-fluorescent media. Time-lapse studies were obtained by a spinning-disc confocal imaging system (PerkinElmer) equipped with a microscope (TE2000; Nikon), a 100× plan-Apo NA 1.4 objective, camera (Orca ER; Hamamatsu), and UltraVIEW software (PerkinElmer) using 2 × 2 binning. For time-lapse studies, confocal slices were taken every 0.7µm. Static images were taken with 0.5µm between z-planes. Images were stacked to max z-projections and pseudo-colored (when using multiple channels) using Volocity demo software (PerkinElmer). Analysis was then performed using ImageJ (NIH).

Analysis of Microscopy

The detachment of cytoplasmic MTs from the SPB was quantified by taking time-lapse movies as described above for 10min and taking a z-series every 10sec. Max-projection images were then examined for MTs that were attached at the SPB and detached into the cytoplasm within this 10min window. The frequency of detachment was then taken as a fraction of these detaching MTs against the total number of attached MTs at the beginning of the movie. Some strains exhibited MTs in the cytoplasm that were not attached at the beginning of the movie and persisted throughout the observation time. These MTs were not included as detaching MTs and were put into a “free MTs” category. The frequency for microtubule detachment was calculated using a Poisson distribution model.

Cells over-expressing She1 were scored in two different assays. Firstly, GFP-Tub1-labeled cells with an anaphase spindle between 3 and 6µm were scored as mis-oriented spindles if the spindle had failed to enter the daughter cell. The second assay examined localization of GFP-labeled dynactin subunits in cells containing the She1 over-expression plasmid that were grown in either glucose, mimicking the WT condition, or in galactose. Cells with spindles were put into three categories, if the GFP signal was found at only the SPB, only the plus-end of a cytoplasmic MT, or if signal was found at both locations simultaneously.

GST-She1 Purification from *E. coli*

Plasmid pCU1215 was transformed in to BL21 bacterial expression cells. Bacteria were grown at 26º in 1L LB broth containing kanamycin until OD600≈ 0.5 and then induced with 20mM IPTG for 4hrs. Cells were then spun down and washed with cold PBS. Cells were resuspended in 8.5mL cold PBS and one Complete EDTA-free protease inhibitor tablet (Roche) and moved to a 50mL conical tube. 10µL of 100mg/mL lysozyme was added to the cells on ice for 30min. Cells were lysed using sonication. Triton X-100 was added to 1% to the lysate and the mixture was rocked at 4º for 20min. Cell debris was pelleted at 12,000rpm for 25min at 4^{o} in a Sorvall RC5. Supernatant was then incubated with PBS-equilibrated glutathione-sepharose for 2.5hrs at 4º. Beads were then pelleted by low-speed centrifugation and washed 4X with cold PBS. Beads were then concentrated and resuspended in 350µL 80mM reduced glutathione in

PBS (pH 7) and rocked O/N at 4º. Purified GST-She1 was then eluted by adding mixture to a Mini Chromotography column (BioRad) and spinning at 7500rpm for 2min.

Microtubule Co-Sedimentation Assay

For assays with whole cell extracts, log phase yeast cells (CUY1865 She1-13Myc) (OD_{600}=0.75-1.0) were centrifuged for 5min at 2,000rpm, washed once in water, and once in lysis buffer (80mM PIPES, 1mM EGTA, 1mM $MgSO_4$, 5% glycerol, 100 mM KCl, 0.25% Brij-35, 2mM DTT pH 6.8 with KOH). Final pellet was resuspended in lysis buffer plus 20µM taxol, 1mM PMSF, 10µg/ml Leupeptin, 10µg/ml Pepstatin. Cells were homogenized in bead beater for two minutes, followed by a rest of one minute, and then an additional two minutes. Lysates were pre-cleared by centrifugation at 100,000rpm in TLA100.3 for five minutes at 4º. Tubulin (Cytoskeleton) was diluted to 1mg/ml in PEM-DGT (100mM PIPES, 2mM EGTA, 1mM $MgCl_2$ with 20µM taxol, 1mM GTP, and 4mM DTT) and pre-cleared by centrifugation in a TLA100.3 rotor at 4º for five minutes at 65,000rpm. Supernatant was incubated at 37° for 20min to allow microtubule polymerization, followed by centrifugation at room temperature in a TLA100.3 rotor at 32,000rpm for 20min. Microtubules in the pellet were resuspended in PEM-DGT to a final concentration of 5mg/ml. Dilutions of microtubules were added to 20µl of pre-cleared cellular lysate and incubated on ice for 20min. Samples were centrifuged 10min at 70,000rpm in TLA100.3 at 4º. SDS-PAGE loading buffer was added to supernatant. Pellet was resuspended in PEM+DGT prior to addition of SDS-PAGE loading buffer. Following SDS-PAGE electrophoresis, She1-13myc and tubulin were

detected by immunoblot with anti-Myc (9E10, Covance) and anti-tubulin (DM1α, Sigma) antibodies.

Assays with purified GST-She1 were similar. Purified tubulin from porcine brains were used (Blake-Hodek et al., 2010) instead of tubulin from Cytoskeleton. Prior to mixing with assembled MTs, GST-She1 was spun at 65,000rpm at 4º for 12min to clear insoluble material. The assay buffer was 80mM PIPES, not 100mM. Once 10µL of pre-cleared GST-She1 was mixed with assembled MTs at room temperature for 5min, they were spun at 70,000rpm for 40min at 25º. The contents of the supernatant and pellet were analyzed by Western blot, as with whole-cell extract, with anti-GST used to detect She1 instead of anti-myc.

Yeast Protein Extracts and Western Blots

Yeast strains were grown as described above in 50-100mL cultures until mid-log phase. Cells were then collected by centrifugation at 2,000rpm in a Beckman swinging-bucket table-top centrifuge, washed with H_2O, and a second wash in breakage buffer (30mM $NaPO_4$, 60mM β-glycerphosphate, 150mM KCl, 6mM EGTA, 6mM EDTA, 10% glycerol). Cells were spun and resuspended in a minimum volume of breakage buffer. Protease inhibitors were added (5µL 100mM PMSF, 1.5µL 10mg/mL Pepstatin, and 1.5µL 10mg/mL Leupeptin) and the mixture was frozen in liquid nitrogen drop by drop. Frozen cells were stored at -80º until the liquid nitrogen boiled away. Cells were then ground by mortar and pestle and collected in a microfuge tube. Lysates were cleared of

cell debris by spinning at top speed for 20min at 4º. The supernatant was then transferred to a new tube for a second spin for 10min. Protein extract was moved to a new tube and assayed for protein concentration by Bradford Assay.

To examine protein contents of whole cell extracts, 50µg of lysate was loaded per lane into a 10% SDS-PAGE. Once lysates had migrated through the gel matrix; the gel, filter paper, and nitrocellulose membrane were equilibrated in wet transfer buffer (48mM Tris, 39mM glycine, 20% methanol) for 20min. A Bio-Rad Trans-Blot Cell was used to transfer proteins onto the nitrocellulose membrane at 100mA overnight. Membranes were then blocked with 5% non-fat dry milk (NFDM) in TBS-T (20mM Tris, 0.1% Tween-20, 137mM NaCl, pH 7.6) for 1hr. Blocked membranes were probed for proteins in a variety of ways, but typically a 1:1,000 dilution of myc-antibody (9E10; Covance) or 1:500 dilution of HA-antibody (HA.11; Covance) in 5% NFDM TBS-T was replaced the blocking solution for 2hrs. Membranes were washed 3 times with TBS-T for 10min. Secondary antibody, either a 1:5,000 dilution of anti-Mouse (BioRad) or 1:12,500 dilution of light-chain specific anti-Mouse (Jackson ImmunoResearch) in 5% NFDM TBS-T was then added for 1hr. Membranes were again washed 3 times with TBS-T for 10min. Tagged-proteins were visualized by adding 250µL of standard ECL reagents (Pierce) or Dura ECL reagents (Thermo) and exposing to film.

Co-Immunoprecipitations

Protein extracts for Co-IPs were prepared as detailed above, except for cells over-expressing She1. 20mL starter cultures of strains containing She1-GFP over-expression plasmids were grown to late-log phase. These were spun down and washed with 10mL of distilled H_2O and resuspended in 10mL CSM with raffinose. These were then split into two 100mL CSM-raffinose cultures and grown at 30º for 36-48hrs until they reached mid-log phase. These cultures were then spun down and the media was replaced with either CSM-glucose or CSM-galactose and grown for an additional 6hrs. These cells were then collected and extracts were prepared as described above.

Co-immunoprecipitations were mixed as described by Wolyniak and colleagues (Wolyniak et al., 2006). For CoIPs of the dynactin complex, 50µL of myc or HA affinity resin (Sigma) was used to precipitate epitope-tagged proteins from lysates. Western blots were probed with either anti-myc (9E10, Covance) or anti-HA (HA.11, Covance) and followed with an anti-mouse secondary antibody (BioRad) or a light-chain specific anti-mouse secondary antibody, both of which were conjugated to HRP.

Yeast Two-Hybrid Assays

Yeast two-hybrid assays were performed as described by Wolyniak and colleagues (Wolyniak et al., 2006). Plasmids used are designated in Table 2.2. Vectors containing *SPC97*, *SPC98*, and *TUB4* were gifts from T. Davis. The She1-AD plasmid

(pCU1214) was constructed by Xue Xia and the *SHE1-BD* (pCU1305) construct was made by Alex Amaro. Control plasmids that were either empty (pCU369 and 370) or had known interactors (pCU371 and 372; *SNF1/SNF4*) were obtained from S. Elledge. Plasmids were transformed into the Y190 yeast strain (CUY943). For strains that used a plasmid containing *SHE1*, that plasmid was transformed in second to alleviate the slow growth phenotype associated with over-expressing *SHE1*. Interaction of query genes was assayed by either examining β-galactosidase activity on a filter assay and scoring for blue color or by complementation of auxotrophy on CSM-Leu-Trp-His+3-AT plates.

Chromatin Immunoprecipitation

Strains were grown in 50mL of YPD to mid-log phase. Cells were then fixed by adding formaldehyde to a final concentration of 1.25% for 20min. The fixation reaction was quenched by addition of 0.5g of glycine for 5min. Fixed cells were then collected by centrifugation at 2,000rpm for 5min and washed twice with 25mL cold TBS. Cell pellets were resuspended in 0.45mL of lysis buffer (50mM HEPES, 1mM EDTA, 140mM NaCl, 1% Triton X-100, 0.1% NaDOC, 10µg/mL Leupeptin, 10µg/mL Pepstatin, 0.5mM PMSF) with 0,5mL of glass beads added. Lysates were then generated by subjecting cells to continuous vortexing for 1hr at 4º. To separate liquid from beads, a small-gauge needle was heated and used to lance a small hole in the bottom of the tube containing the lysate. This was then inserted into a 15mL conical tube and spun at 384×*g* for 1min at 4º. Pelleted material was resuspended and the mixture was divide into two equal

volumes kept on ice. DNA was then sheared by sonication in a Diagenode Bioruptor set on High with 30sec pulses and 1.5min rests for a total of 15min. Cell debris was cleared from lysates by spinning at top speed for 15min at 4º. Supernatants were pooled into one tube. Antibody was then added to 350µL of lysate and incubated on an inverter for 2hrs at 4º. 40µL of Protein-G-Sepharose beads equilibrated in lysis buffer and blocked with 2µg of sheared λ DNA was then added to the reaction and incubated at 4º for 1hr. Beads were then collected by low-speed centrifugation and put through a series of 1mL 5 minute washes: 4 times with lysis buffer, one wash of high-salt lysis buffer (50mM HEPES, 1mM EDTA, 750mM NaCl, 1% Triton X-100, 0.1% NaDOC, 10µg/mL Leupeptin, 10µg/mL Pepstatin, 0.5mM PMSF), one wash in Wash buffer (10mM Tris, 1mM EDTA, 0.25M LiCl, 1% NP-40, 0.5% NaDOC), and 2 washes in 1X TE (10mM Tris, 1mM EDTA). Protein-DNA complex was eluted from the beads by adding 100µL of elution buffer (50mM Tris, 10mM EDTA, 1% SDS) to the beads and incubated at 65º for 15min. Beads were spun and the supernatant moved to a new tube. Further elution was performed by adding 150µL elution buffer plus 0.67% SDS and incubating at 65º for an additional 10min. This supernatant was combined with the previous one and cross-linking of DNA to protein was reversed by incubating at 65º overnight. Protein was removed from samples by digestion by addition of 250µL of 5mg/mL Proteinase K in TE and incubated at 42º for 2hrs. Extraction of DNA was performed by addition of 55µL of 4M LiCl and 500µL of Phenol/Chloroform and mixed for 1 min. The mixture was then centrifuged for 10min at top speed to separate phases. DNA was further extracted by moving the top layer to a new tube and adding 500µL of chloroform, mixed, and centrifuged for 10min at top speed. DNA was pelleted by

addition of 40µg of glycogen and 1mL 100% ethanol, incubated at -20º for 15min, and spun at top speed for 10min. The pellet was washed with 1mL 75% ethanol and spun again. After drying the pellet, DNA was resuspended in 50µL TE. DNA content was then analyzed by amplifying either the CEN locus or a non-target locus. Samples were compared to 1:10 dilutions of input DNA.

CHAPTER THREE

Results

Detachment of cMT from the SPB in *she1*Δ Mutants

SHE1 (YBL031w) was identified in a synthetic genetic array (SGA) screen looking for gene deletions that are lethal in combination with the temperature-sensitive *stu2-12* allele performed by the Boone lab at the University of Toronto. She1 was of interest because it had previously been shown to localize to microtubules in yeast cells (Huh et al., 2003). She1's function was first characterized by Xue Xia by examining MT morphology and behavior in *she1*Δ cells expressing GFP-Tub1. She found that the loss of She1 did not produce any change in the length or number of cytoplasmic microtubules, and it did not affect the assembly or elongation of mitotic spindles. In addition, loss of She1 did not significantly alter the dynamics of cytoplasmic microtubules. However, using time-lapse microscopy, I observed dramatic movements of spindles around the cell; metaphase spindles moved back and forth between the mother cell and bud, and anaphase spindles were bent to such extremes that they often broke. These spindle movements in *she1*Δ cells were previously described by Woodruff and colleagues (2009) and attributed to inappropriate dynein activity.

Xue and I also noticed that cytoplasmic microtubules in *she1*Δ cells frequently released from their anchor point at the SPB and moved freely around the cell periphery before depolymerizing (Figure 3.1A). Similar cytoplasmic microtubule detachment from the SPB has previously been observed in cells containing mutations that affect the integrity of the SPB outer plaque, such as *cnm67Δ* or $SPC72^{stu2\Delta}$

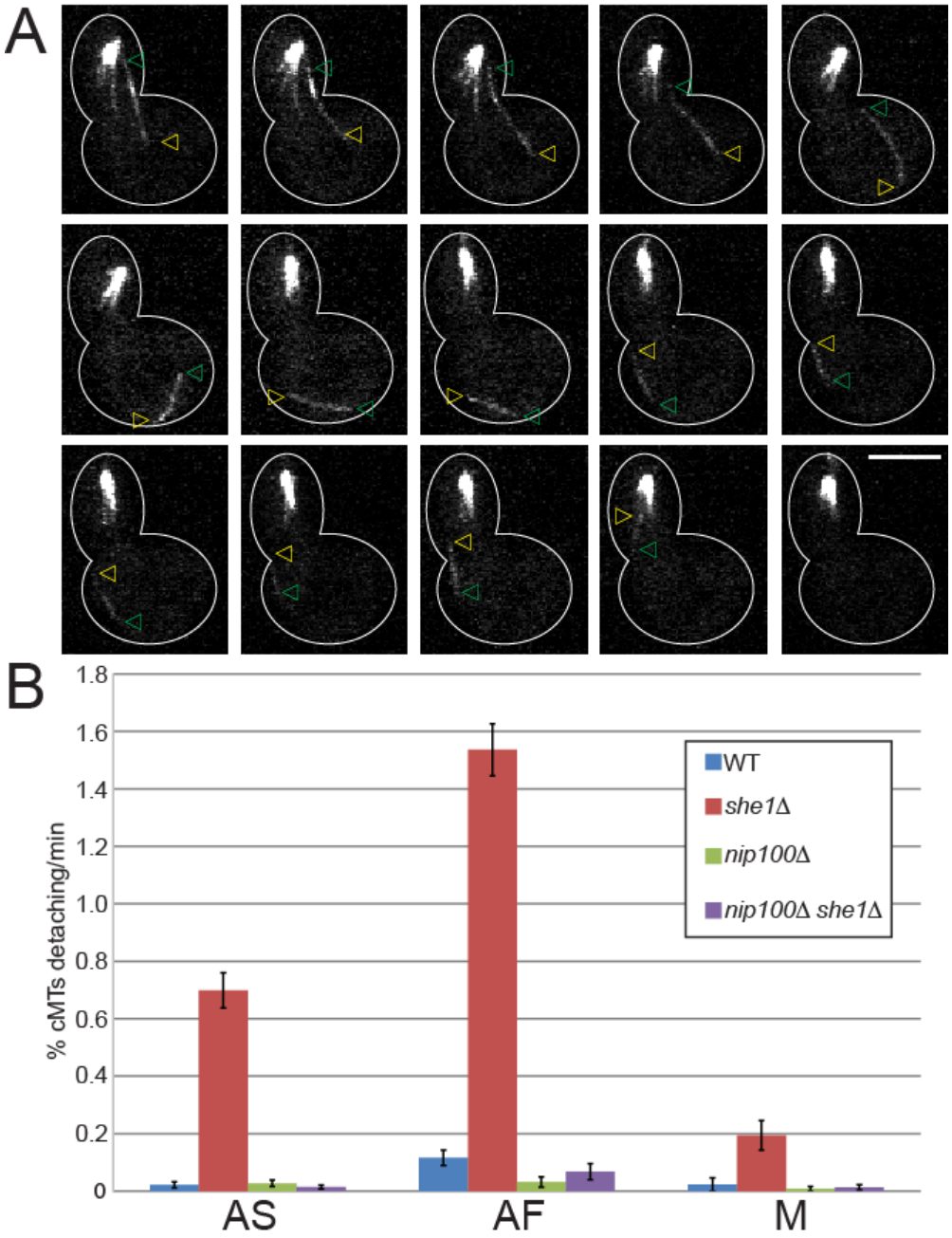

Figure 3.1 Cytoplasmic MTs Detach from the SPB in *she1Δ* Mutants. (A) Time-lapse of *she1Δ* cell arrested in α-factor. The yellow arrowhead points to the minus-end and the green arrowhead points to the plus-end of a cMT that detaches from the SPB. Each frame advances 10sec. (B) Quantification of the rate of detachment of cMTs as a fraction of the total number of cMTs observed. AS = asynchronous, AF = α-factor arrested, M = metaphase arrested. CUY Strains: WT = 2015 and 2018, *she1Δ* = 2016 and 2019, *nip100Δ* = 1991 and 2033, *nip100Δ she1Δ* = 2017 and 2034. Error bars are standard deviations from Poisson approximation.

(Hoepfner et al., 2000; Usui et al., 2003). I quantified this effect by determining the fraction of cytoplasmic microtubules that detach from the SPB per minute. In asynchronously growing wild-type cells, only 0.02% of microtubules detach. I found that in asynchronously growing *she1*Δ cells, 0.7% of microtubules detach (Figure 3.1B).

cMT Detachment Rates Depend on the Cell Cycle and Dynein Activity

Careful observation of microtubule detachment in asynchronous cultures revealed to me that the majority of these events occurred in cells that were growing in the early portion of the cell cycle, prior to the formation of a bipolar spindle. To measure this difference, I create uniform populations of cells by arresting them in G1 by exposure to α-factor or in metaphase by depletion of Cdc20, the ubiquitin ligase of the anaphase promoting complex. As shown in Figure 3.1B, during α-factor arrest, 0.01% of microtubules detach in wild-type cells and 1.5% of microtubules detached in *she1*Δ cells. During metaphase arrest, 0.02% of microtubules detached in wild-type cells and 0.2% of microtubules detached in *she1*Δ cells. Thus, in both wild-type and *she1*Δ cells, microtubules detachment is ~5-fold more frequent in α-factor arrested cells. In both α-factor and metaphase-arrested cells, microtubule detachment is nearly 15-fold more frequent in *she1*Δ cells than in wild-type cells.

Woodruff and colleagues (2009) reported that She1 inhibits dynein activity by limiting the recruitment of dynactin to cytoplasmic microtubules ends. This result suggests that the increased microtubule detachment observed in *she1*Δ cells could be due to excessive dynein activity. To test this possibility, I measure microtubule detachment in cells lacking the dynactin complex protein, Nip100, which is essential for

dynein activity. Microtubule detachment rates in *she1*Δ *nip100*Δ cells were less than those in wild-type cells for asynchronous, α-factor-arrested, and metaphase-arrested populations (Figure 3.1B). Thus, the increased frequency of microtubule detachment in *she1*Δ cells depends on dynein activity.

Detachment Rate Depends on the site of cMT Anchorage

Why do MTs detach more readily in α-factor-treated cells than in metaphase cells? This could arise from differences in the strength of attachment of cMTs to the SPB, which are anchored at the half-bridge in α-factor-arrested cells and at the outer plaque in metaphase cells (Figure 1.2C). Alternatively, the force pulling on cMTs may differ during these two stages of the cell cycle. To distinguish between these two possibilities, I use the *kar1*-Δ*15* mutation (Vallen et al., 1992). Kar1-Δ15 lacks the portion of Kar1 that binds Spc72 and, thus, eliminates cMT nucleation from the half bridge (Figure 3.2A). In metaphase cells when cMTs nucleate from the outer plaque, the *kar1*-Δ*15* mutation should have little effect on cMT detachment, and this is what I observe for wild type and *she1*Δ cells (Figure 3.2B).

In α-factor-arrested cells when cMTs normally originate from the half-bridge, the *kar1*-Δ*15* mutation should eliminate most cMTs. In fact, I observe about half the normal number of cMTs in *kar1*-Δ*15* and *kar1*-Δ*15 she1*Δ cells. These cMTs presumably arise from the outer plaque where Spc72 can bind to Nud1. At this stage of the cell cycle, when Spc72 binding to Kar1 is favored, Spc72 binding to Nud1 is not optimal (Pereira et al., 1999). In addition to reduced cMT numbers, I observe a significant number of unattached cMTs (0.5 and 0.6 per cell in *kar1*-Δ*15* and *kar1*-Δ*15 she1*Δ cells,

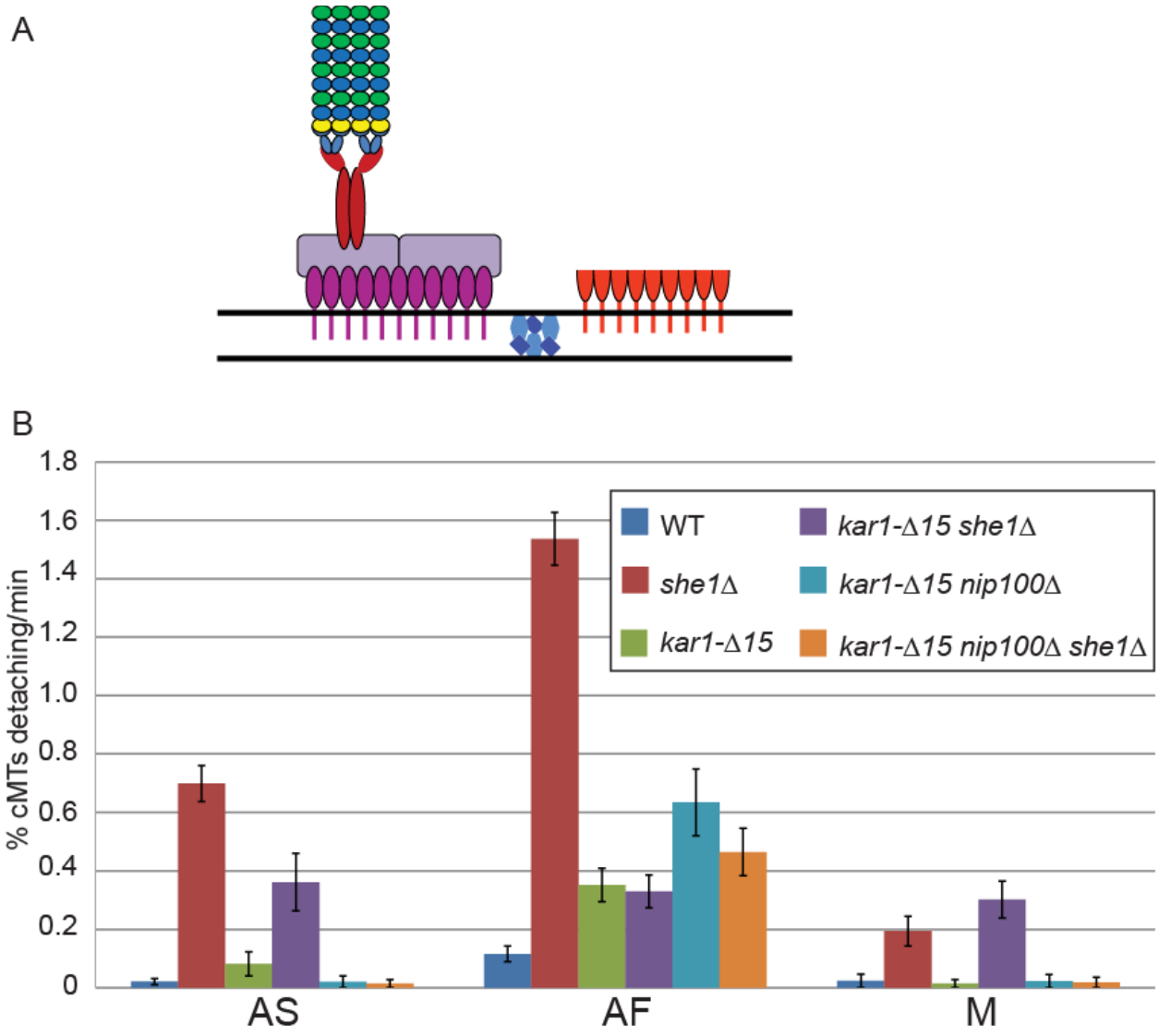

Figure 3.2 cMT Detachment Depends on Anchorage Site. (A) In *kar1-Δ15* cells, cMTs can only anchor at the outer plaque. (B) This change in anchorage reduces the rate of cMT detachment. However, a basal amount of detachment still occurs through spontaneous detachment that is not dependent upon dynein. AS = asynchronous, AF = α-factor arrested, M = metaphase arrested. CUY Strains: *kar1-Δ15* = 2008 and 2020, *kar1-Δ15 she1Δ* = 2009 and 2021, *kar1-Δ15 nip100Δ* = 2062 and 2064, *kar1-Δ15 nip100Δ she1Δ* = 2063 and 2065. Error bars are standard deviations from Poisson approximation.

respectively), most likely nucleated by cytoplasmic aggregates of Spc72 that fail to attach to the SPB (Pereira et al., 1999). The *kar1-Δ15* mutation also increased the rate of cMT release 2.7-fold above that observed in wild type cells. Although the mechanism of this increased rate of release is not known, I refer to it as spontaneous release because it does not depend on dynein activity; introducing the *nip100Δ* mutation does not lower cMT detachment in *kar1-Δ15* cells.

As shown in Figure 3.2, in *kar1-Δ15 she1Δ* cells, cMT detachment is nearly four-fold lower than in *she1Δ* cells. This rate is only slightly higher than the spontaneous release rate observed in *kar1-Δ15* cells, indicating that *she1Δ* has little effect in *kar1-Δ15* cells. cMT detachment in *kar-Δ15 she1Δ* cells is not altered by introducing *nip100Δ*, indicating that this residual release is not due to dynein activity. Thus, forcing cMTs to nucleate from the outer plaque greatly diminshes the effect of *she1Δ* on cMT detachment in α-factor-arrested cells. This result supports the argument that cMTs are attached more strongly to the outer plaque than the half-bridge.

Detachment Occurs at the γ-tubulin Ring Complex

I next set out to establish the point at which cMT detachment occurs. The first aim was to find if cMTs broke somewhere along the length of the polymer or if they were pulled intact from the SPB. If the latter were true, it would be possible that anchoring proteins from the γ-Tubulin Small Complex (γ-TuSC) or even the SPB would be on the end detaching from the SPB (the minus-end). I initially imaged *she1Δ* cells expressing mCherry-Tub1 and GFP-Tub4 following arrest in α-factor (Figure 3.3). Of the 72 cMTs

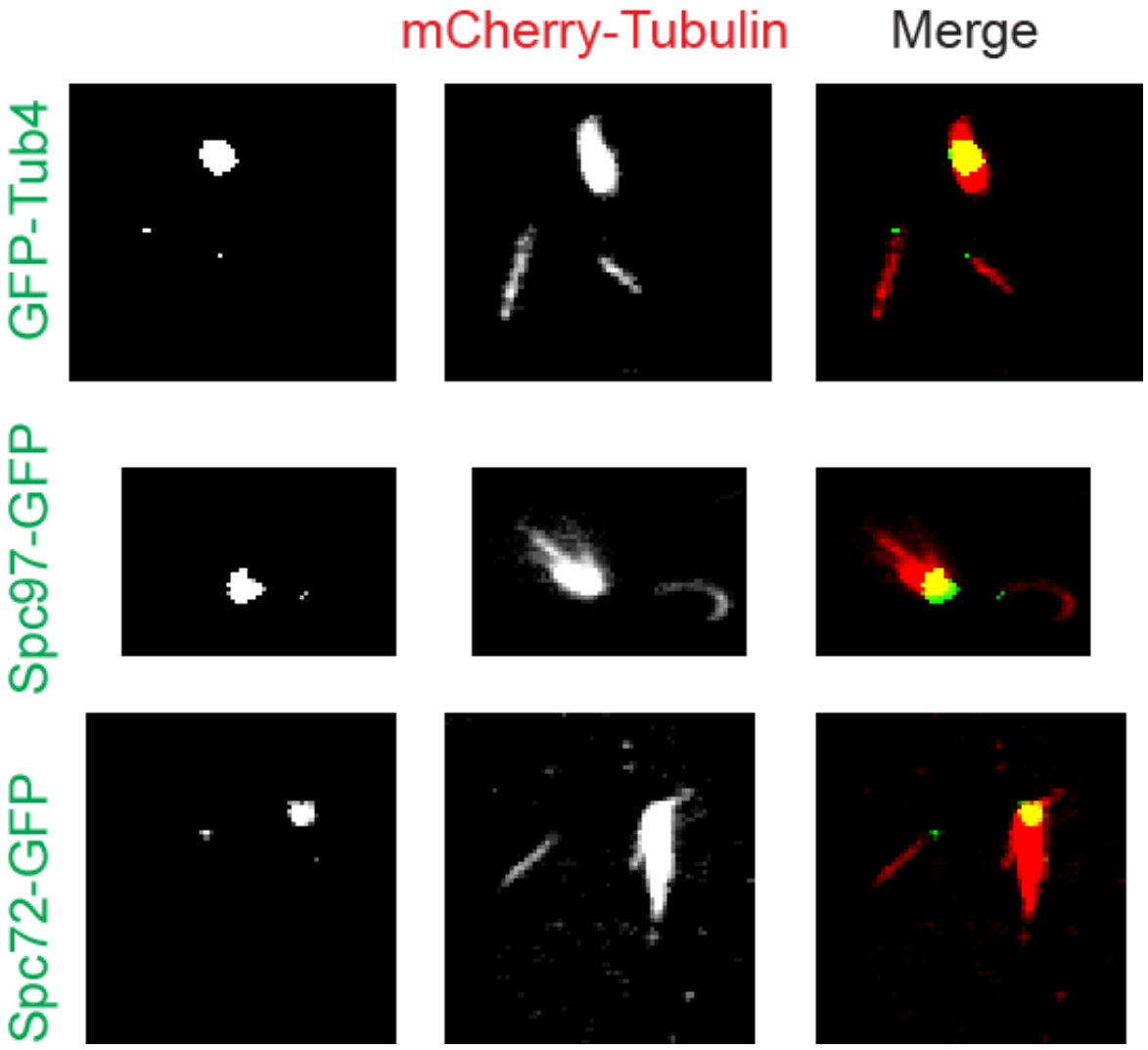

Figure 3.3 γ-TuSC Proteins on the Ends of Detached cMTs. Time-lapse fluorescence microscopy of mCherry-Tub1 *she1Δ* cells arrested in α-factor reveals cMTs detaching from the SPB have their minus-ends labeled with either GFP-Tub4 (CUY 2028), Spc97-GFP (CUY 2039), or Spc72-GFP (CUY 2037).

observed detaching from the SPB, 62 (86.1%) had GFP-Tub4 at the end detaching from the SPB. Detached cMTs existed for an average of 103±38sec if there was a GFP signal on their minus-end. I also imaged cMT detachment in *she1*Δ cells expressing mCherry-Tub1 and Spc72-GFP (Figure 3.3). Spc72-GFP was observed on the ends of 21 of 26 (81%) detached cMTs. On the other hand, I never observed Spc42 on the ends of detached cMTs in cells expressing GFP-Tub1 and Spc42-mRFP (data not shown). This result was expected since Spc42 is in the central core of the SPB. In summary, these result indicate that detached cMTs contain the γ-TuRC and Spc72 at their minus ends so that the break must occur somewhere on the SPB-proximal side of Spc72.

In budding yeast, MTs only have dynamic plus ends since their minus ends are anchored at the SPB. Treadmilling of tubulin sub-units has not been observed in *S. cerevisiae* as in flies and higher eukaryotes. Detached cMTs eventually depolymerize as they are being pulled around the cell. This could happen from the plus end of the cMT or from the minus end, now that it is free. While observing detaching cMTs in strains expressing GFP-Tub4, I found that the GFP signal would remain while the length of the cMT decreased. This indicates that the proteins remaining on the minus-ends of detached cMTs are still able to cap them and prevent tubulin subunits from dissociating from this site.

I next examined whether the break point in α-factor treated cells was between Spc72 and Kar1. $Spc72^{1-276}$-$Kar1^{192-433}$ is a fusion protein that combines the Tub4-binding portion of Spc72 and the half-bridge-binding region of Kar1. This construct was expressed in a strain lacking the native Spc72 and Kar1 proteins so that the only source

of these proteins is the fusion protein (Pereira et al., 1999). Addition of the Spc72-Kar1 fusion protein lowers the rates of cMT detachment 2.4-fold in wild-type cells and 10.6-fold in *she1*Δ cells (Fig 3.4). Because the fusion protein substantially reduces cMT detachment, I conclude that the interaction between Spc72 and Kar1 is the linkage that is normally broken during cMT release α-factor-arrested cells.

I used a second fusion protein to examine whether the break point in metaphase cells was between Spc72 and Cnm67. $Spc72^{1-276}$-$Cnm67^{1-581}$ is a fusion protein that combines the Tub4-binding region of Spc72 and the outer plaque-binding portion of Cnm67. This fusion protein by-passes the need for the SPB functions of Nud1, which normally bridges these two proteins (Gruneberg et al., 2000). Cells expressing Spc72-Cnm67 fusion lack the native Spc72 and Cnm67 loci so that the only source of cMT anchorings is through the fusion protein located in the outer plaque. The presence of the Spc72-Cnm67 fusion protein did not reduce the rate of cMT detachment; in fact, release rates rose 5.2-fold in wild-type cells and 1.3-fold in *she1*Δ cells (Figure 3.4). Thus, I cannot conclude that it is linkage between Spc72 and Cnm67 that is normally broken during cMT release in metaphase cells.

Interestingly, the Spc72-Kar1 fusion did not reduce cMT detachment rates in metaphase-arrested cells; in fact, these rates were raised 16.6-fold in wild-type and 1.8-fold in *she1Δ* cells. Thus, even the enhanced stability provided by this fusion protein at the half-bridge is still less than that provided by the normal outer plaque connection in metaphase cells. In addition, the Spc72-Cnm67 fusion reduced the rate of cMT detachment in α-factor arrested cells: 2.3-fold for wild-type cells and 8.8-fold for *she1*Δ cells. This indicates that even the weakened outer plaque connection provided by this

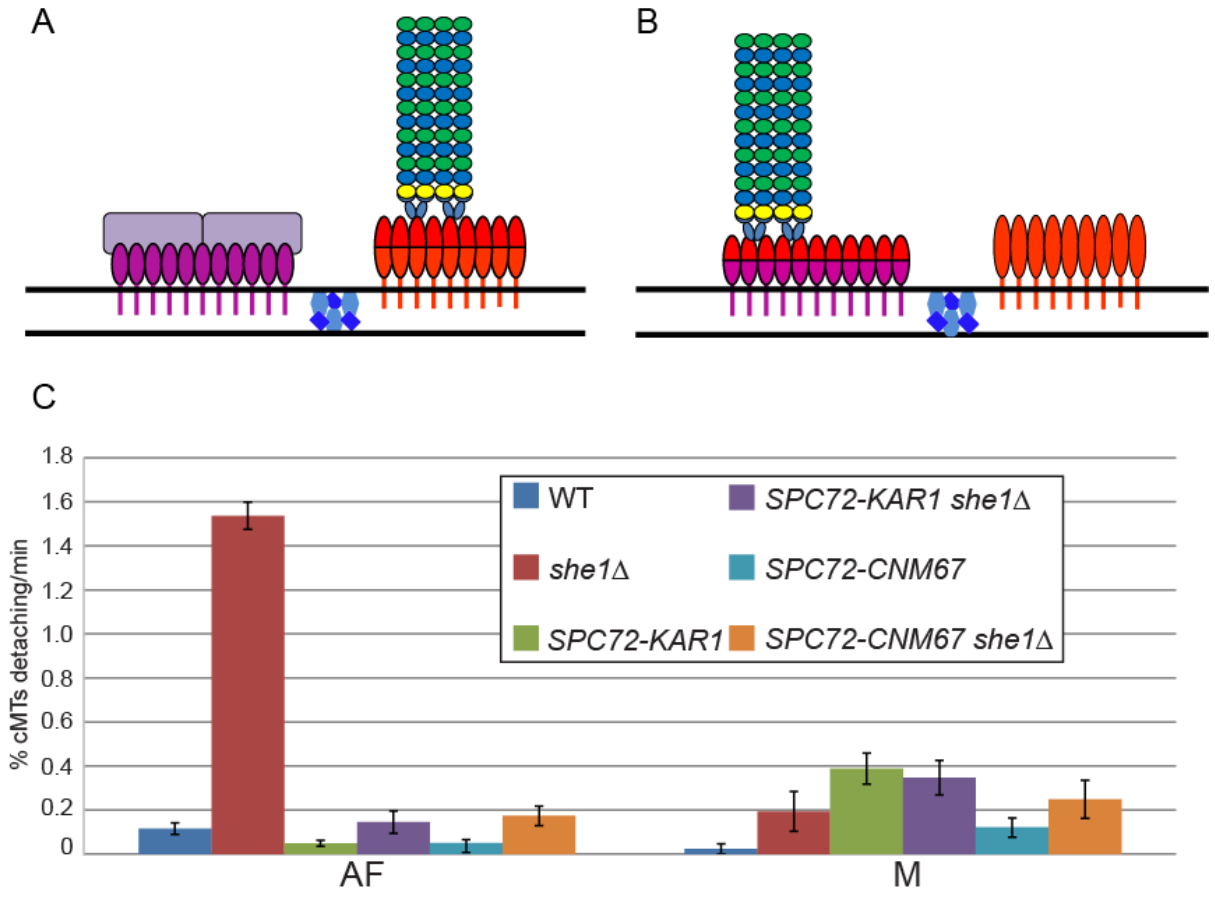

Figure 3.4 Tethering cMTs to the SPB Rescues Detachment. (A) The Spc72-Kar1 fusion protein (red and orange) can only organize cMTs at the half-bridge since the native Spc72 is deleted. (B) Similarly, the Spc72-Cnm67 fusion protein (red and purple) can only anchor cMTs to the outer plaque. Num1 is normally the binding partner of Spc72, but is no longer necessary here because of the fusion protein. (C) Quantification of the detachment rates in these strains. AS = asynchronous, AF = α-factor arrested, M = metaphase arrested. *SPC72-KAR1* = 2010 and 2025, *SPC72-KAR1 she1Δ* = 2011 and 2035, *SPC72-CNM67* = 2022 and 2024, *SPC72-CNM67 she1Δ* = 2023 and 2030. Error bars are standard deviations from Poisson approximation.

fusion protein is still stronger than the normal half-bridge connection. Both of these results support the conclusion of the previous section that the outer plaque connection is stronger than that at the half-bridge.

Over-expression of SHE1 Phenocopies Dynein Mutants

The fact that excessive cMT detachment in *she1*Δ cells depends on dynein activity suggests that She1 negatively regulates dynein activity. A hallmark of dynein pathway mutants is the elongation of anaphase spindles within the mother cell due to incorrect spindle orientation. Thus, I hypothesized that over-expression of She1 would produce this dynein phenotype. To test this, I expressed She1 from the highly efficient *GAL 1/10* promoter. Cells were imaged following a shift to galactose-containing media for four hours. I quantified mid-anaphase spindles (between 3 and 6µm) that were incorrectly oriented with both SPBs in the mother. Cells over-expressing She1 had a level of spindle mis-orientation similar to that in *dyn1Δ* and *nip100Δ* cells (Figure 3.5). Over-expressing She1 in *dyn1Δ, arp1Δ* or *nip100Δ* cells did not increase the frequency of spindle mis-orientation, indicating that She1 acts through the dynein pathway.

To investigate the mechanism of She1 inhibition of dynein activity, She1 was over-expressed in cells expressing GFP-tagged dynactin complex proteins and *mCherry-TUB1*, and cells were scored for GFP staining at MT plus ends only, the SPB only, or both. For cells expressing Nip100-GFP, Arp1-GFP, and Jnm1-GFP, She1 over-expression decreased the number of cells with cMT plus-ends labeling (9.1-fold, 7.4-fold, and 7.6 fold, respectively), and increased the number of cells with only SPB

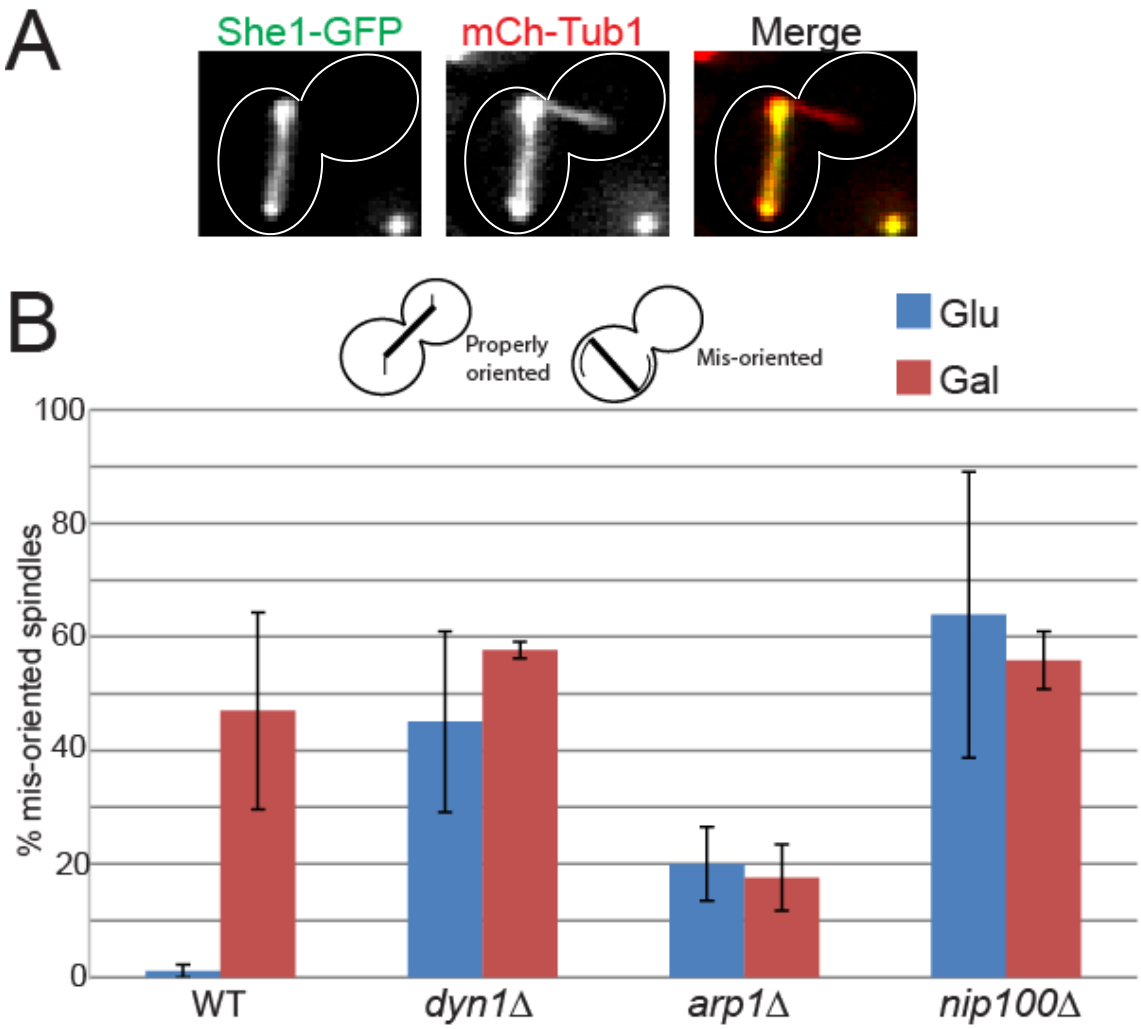

Figure 3.5 Over-expressing She1 Increases Spindle Mis-orientation in Cells. Cells with mCherry-Tub1 and a plasmid with She1-GFP under the inducible Gal promoter were grown at 30° in glucose and then shifted to galactose media for 4hrs. (A) Example of a cell that has extended its spindle within the mother cell. (B) Percent of mid-anaphase spindles that elongated within the mother cell. CUY strains + CUB plasmid: WT = 1972+1263 (n=62 for Glu, n=132 for Gal), *dyn1Δ* = 1930+1288 (n=207 for Glu, n=183 for Gal), *arp1Δ* = 1990+1299 (n=275 for Glu, n=140 for Gal), *nip100Δ* = 1991+1299 (n=512 for Glu, n=275 for Gal). Error bars are standard deviation.

staining (6.5-fold, 16.9-fold, and 4.3-fold, respectively) (Figure 3.6). The overall number of cells that displayed a GFP-signal was relatively unchanged. Over-expression of She1 did not substantially affect the localization of Dyn1-GFP. These results indicate that She1 inhibits dynein activity by preventing the proper loading of the dynactin complex onto the plus-ends of cMTs.

One possible mechanism by which She1 could inhibit dynactin loading onto MT plus-ends is by interfering with dynactin assembly. Over-expression of She1 might prevent the complete dynactin complex from assembling and correctly localizing to cMT plus-ends. The timing of the loading of the dynactin complex onto cMT plus-ends could also be due to a direct binding of She1 interacting with subunits of the dynactin complex, preventing their binding to cMTs. In the over-expression studies shown in Figure 3.7, She1-GFP was over-expressed and the interaction between dynactin complex proteins was examined by co-immunoprecipitation. Binding between Arp10-3HA and Nip100-13myc, Nip100-3HA and Ldb18-13myc, Jnm1-3HA and Arp1-13myc, and Jnm1-3HA and Nip100-13myc was not disrupted in cells over-expressing She1-GFP. In addition to these experiments, the She1-GFP content of the immunoprecipitated samples was probed by Western blot using a GFP-targeted antibody. Although bands at the predicted molecular weight for She1-GFP were found in the protein lysate inputs, no such bands were present in the Co-IP samples, corroborating the conclusion that over-expression of She1-GFP does not disturb dynactin localization through interaction with its subunits.

Figure 3.6 Over-expressing She1 Changes the Localization of Dynactin Components. Cells expressing mCherry-Tub1 and GFP-labeled dynactin and harboring a plasmid containing *GAL 1/10 SHE1* were observed after growing in glucose or switched to galactose media. (A) The localization of dynactin proteins Nip100, Arp1, and Jnm1 is normally at the SPB and cMT plus ends (white arrow). When She1-is over-expressed, Nip100, Arp1, and Jnm1 were excluded from the plus-ends (yellow arrows). However, dynein's localization did not change with over-expression of She1. Scale bar in upper corner of merged images is 5µm. CUY strain + CUB plasmid used: Nip100-GFP = 2055+1293, Arp1-GFP = 2056+1293, Jnm1-GFP = 2057+1293, Dyn1-GFP = 2040+1299. (B) This change in localization was quantified and compared against the localization of dynein in similar conditions.

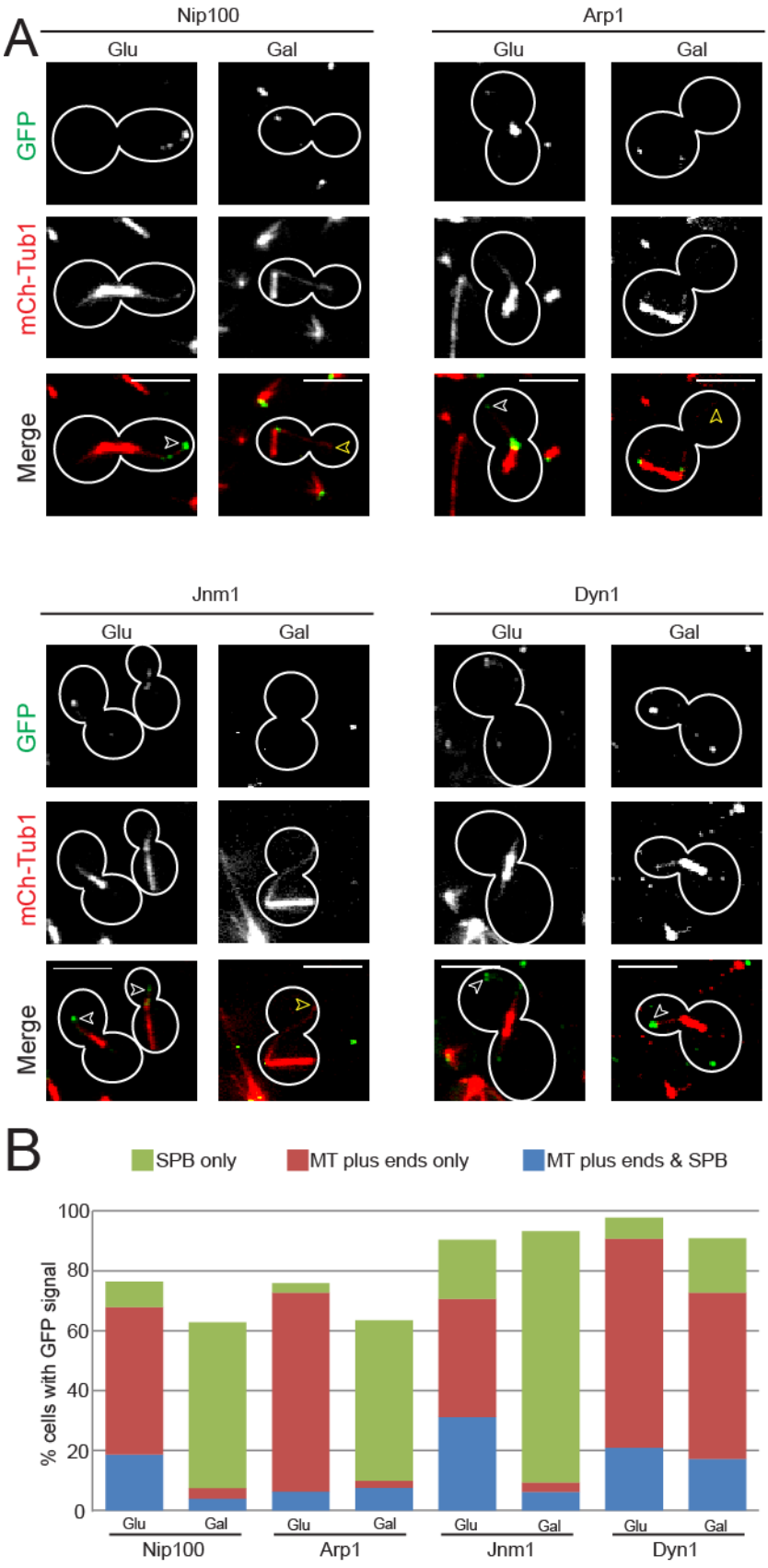
A
Nip100
Arp1
Glu
Gal
GFP
mCh-Tub1
Merge
Jnm1
Dyn1
B
SPB only
MT plus ends only
MT plus ends & SPB
% cells with GFP signal
100
80
60
40
20
0
Nip100
Arp1
Jnm1
Dyn1

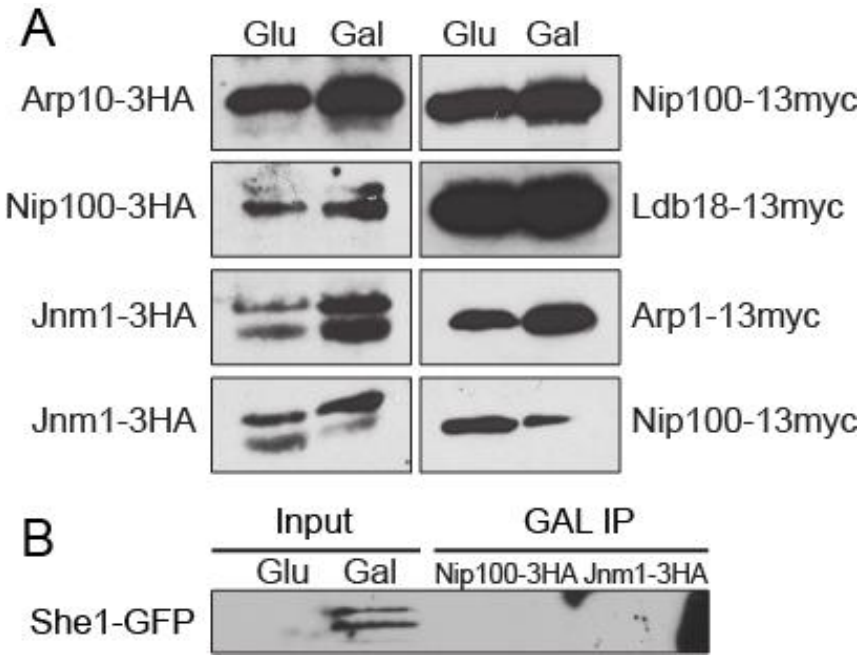

Figure 3.7 Association of Dynactin Proteins is Unaffected by She1 Over-expression. Cells with HA and MYC tagged dynactin complex proteins with She1-GFP under an inducible Gal promoter were grown in glucose or galactose. Whole cell lysates were incubated with HA-affinity gel and the bound fraction was analyzed by Western blot for associating proteins. (A) Immunoprecipitated material from glucose and galactose cultures were blotted for either HA (left panels) or myc (right panels) CUY strains + CUB plasmid: Top = 1909+1213, 2nd = 1933+1213, 3rd = 1936+1263, Bottom = 1938+1263. (B) 50µg of protein lysate from 1933+1213 was probed for She1-GFP, which is present when over-expressed in galactose media. HA-resin immunoprecipitated material from 1936+1263 or 1938+1263 was probed for She1-GFP. No detectable amount of protein was observed.

Protein and Genetic Interactions of She1

She1-GFP localizes along the lengths of cMTs, ipMTs, and at the SPBs (my observations and (Huh et al., 2003; Wong et al., 2007; Woodruff et al., 2009). She1's association with these structures could be a result of direct interaction with MTs or through other MT-associated proteins. In order to find binding partners of She1 to dissect its association with these structures, we performed a series of yeast two-hybrid experiments. Prior to learning of She1's role at the plus-ends of cMTs, I reasoned that She1 could be interacting with SPB proteins, causing a weak cMT anchorage point when She1 was missing. I began with vectors containing genes of the γ-TuSC, including *TUB4*, *SPC97*, and *SPC98*, fused to either the activating or binding domain of Gal4. In addition, I tested if She1 interacted with *TUB1* (α-tubulin) and *TUB2* (β-tubulin) and if it interacted with itself. When compared to the positive control interaction of *SNF1* and *SNF4*, *SHE1* only showed positive interactions with *TUB4*, *SPC97*, and *SPC98* in the β-Gal colorimetric assay (Figure 3.8). These three interactions were further investigated by scoring for colony growth on CSM-histidine + 3-AT plates, where only cells with a positive interactions between the bait and prey proteins will survive. In this assay, *SHE1* interacted with both *SPC97* and *TUB4*. In order to fully confirm that these partners physically interact, strains were made that contained *SHE1-13MYC* paired with either *TUB4-3HA* or *SPC97-3HA* to be used in co-immunoprecipitations. Despite extensive trials, a positive interaction between either of these protein pairs was never observed.

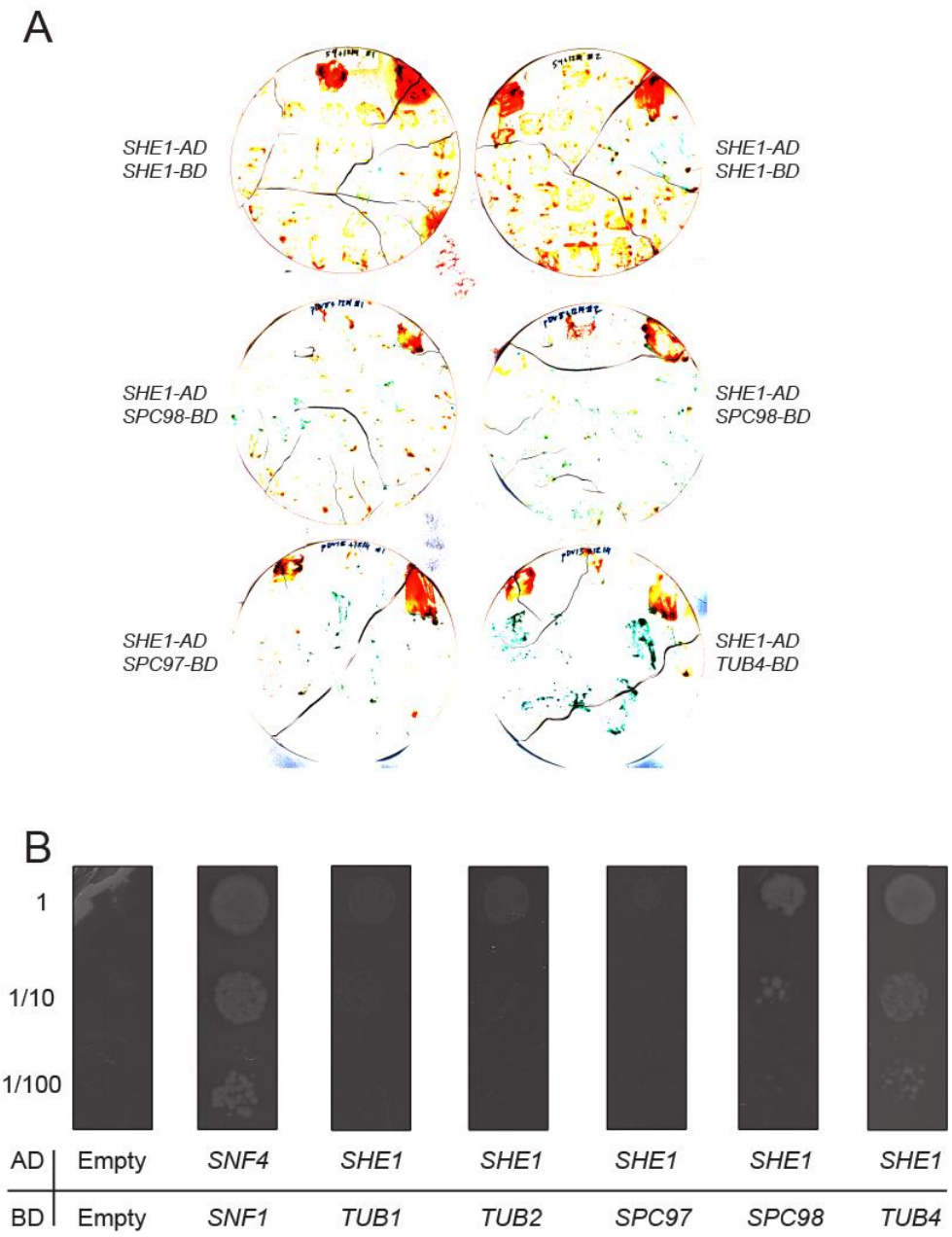

Figure 3.8 Yeast Two-hybrid Interactions of *SHE1*. (A) CUY943 (Y190) containing plasmids listed on next to each disc were grown on CSM-leu-trp plates. Colonies were then transferred to Whatmann paper and stained for β-galactosidase activity. (B) Similar strains were grown in CSM-leu-trp liquid media. Cells were washed with water and then serially diluted. Cells were then transferred by pinning device onto CSM-his + 3-AT plates to score for genetic interactions allowing growth.

Wong and colleagues performed a two-hybrid screen characterizing the protein interactions at the yeast kinetochore (Wong et al., 2007). Here, they found that She1 interacts with Bim1 and other outer kinetochore proteins. In order to confirm this interaction, I immunoprecipitated samples of She1-13myc and probed for Bim1 by Western blot using an antibody targeted against native Bim1 (Figure 3.9). She1's interaction with Bim1 could not be confirmed by this method.

She1 Associates Directly with Microtubule Structures

As previously reported, She1-GFP localizes to mitotic spindles, cMTs, and a ring structure at the bud neck (Wong et al., 2007). Alex Amaro assessed She1's ability to associate with MTs by incubating whole cell protein extracts of a strain containing She1-13myc with pre-assembled, taxol-stabilized, bovine MTs (Figure 3.10A). The MTs were then spun down and the amounst of She1-13myc in the pellet and supernatant were compared. She1-13myc bound to MTs in a MT concentration-dependent manner. The apparent dissociation constant, equal to the concentration of polymerized tubulin required to cosediment half of the She1-13myc protein is ~2μM. This association between She1 and MTs could be direct or could be mediated by another protein in the extract. To determine whether She1 can bind directly to MTs, I purified GST-She1 from bacterial cells and incubated it with taxol-stabilized MTs. GST-She1 bound to MTs with an apparent dissociation constant of ~1μM (Figure 3.10B). Thus She1 can bind to MTs directly and with an affinity similar to other MAPs (Blake-Hodek et al., 2010).

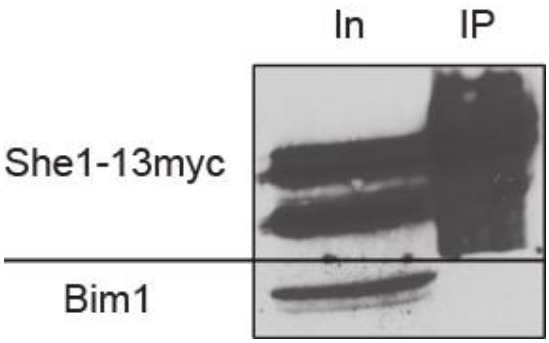

Figure 3.9 Immunoprecipitation of She1-13myc. Protein lysate from CUY1865 was immunoprecipitated with α-myc antibody. Input (In) and immunoprecipitated (IP) material was analyzed for She1-13myc with α-myc and Bim1 with α-Bim1. No detectable amount of Bim1 was found in the IP lane.

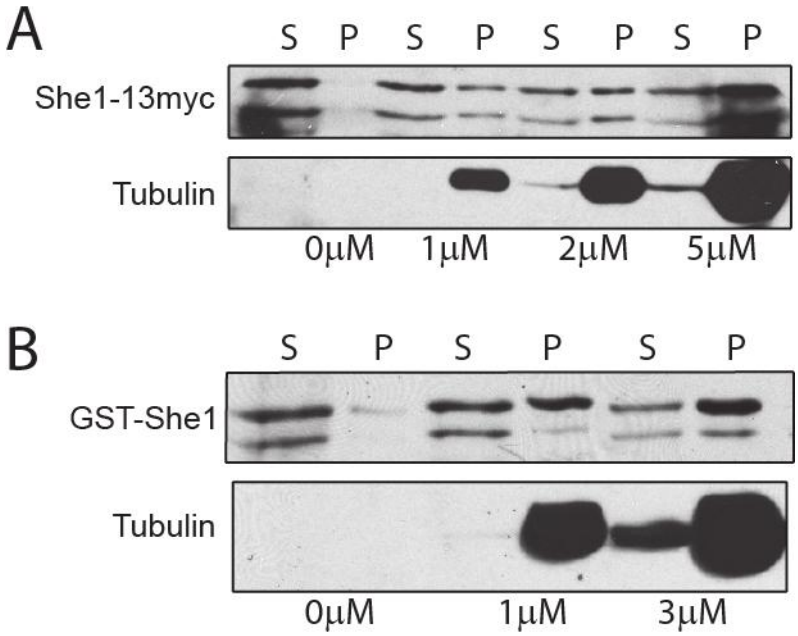

Figure 3.10 She1 Associates with MTs. Protein was mixed with increasing molar amounts of pre-assembled MTs and pelleted at high speed. Contents of the supernatants (S) and pellets (P) were analyzed by Western blot. (A) Protein lysate from cells expressing She1-13myc (CUY1865) were incubated with increasing molar amounts of tubulin. (B) Similar assay was performed with GST-She1 (CUB 1215) purified from bacterial BL21 cells. GST-She1 was probed for with α-GST antibody.

Post-Translational Modification of She1

The predicted molecular weight of She1 is 38kDa and protein analysis was performed with a 13myc epitope-tagged version of this protein which adds 20kDa to the predicted size, for a total of 58kDa. When I examined She1-13myc by Western blot, a pair of prominent bands was found at 81 and 74kDa. Since the localization of She1 to cMTs is lost during mitosis, I hypothesized that a post-translational modification could be the mechanism for this change, which would explain the multiple bands at higher molecular weights observed for She1-13myc. I first wanted to see if the shifts in She1-13myc were cell cycle-dependent. My first approach was to use the P_{MET3}-*CDC20* allele to synchronize the cells in metaphase and release them, taking samples of cells every 20min to observe a change in the band pattern as cells progressed through the cell cycle. This construct attenuates transcription of Cdc20 upon addition of methionine to the media, blocking cells in metaphase since cohesin can no longer be degraded. To confirm that the cells were arrested in metaphase, I simultaneously analyzed Pds1-13myc for cleavage at anaphase. Pds1 is the securin homolog in *S. cerevisiae* and is cleaved during anaphase so that separin can activate. There was no observable change in the She1-13myc bands as the cells progressed through the vegetative cell cycle (Figure 3.11A).

Since cMTs detach more readily in cells in the mating phase, I arrested cells with α-factor and probed for She1-13myc. Here, the middle band at 74kDa was vastly decreased while there was no strong change in the slower migrating band (Figure 3.11B). I further investigated this α-factor-induced change in She1-13myc by

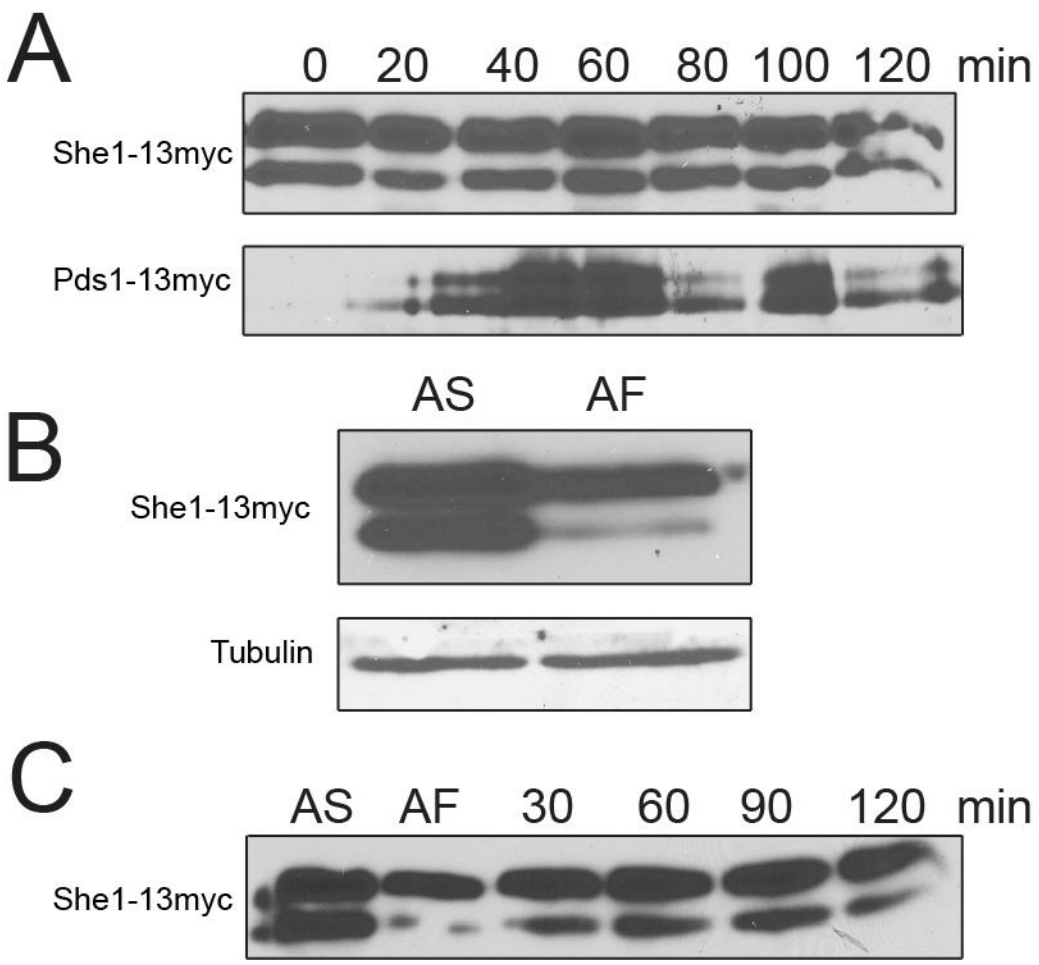

Figure 3.11 She1 Protein Levels During the Cell Cycle (A) Culture of She1-13myc cells were arrested in metaphase and released. Samples were taken every 20min. (B) Cultures were alternatively arrested in mating factor and compared to asynchronous cells. Lower panel is tubulin as a loading control. AS = asynchronous cells, AF = α-factor-arrested cells. (C) α-factor arrested cells were released by replacing media with fresh media. Samples were taken every 30min. CUY 1865 was used in all panels.

performing a time-course of She1-13myc of cells that had been released from an arrest in α-factor. The lower band in She1-13myc recovered to a level similar to that seen in asynchronous cells between 30 and 60 minutes (Figure 3.11C). She1 seems to be modified only in cells that have entered the mating pathway.

I next tried to identify what modification was shifting She1's molecular weight by as much as 24kDa. Phosphorylation of the protein to alter its migration by this much seemed unlikely, and was ultimately ruled out when treatment with λ phosphatase exhibited no effect on the observed size of She1-13myc (Figure 3.12A). Ubiquitin and the ubiquitin-like modifiers are ~8kDa and multiple additions of these can occur. *Saccharomyces cerevisiae* has several of these small post-translational modifications, including ubiquitinylation, SUMOylation, urmylation, neddylation, and hubbylation (Dittmar et al., 2002; Hochstrasser, 1998; Hochstrasser, 2000; Pedrioli et al., 2008). The urmylation, neddylation, and hubbylation pathways are not required for viability and deletions of the ORFs of the small peptides (*URM1*, *RUB1*, and *HUB1*, respectively) were paired with *SHE1-13MYC*. Western blots of these strains showed no change in the migration pattern of She1-13myc, indicating that She1 is not modified in any of these pathways (Figure 3.12B). Ubiquitin and SUMO are necessary for survival, so antibodies targeted for these small peptides were used to probe Western blots of immune-precipitated samples of She1-13myc. Neither of these antibody's had bands that aligned with She1-13myc (Figure 3.12C). Another approach to examining these modifications was to treat the cells with N-ethylmaleimide (NEM) which blocks the activity of reactive cysteines, which these pathways depend on for ubiquitin-meidated degradation. If these pathways are blocked, then the lower band of She1-13myc may

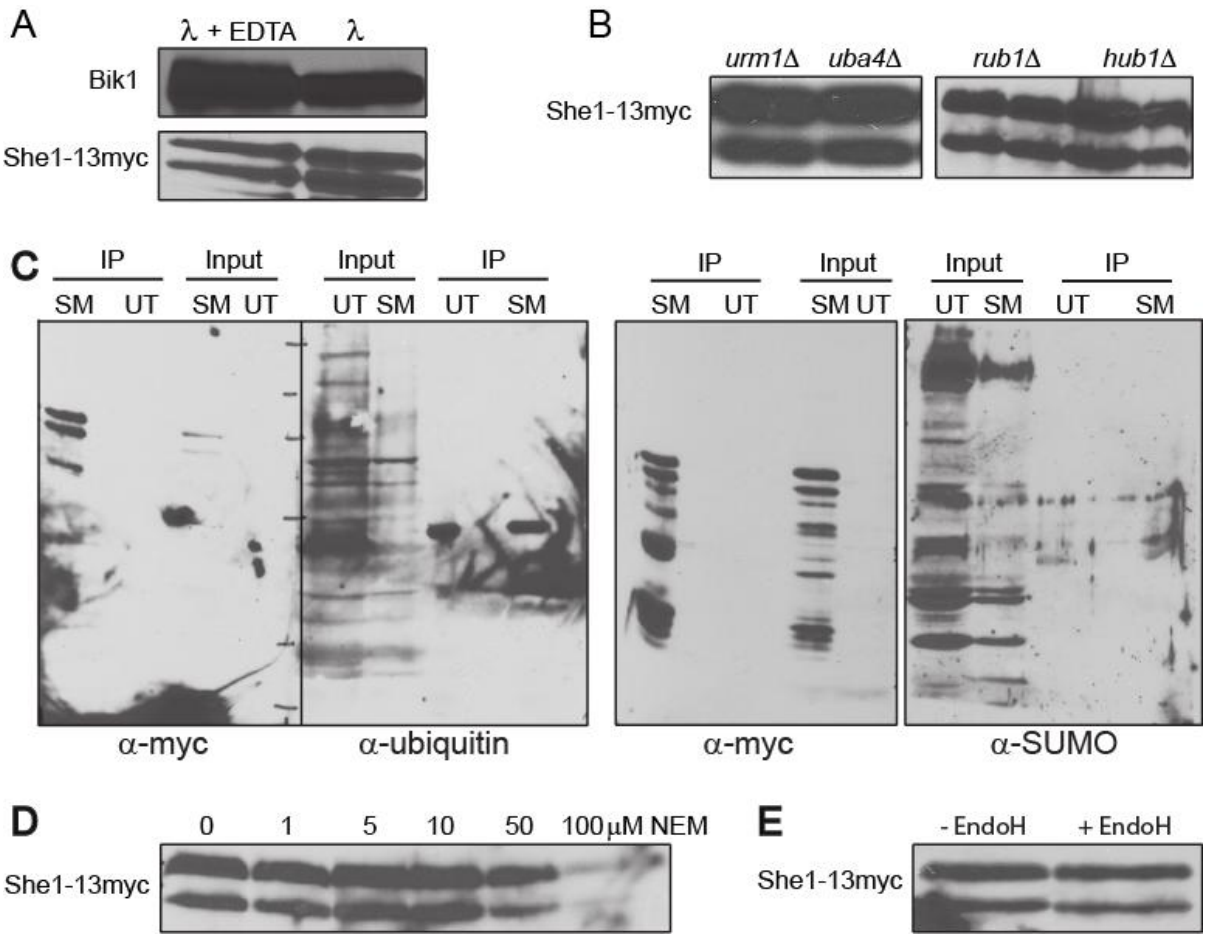

Figure 3.12 Examination of Possible Modifications of She1. (A) Protein lysates were treated with either λ phosphatase or λ phosphatase with EDTA to inhibit the reaction, as a control. The Bik1 band collapses upon treatment, where She1-13myc does not change migration. (B) She1-13myc in strains deleted for ubiquitin-like modifiers. All bands are at the same position in the gel. (C) 50 µg of protein lysate (Input) from a strain with no tagged proteins (UT) and a strain expressing She1-13myc (SM) and α-myc immunoprecipitations of these lysates (IP) were probed with either α-myc, α-ubiquitin, or α-SUMO anitibodies. None of the immunoprecipitated material reacted with the α-ubiquitin or α-SUMO antibodies. (D) 5min prior to harvesting, cells were treated with increasing molar amounts of NEM. Lysates from treated cells showed no difference in the migration of She1-13myc bands. (E) Cells were treated with Endoglycosidase H before harvesting. No difference in migration pattern of She1-13myc

disappear, similar to when cells are exposed to α-factor. No difference in She1-13myc migration in cells treated with concentrations of NEM between 1 and 50µM prior to lysis, but may have been affected at 100µM (Figure 3.12D). These negative results were not confirmed because I lacked positive controls for these antibodies. Since She1-GFP also localizes as a ring around the bud neck (Wong et al., 2007), there was a remote possibility that this modification was a glycosylation event. Protein lysates of She1-13myc strains were treated with Endo H, which cleaves N-linked glycosylation modifications. Again, there was no change in the pattern of bands seen in She1-13myc Western blots (Figure 3.12E). As of now, the modification of She1 is currently unknown.

CHAPTER FOUR

Discussion and Future Directions

She1 Regulates Dynein Activity

In *Saccharomyces cerevisiae*, cytoplasmic dynein has only one main function which is to orient the spindle through the bud neck during anaphase so that the nuclear material is partitioned equally between mother and bud before cytokinesis. To ensure the proper timing of this function, dynein activity is restricted to a small window after spindle migration to the bud neck and until the end of anaphase B (Moore et al., 2009). Pac1, Bim1, and Kip2 are responsible for bringing dynein to the cMT plus-ends where it can be loaded onto cortical Num1 sites in the daughter cell (Markus and Lee, 2011). The association of the dynactin complex activates dynein at these cortical sites when they are in contact with a cMT (Markus et al., 2009). Dynein can be found on cMTs during the majority of the cell cycle, so the timing of dynein activity is restricted by the loading of the dynactin complex which is absent from cMT plus-ends in G1 and pre-anaphase. Dynactin proteins become enriched at cMT plus-ends during anaphase, activating dynein for spindle orientation (Woodruff et al., 2009).

Woodruff and colleagues (2009) demonstrated a unique phenotype in *she1Δ* cells where metaphase spindles are rapidly translocated around the cell and anaphase spindles are pulled around the cell by their SPBs, at times curling the spindle around itself. These phenotypes could be rescued by deletion of the dynein heavy chain,

DYN1, disabling the dynein pathway. I also observed aberrant spindle movement phenotypes in *she1Δ* cells; in addition, I observed cMTs detaching from the SPB which were then pulled around the cortex before depolymerizing (Figure 3.1). MTs detaching from the SPB have been observed in cells of SPB mutants (Hoepfner et al., 2000; Usui et al., 2003; Vallen et al., 1992), but I do not believe that She1 has a specific function at this site because of its proposed regulatory interaction with the dynein pathway at the plus-ends of cMTs and because She1-GFP is found along MTs, not just at the SPB (Wong et al., 2007; Woodruff et al., 2009). When I disrupted the dynein pathway by deleting *NIP100*, a dynactin complex protein necessary for dynein function (Kahana et al., 1998), the spindle movement and cMT detachment phenotypes were all attenuated. I also have found that over-expression of She1 leads to spindle elongation within the mother cell, evidence of a disrupted dynein pathway (Figure 3.5). These data support She1's role in the inhibition of dynein activity.

In budding yeast, a number of microtubule motor proteins associate with cMTs (Hildebrandt and Hoyt, 2000). However, none of the kinesins produce a direct pulling force on cMTs. Only dynein and Myo2, a class-V myosin, produce pulling forces on cMTs at any point in the cell cycle (Hwang et al., 2003; Li et al., 1993). It was interesting to note that deletion of *NIP100* lowers the rate of cMT detachment in WT cells that have been arrested in α-factor and in metaphase when dynein function is thought to be inhibited. I believe that this indicates that there is a basal level of dynein that is functioning during the early parts of the cell cycle despite regulatory elements in action to prevent such activity and that this activity is strong enough to account for 75% of the cMT detachment seen in WT cells (Figure 3.1). In *she1Δ* mutants dynein activity

is not inhibited and cMTs detach from the SPB at a much higher rate (Figure 3.1). From these data I conclude that the major pulling force on cMTs at all points in the cell cycle is produced by dynein activity and that this activity is much higher when She1 is eliminated.

Cytoplasmic MTs Attach to the Outer Plaque More Strongly than to the Half-Bridge

The rate of cMT detachment was highest in *she1Δ* cells arrested in the mating pathway when dynein function is thought to be restricted (Yeh et al., 1995). If dynein is responsible for pulling cMTs from the SPB during G1, why do cMTs detach at such an incredibly low rate when dynein is actively pulling the spindle through the bud neck? Even in *she1Δ* cells arrested in metaphase when dynein is over-active, the rate of cMT detachment is 8-fold lower than *she1Δ* cells arrested in α-factor. I reasoned this could be due to a difference in attachment of cMTs to the SPB during the different portions of the cell cycle. The site of cMT anchorage changes from the half-bridge prior to SPB duplication and migrates to the outer plaque after daughter SPB separation (Byers and Goetsch, 1975). This change in cMT anchorage point may be mediated by the phosphorylation state of Spc72 which binds to the γ-TuSC that seeds cMTs (Gruneberg et al., 2000). Co-immunoprecipitations have suggested that Spc72's interaction with Kar1 at the half-bridge is weaker than with Nud1 at the outer plaque (Gruneberg et al., 2000; Pereira et al., 1999). Cells harboring the *kar1-Δ15* mutation (Vallen et al., 1992) do not organize cMT at the half bridge and any observed cMTs are assumed to be anchored at the outer plaque. These *kar1-Δ15* cells have a rate of cMT detachment

much lower than that seen in *she1Δ* cells (Figure 3.2). This indicates that cMTs that are organized at the outer plaque have a stronger attachment to the SPB than those anchored at the half-bridge.

I further corroborated this hypothesis by tethering cMTs to the half-bridge with the Spc72-Kar1 fusion protein (Pereira et al., 1999) which greatly reduced the rate of cMT detachment in cells arrested in α-factor (Figure 3.4). This rate was almost identical to that of a fusion protein, Spc72-Cnm67 (Gruneberg et al., 2000), which tethered cMTs to the outer plaque. These fusion proteins must provide a stronger connection for cMTs than the normal half-bridge connection in α-factor-arrested cells. However, during metaphase, the Spc72-Kar1 fusion protein releases cMTs at rates increased over both wild-type and Spc72-Cnm67 fusion cells. These data indicate that the normal outer plaque connection for cMTs is stronger than cMTs tethered to the half-bridge via Spc72-Kar1.

The reason for switching the anchor points of cMTs during the cell cycle is not well understood since cells can survive with either the half-bridge or outer plaque cMT anchorage sites missing (Brachat et al., 1998; Vallen et al., 1992). We reason that, in part, this migration of cMTs from the half-bridge to the outer plaque is a necessity in order for the attachment of cMTs to withstand the pulling force of dynein that mainly occurs when the cMTs are anchored at the outer plaque.

Cytoplasmic MT Detachment Occurs Between Spc72 and the Half-Bridge

Detachment of cMTs in *she1Δ* cells occurs through the pulling force of dynein on the plus-ends and reeling the cMT to a cortical site through dynein's minus-end-directed locomotion (Yeh et al., 2000). This detachment could then be the result of a break along the length of the cMT or due to the weakened connection of the cMT to the half-bridge discussed above. Tub4-GFP in *she1Δ* cells arrested in α-factor was observed on the majority of the ends of mCherry-Tub1-labeled cMTs leaving the SPB (Figure 3.3) revealing that breakage of the cMT along its length was not the primary method of detachment. I also observed Spc72-GFP (Figure 3.3) on the ends of detaching cMTs, but not Spc42-mRFP (data not shown) which led us to conclude that the break occurs at the weak interface of Spc72 with Kar1.

These data combined with the fusion protein experiment results point to a poor connection for Spc72 to Kar1. Yet, it is still puzzling why the Spc72-Cnm67 fusion protein did not rescue detachment during metaphase. Perhaps, Spc72's binding to Nud1, which is by-passed in the Spc72-Cnm67 fusion strain, may be a better connection during mitosis (Gruneberg et al., 2000).

Proposed Mechanism of She1's Regulatory Effect on Dynein Activity

The activation of dynein is an important regulatory event in ensuring proper spindle orientation during mitosis. There are several mechanisms for targeting dynein activity to cMTs that have made it into the bud. Dynein localization is unaffected by

She1 levels in the cell (Figure 3.6 and (Woodruff et al., 2009)) indicating that the Pac1/Bim1/Kip2 pathway is not regulated by She1. Thus, She1 must somehow control the loading of the dynactin complex proteins. In *she1Δ* cells, dynactin components localize at cMT plus-ends at an earlier point in the cell cycle (Woodruff et al., 2009) and in greater number (Markus et al., 2011), activating dynein forces at a point in the cell cycle that is incorrect and unnecessary. This early activation of dynein leads to cMT detachment and aberrant spindle movements. I also show that over-expression of She1 excludes dynactin components from cMTs leading to a lack of normal dynein function and accumulation of cells with mis-oriented spindles (Figure 3.6).

She1 may either affect the assembly of the dynactin holo-complex as suggested by Woodruff and colleagues (2009) or it may obscure the binding substrate for dynactin on the cMT (Kardon et al., 2009). Over-expression of She1 does not affect the assembly of dynactin (Figure 3.7) and the ratio of dynactin components that are loaded onto the cMT in *she1Δ* cells is unaffected (Markus et al., 2011). She1-GFP associates with cMTs during G1 and pre-anaphase when dynein is mostly inactive, but is lost from these sites during anaphase (my observations and (Wong et al., 2007; Woodruff et al., 2009)). I have shown that She1 does bind to MTs on its own (Figure 3.10). I suggest that She1 binds to the cMT plus-ends during the early part of the cell cycle. At this site, She1 prevents dynactin from loading onto the cMT, attenuating dynein activity and preventing the detachment of cMTs and aberrant spindle movement during metaphase. Upon anaphase, She1's localization to cMTs is lost allowing dynactin to properly activate dynein and orient the spindle through the bud neck (Figure 4.1).

Figure 4.1 Proposed Model for She1's Control of Dynein Activity. (A) During G1 and in the mating phase, She1 (brown hexagon) is found on cMTs, blocking dynactin's association with dynein at the plus-end. This prevents the activation of the majority of dynein's minus-end directed motility (green arrow). Detachment of cMTs rarely occurs (red arrow). (B) During spindle orientation in metaphase, She1's localization to cMTs is only slightly diminished, still blocking dynactin from activating dynein. Detachment of cMTs during this portion of the cell cycle when cMTs are organized at the outer plaque is much less than during α-factor. (C) In *she1Δ* mutants, cells arrested in α-factor experience a large increase in dynein pulling forces since dynactin is free to associate with dynein. The weak association between Kar1 and Spc72 leads to a greatly increased rate of cMT detachment from the SPB. (D) When *she1Δ* cells are arrested in metaphase there is the possibility of more active dynein molecules than in WT cells. This leads to an increased rate of cMT detachment as well, but it is still less since the association of Spc72 with Nud1 is stronger than Spc72 with Kar1.

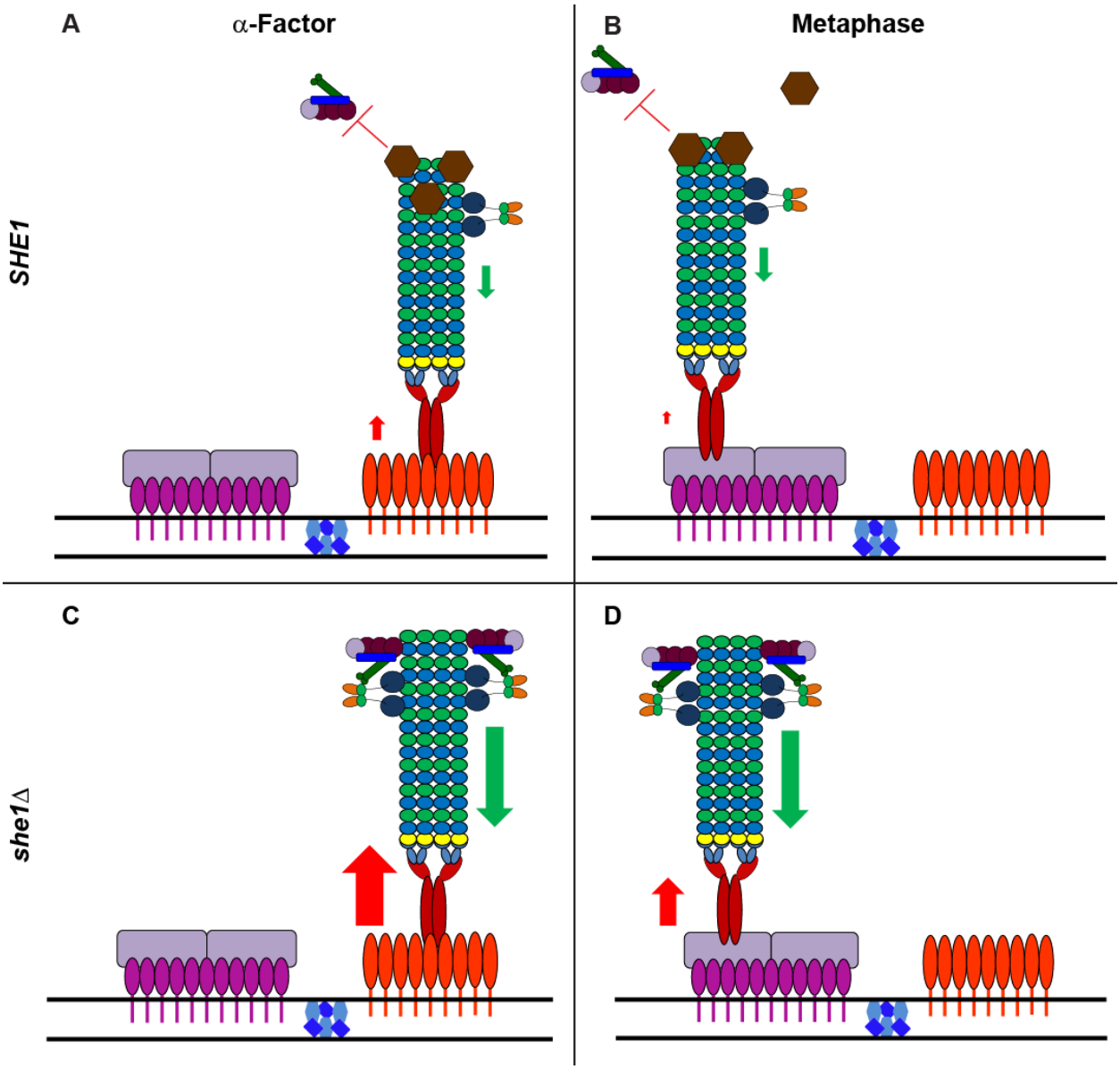
A
α-Factor
B
Metaphase
SHE1
C
D
she1Δ

Future Directions

In order to fully characterize the dynein regulatory network, it will be necessary to find up-stream effectors of She1. Efforts to find proteins that physically interact with She1 have been difficult and have not provided any positive interactions with known proteins (my unpublished data and (Woodruff et al., 2009). One approach to finding proteins that interact with She1 is SILAC. Here, cells are grown in two different media, one with heavy isotope labeled lysine and arginine, the other with light isotope lysine and arginine. She1-13myc would then be immunoprecipitated from cultures grown in heavy isotope media and the precipitated material would be examined by mass-spectrometry. This procedure is more sensitive than traditional mass-spec analysis because the lighter isotope sample will identify any background seen in the data. Again, this procedure may not be sensitive enough if She1 only enzymatically modifies parts of the dynactin complex or other effectors since these interactions are often too quick and with affinity too low to find by immunoprecipitation.

Identifying the modification of She1 could be very telling on how She1 is regulated and perhaps even offer a glimpse at its function. I believe that She1 is post-translationally modified in yeast because the GST-She1 purified from *E. coli* runs on a SDS-PAGE gel at its expected size of 64kDa (She1 is 38kDa and GST is 26kDa). Over-expression of Bud14, a component of the Glc7-Bud14 phosphatase, generates phenotypes similar to those observed in *she1Δ* cells where the metaphase spindle has aberrant movement around the cell and cMTs detach from the SPB (Knaus et al., 2005). She1 does appear to be post-translationally modified (Figure 3.11) which would be expected to change when the cell begins anaphase. However, She1 does not seem to

undergo any changes during the vegetative cell cycle (Figure 3.11A). Exposure to α-factor decreases the intensity of the lower band of She-13myc (Figure 3.11B and C). I have tried to determine if She1 is modified through ubiquitin and ubiquitin-like systems (Figure 3.12), but have not found strong evidence to conclude if it is or is not. She1 purified from yeast could be analyzed by mass-spec to help determine the modification seen on She1-13myc. Global expression analysis estimates that there are only ~256 molecules of She1 in each yeast cell (Ghaemmaghami et al., 2003), so a large volume of yeast would need to be grown to attain enough material to perform mass-spec analysis.

She1 was found to genetically interact with a number of kinetochore and spindle-associated proteins through a yeast two-hybrid screen (Wong et al., 2007) and has very strong localization to the mitotic spindle (my observations, (Wong et al., 2007)). There is some indication that She1 has a second function within the nucleus that is involved with the timing of the breakdown of the spindle after anaphase (Woodruff et al., 2010). The post-translational modifications discussed above may regulate She1's shuttling between the nucleus and cytoplasm.

She1's synthetic lethality with *stu2-12* and *kip3Δ* may also stem from She1's proposed nuclear function. Stu2 aids in the elongation of the mitotic spindle and is found on the spindle mid-zone (Severin et al., 2001). Kip3 has numerous functions within the nucleus and *kip3Δ* cell also exhibit a similar defect in spindle breakdown as *she1Δ* cells (Woodruff et al., 2010). Studying the interplay of these three proteins on the spindle mid-zone would yield information on the mechanism of spindle breakdown

and if She1 has a regulatory role in the nucleus as well. I would combine deletions of *SHE1* with other *STU2* conditional alleles to see if a synthetic interaction occurs at temperatures lower than the known restrictive temperatures for those *STU2* alleles. These strains could then be labeled with GFP-Tub1 and spindle morphology could be observed for defects. A similar assay could be done by first making KIP3 conditional alleles in a ***she1Δ*** strain. Combining any new conditional *KIP3* alleles with ***she1Δ*** could give rise to phenotypes with spindle defects or new cMT defects since Kip3 also is involved with cMT dynamics and functions.

It seems as though She1 and does not have any direct homologs in higher eukaryotes. Spindle positioning is important and evolutionarily conserved in higher eukaryotes. Identifying a protein or protein complex that performs an analogous function in other organisms will aid in elucidating dynein regulation pathways in higher eukaryotes.

APPENDIX 1

Localization of Stu1 to the Kinetochore

Stu1 belongs to the CLASP family of MAPs and has roles in both regulating MT dynamics and maintaining attachments between MTs and cellular structures (Pasqualone and Huffaker, 1994; Yin et al., 2002). During metaphase in budding yeast, Stu1 binds to the plus-ends of kinetochore MTs and tracks them, possibly aiding in their dynamics to correctly find the centromere of chromatids (Ma et al., 2007; Ortiz et al., 2009). After anaphase begins, Stu1 migrates to the spindle mid-zone, perhaps stabilizing and polymerizing the inter-polar MTs as they elongate (Yin et al., 2002). Recent work on Stu1's function at the kinetochore has shown that it may play a role in the spindle assembly checkpoint and be part of the complex that relays an unoccupied kinetochore signal to cells (Jones et al., 1999; Ortiz et al., 2009). I wanted to examine this process more closely by observing the Stu1 occupancy of kinetochores in a variety of circumstances.

Stu1's localization to kinetochores was assayed by chromatin immunoprecipitation (ChIP) of a myc-epitope tagged version of Stu1 in WT cells, cells treated with nocadozole, or in a temperature-sensitive *ndc10-1* background that ablates kinetochores at restrictive temperatures. I targeted the centromere of chromosome III for Stu1 occupancy and I also designed a set of primers amplify a portion of the *SSC1* locus which is located ~100 kbp away from the centromere, as a negative control. The outer kinetochore protein Dam1-9myc and the inner kinetochore protein Ndc10 were used as a positive control in the assay.

As shown in Figure A1.1, Dam1-9myc, Ndc10-13myc, and Stu1-13myc are all found at kinetochores in WT cells under normal growth conditions. When cells containing the *ndc10-1* allele were shifted to restrictive temperature both Ndc10-1-13myc and Stu1-13myc no longer associated with the centromere within the limits of detection for this assay. This result suggests that Stu1 associates with proteins of the kinetochore and not directly with centromeric DNA.

Next, I wanted to see if Stu1 associated with unattached kinetochores. To increase the amount of kinetochores not making contact with a MT, cells were treated with nocodazole for 30min to depolymerize MTs. ChIP analysis confirmed Stu1-13myc's association with unattached kinetochores. This is in agreement with fluorescence microscopy data from Ortiz and colleagues (Ortiz et al., 2009).

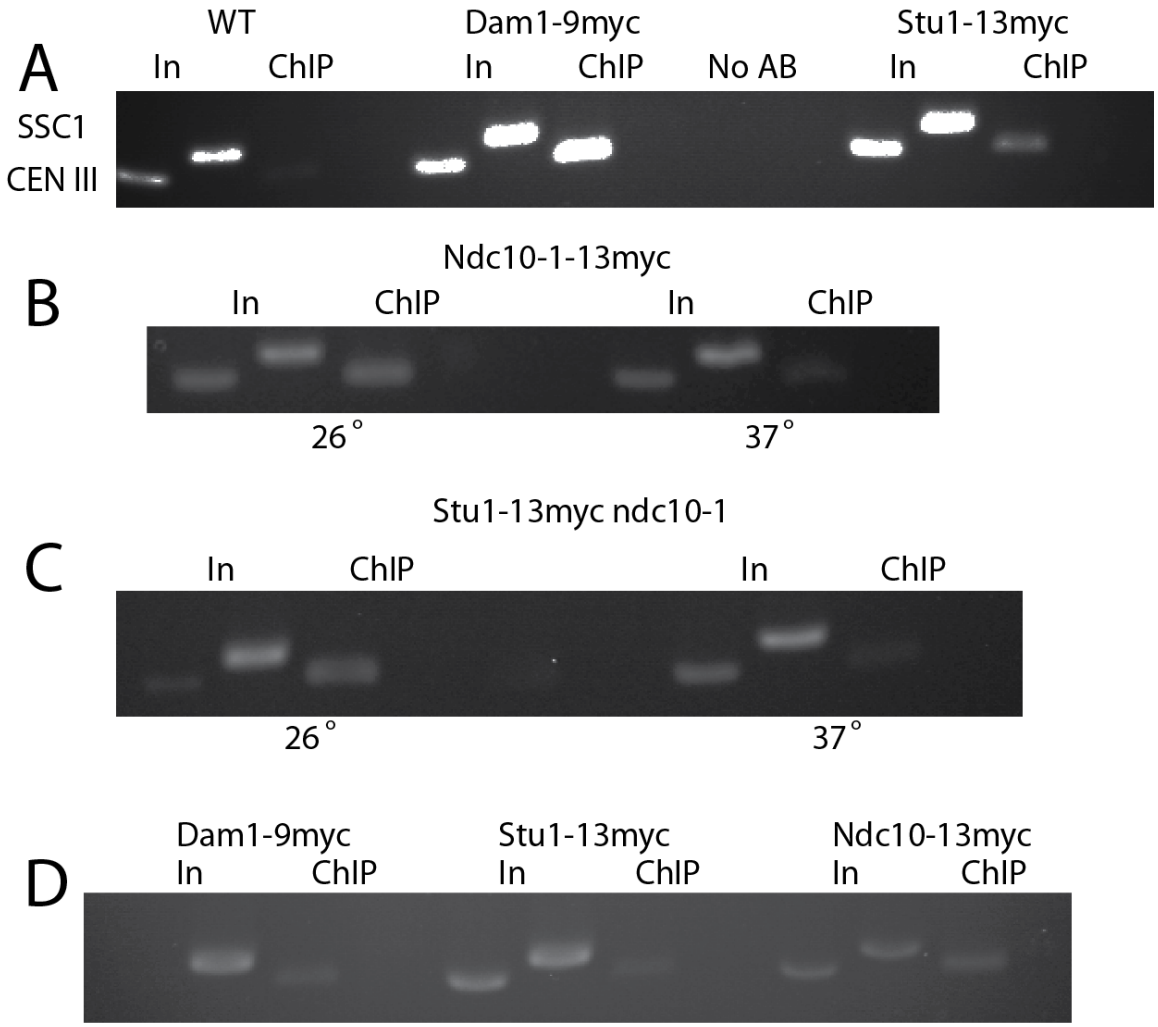

Figure A1.1 Chromatin Immunoprecipitation of Stu1. Immunoprecipitated content was analyzed for either centromeric (CEN III) or non-specific (SSC1) DNA bound by epitope-tagged protein (ChIP samples) and compared to a 1:10 dilution of starting material (In). (A) An untagged strain (WT) was compared to Dam1-9myc and Stu1-13myc. Antibody was not added to a preparation of Dam1-9myc to control for non-specific binding by Protein-G beads (No Ab). (B) The temperature-sensitive Ndc10-1-13myc protein does not bind CEN III as efficiently at restrictive temperature. (C) Stu1-13myc can no longer bind CEN III in a *ndc10-1* strain at restrictive temperature. (D) Dam1-9myc and Stu1-13myc, but not Ndc10-13myc, are excluded from the kinetochore when cells are treated with nocodazole. CUY strains used WT (28), *DAM1-9MYC* (1288), *STU1-13MYC* (1386), *ndc10-1-13MYC* (1927), *STU1-13myc ndc10-1* (1923), *NDC10-13MYC* (1926).

APPENDIX 2

Quantitative PCR Screen for Tubulin Regulatory Genes

Microtubules are assembled from α/β heterodimers essentially making the polymer half α-tubulin and half β-tubulin. One could assume then that the number of molecules in the cell of each subunit would be equal to the other. Cells would most likely then have an equal number of loci for these genes that were expressed co-incidentally in order to maintain the ratio of α to β tubulin. However, in vertebrate cells, there can be as many as six different loci for each tubulin gene as well as other pseudogene loci (Wade, 2009). *Saccharomyces cerevisiae* has two loci for α-tubulin, *TUB1* and *TUB3*, and a single locus for β-tubulin, *TUB2* (Schatz et al., 1986). Coordinated expression of these three loci is critical for cell viability as an excess of β-tubulin is lethal (Burke et al., 1989; Katz et al., 1990). The lethal phenotype of over-expressing *TUB2* can be rescued by over-expression of one of the α-tubulin genes (Weinstein and Solomon, 1990). In contrast, cells can tolerate excess amounts of α-tubulin, as shown by insertion of a *GFP-TUB1* cassette that effectively duplicates the locus and does not greatly affect viability. The mechanism of this lethality is not understood, as it could be a function of titrating available monomers or dimers out of the usable pool, a change in MT dynamics, incorrect incorporation of β-tubulin into the MT creating structural anomalies, or a number of other possibilities.

Identification of genes involved with the expression and maintenance of tubulin monomer levels within the cell would be of interest, to help understand why this process is important. In order to find genes possibly involved in these processes, transcriptional

levels of the three tubulin genes were to be screened in cells that have single ORF deletions in non-essential genes or in cells in restrictive conditions for conditional alleles of essential genes. Transcript levels of *TUB1*, *TUB2*, and *TUB3* would then be quantified by real-time PCR (QPCR) by measuring the intensity of SYBR green fluorescence after each round of replication. Strains that have a reduced or elevated level of tubulin transcripts compared to WT cells potentially would have disruptions in genes involved in maintaining the balance of tubulin monomers within the cell.

In order to screen the entirety of *Saccharomyces cerevisiae's* ~6,000 ORFs, a high-throughput screen was devised and implemented by the Pleiss lab that utilizes both the gene-deletion library from Open Biosystems (Giaever et al., 2002) that has single ORF deletions of the ~4,300 non-essential genes. The remaining essential ORFs have had temperature sensitive mutations created and these alleles have been singly transformed into strains. When grown at restrictive temperature, these strains are considered to behave similarly to entire gene deletions. The Pleiss lab grew small volumes of these >5,500 strains in duplicate at either 30° for total deletions or at their restrictive temperature for temperature-sensitive mutants in 384-well dishes. Entire cultures were harvested and mRNA was extracted by chloroform extraction via an automated process for consistency and repeatability, using a Biomek NP liquid handling robot. They then converted the collected mRNA into cDNA by reverse-transcriptase PCR. These cDNA samples were then used in the QPCR assay. These growth conditions were repeated for biological replicants.

I generated primers targeted toward the three tubulin loci using the Primer 3 web-based software to find 25-mers that were highly specific to one of the tubulin genes and had optimal annealing temps between 55° and 60°. Two sets of primers were generated per locus, one set near the 5' end and the other closer to the 3'. I then used these primers to optimize QPCR reactions for the lowest annealing temperature and quickest extension time. I then used the optimal primers for *TUB1* to run QPCR reactions with the cDNA created from the strains listed above. 384-well plates of 10µL reactions were run in a Roche Lightcycler 480. Replicates of the reaction plates were run with each biological replicate, for a total of four reactions per strain. These replicates took into account biological differences in growth rate, mRNA recovery, cDNA synthesis, and technical aspects such as pipette error and thermocycler temperature variation.

The curves generated from the QPCR data were used by the Pleiss lab to calculate the nanogram quantity of tubulin transcript in each strain used in the screen. In order to normalize for variability found between the four values acquired for each strain, a coefficient of variation was determined for each primer pair used. Laura Bud found that the value in the vast majority of samples was reproducible and samples with a coefficient higher than 0.25 were excluded from further analysis. To account for variability due to experimental procedures, data from six different primer pairs were compiled to create a composite normalization value. The details of this formula can be found in Bud et al. 2011 (submitted at time of writing this thesis).

Laura went on to determine the strains that cause changes in tubulin transcriptional levels by using the calculated nanogram amounts of mRNA and comparing them with Single Analysis of Microarrays (SAM), a program intended for use with microarray data (Tusher et al., 2001). For each mRNA, SAM analysis was performed on the four relative amounts or RNA in a strain values, composed of both technical and biological replicates that were generated for each of the ~5500 strains. For each transcript, a one class SAM analysis was performed where the Δ value was adjusted to minimize the false discovery rate (FDR).

From the screen I ran with the *TUB1* primers, ~5,500 query strains were examined, 389 had a significant change in *TUB1* mRNA, 37 up-regulated (positive score) and 352 down-regulated (negative score) *TUB1* transcription (Table A1). The cutoffs for these genes are displayed in Figure A2.1. The data had a median number of false positives of 7.31 and False Discovery Rate of 1.88%.

The candidates for tubulin transcriptional regulation that we found range from a number of processes, such as transcription, translation, biosynthesis, mitochondrial function, chaperone proteins, and stress response. The largest group of genes is ribosomal subunits. The screen did identify 80 ORFs that are either dubious or have uncharacterized function, providing a large number of genes that could be investigated further for a possible role in tubulin regulation. The next phase of the project would be to repeat the QPCR assay using primers directed at *TUB2* and *TUB3*. I would then over-lie the data sets from the 3 experiments and look for the ORFs that changed the nanogram levels of all three of the tubulin genes. I would then confirm the change in

tubulin expression in each of the strains on a smaller scale. Further investigations into these candidate genes would then be warranted to either find defects in known and previously characterized ORFs or to begin finding functions for unknown ORFs.

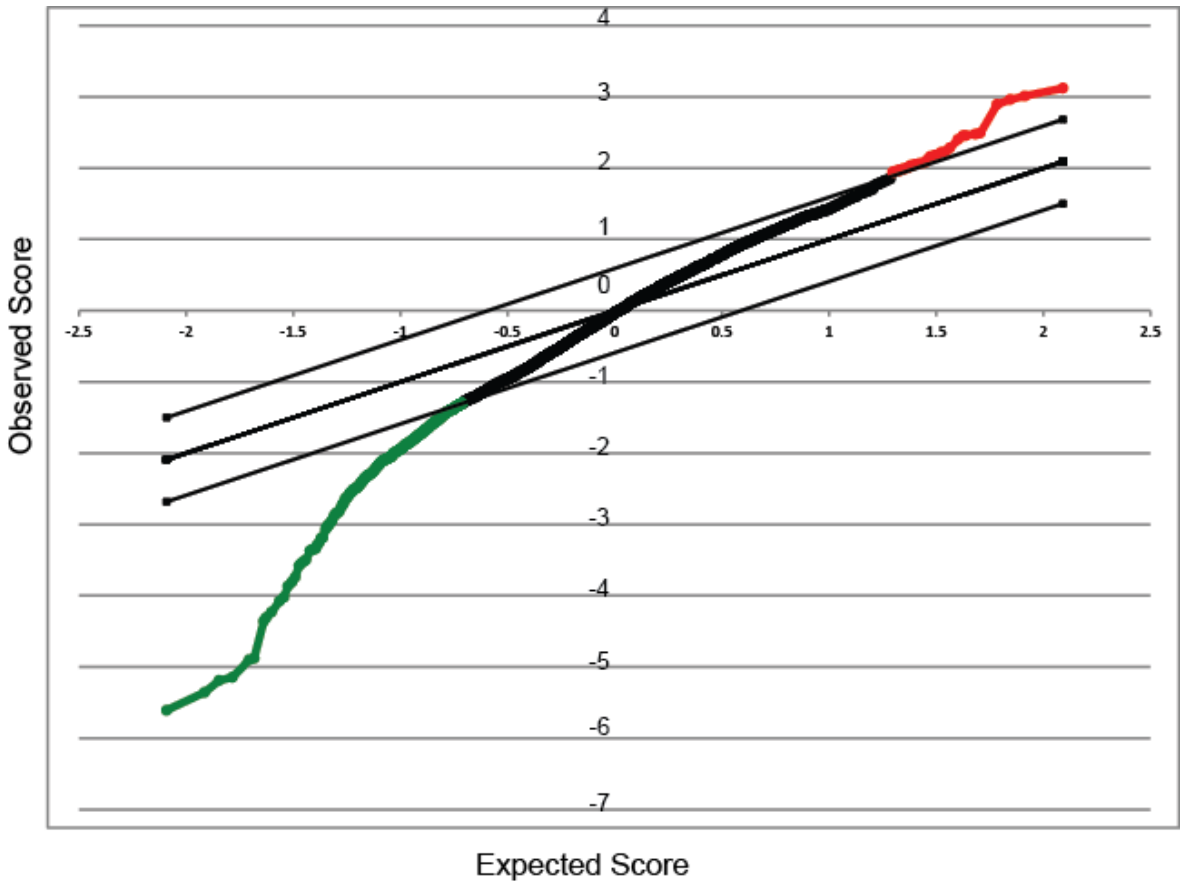

Figure A2.1 SAM Plot of TUB1 Transcriptional Levels. Normalized mRNA nanogram levels from the ~5,500 strains used in the TUB1 QPCR Assay. Strains with increased *TUB1* transcript are marked in red, decreased transcript in green.

TABLE A2.1 Gene Deletions That Alter *TUB1* Transcriptional Levels

Score	Gene Name	GO
3.122463	IRC14	Dubious ORF
3.011555	ORT1	Ornithine Transport
2.963357	EMC6	ER Folding
2.893035	FIP1	Polyadenylation Factor
2.490313	YGR031W	Unknown
2.478781	BNA3	Kynurenine aminotransferase
2.459286	NRM1	Repressor of MBF
2.455777	PHA2	Prephenate dehydratase
2.402823	DNF2	Flippase
2.283398	YBL071C-B	Unknown
2.229075	ATP17	ATP Synthase
2.223559	BUD3	Bud site selection
2.185687	YOR277C	Dubious ORF
2.179277	NFT1	Transporter
2.163599	SAP30	Histone Deacetylase
2.124649	LSM6	mRNA Decay
2.089323	SWD3	Histone Methylation
2.072463	RGA1	GTPase Activating Protein
2.062771	SCS3	Inositol Prototrophy
2.056826	TEL1	Telomere maintenance
2.054288	YOL106W	Dubious ORF
2.043647	MDH3	Peroxisome Dehydrogenase
2.037041	MON1	Vesicle Fusion
2.036286	YKR104W	Transporter
2.008353	TUM1	Mitochondrial Protein
1.999922	YBR072C-A	Unknown
1.990944	RPL26B	60S Ribosome
1.984842	PRM1	Membrane fusion during mating
1.977865	UBP2	De-ubiquitinase
1.974862	GNA1	Acetyltransferase
1.972714	SBA1	Chaperone
1.964662	YOR283W	Unknown
1.959616	RPL20B	60S Ribosome
1.956648	DSE3	Daughter Cell Fate
1.949362	DLS1	Chromatin Accessibility
1.944235	PRS2	Phosphoribosylpyrosphate synthetase
1.937483	YKL133C	Unknown
-1.30354	DDC1	DNA Damage Checkpoint
-1.30441	SYS1	Integral Membrane Protein
-1.30454	MDR1	GTPase
-1.30465	GLR1	Glutathione Oxidoreductase
-1.30657	YDR185C	Mitochondrial Protein
-1.30811	ARC19	Actin Cytoskeleton
-1.3125	RPA49	RNA Polymerase

-1.31315	DST1	Transcription Elongation
-1.31426	RAM1	Mating Pathway
-1.31517	RPL29	60S Ribosome
-1.3166	TFB5	RNA Polymerase
-1.3175	YCL046W	Dubious ORF
-1.32025	MRPL13	Mitochondrial Protein
-1.3212	YFR057W	Unknown
-1.32184	YJL027C	Unknown
-1.32212	NFU1	Iron Metabolism
-1.32222	FOL1	Folic Acid Biosynthesis
-1.32279	HSP30	Stress Response
-1.32492	SUI1	Translation Factor
-1.32607	HOS3	Histone Deacetylase
-1.32781	NPT1	NAD+ Biosynthesis
-1.32813	PTK1	Protein Kinase
-1.32874	YOL019W	Unknown
-1.32911	MET18	DNA Repair
-1.3332	SLM6	Actin Cytoskeleton
-1.33432	YDR115W	Mitochondrial Protein
-1.33556	DID4	ESCRT-III Complex
-1.33745	UGO1	Unknown
-1.33769	PHD1	Transcriptional Activator
-1.34284	CTK2	Trancription Protein
-1.34496	YLR402W	Dubious ORF
-1.34652	SYH1	Unknown
-1.34688	RPS9B	40S Ribosome
-1.3482	SRO9	RNA Binding
-1.35176	VMA21	Vacuolar ATPase
-1.35207	SPP1	COMPASS Complex
-1.35233	RSA3	Ribosomal Maturation
-1.35562	COA2	Cytochrome Oxidase Assembly
-1.35567	UBP8	Ubiquitin Protease
-1.35654	ADO1	Adenosine Kinase
-1.36931	PYK2	Pyruvate Kinase
-1.36945	BNI1	Formin
-1.37184	SFH5	Phosphatidylinositol Transfer
-1.37513	ECM14	Metalloprotease
-1.3771	YDL206W	Unknown
-1.37858	PEX29	Peroxisomal Protein
-1.37861	SNC2	v-SNARE
-1.37942	YGR174W-A	Unknown
-1.38025	YPL150W	Unknown
-1.38507	ADA2	Transcription Coactivator
-1.38529	TOM5	Mitochondrial Import
-1.38569	IKI1	Elongator Complex
-1.38638	HPR1	Transcription Elongation
-1.38643	YMR148W	Unknown

-1.38673	MNI1	Methyltransferase
-1.3879	RPS17B	40S Ribosome
-1.38794	SPT10	Histone Acetylation
-1.388	PEX3	Peroxisomal Protein
-1.38869	RPL27B	60S Ribosome
-1.38995	REV3	DNA Repair
-1.39082	TMA19	Ribosomal Protein
-1.39535	UTP6	Nucleolar Protein
-1.39664	YCK1	Morphogenesis
-1.39961	YJR030C	Unknown
-1.40188	DAT1	DNA Binding
-1.40465	CTF4	Sister Chromatid Cohesion
-1.40465	RPL7A	60S Ribosome
-1.40485	DCW1	Mannosidase
-1.40596	YJR037W	Dubious ORF
-1.40709	ALO1	Oxidative Stress Response
-1.412	IES6	Chromatin Remodeling
-1.41255	STM1	TOR Signaling
-1.41426	VEL1	Unknown
-1.41523	YKU80	Telomere Maintenance
-1.41565	DDR2	Multistress Response
-1.41639	ELO1	Acyl Chain Elongation
-1.42422	ELA1	Ubiquitin Degradation
-1.42517	RRN10	rDNA Transcription Factor
-1.42578	POC4	20S Proteasome Assembly
-1.42713	MDM38	Mitochondrial Protein
-1.42739	YRF1-6	Helicase
-1.43076	STE18	Mating Pathway
-1.43428	SVS1	Vanadate Resistance
-1.43731	PIB2	Gene Repression
-1.43735	YKL187C	Unknown
-1.43765	JJJ1	Chaperone Protein
-1.43837	PPA1	Vacuolar ATPase
-1.43909	MNN5	Oligosaccharide Modifier
-1.43984	SPR3	Sporulation
-1.44239	TPS2	Carbohydrate Storage
-1.44624	UBC8	Ubiquitin Conjugation
-1.45079	YAR029W	Unknown
-1.45508	MET22	Methionine Biosynthesis
-1.45568	PAN2	mRNA Processing
-1.45958	BUB3	Kinetochore Checkpoint
-1.46008	PRD1	Peptidase
-1.46123	HSP26	Chaperone Protein
-1.46278	ATS1	Translation Factor
-1.46468	CDC53	Ubiquitination Factor
-1.46905	IRC13	Dubious ORF
-1.47172	DCC1	Sister Chromatid Cohesion

-1.47688	REF2	mRNA Processing
-1.48141	CBF1	DNA Binding
-1.48309	PAF1	RNA Polymerase
-1.48906	YOL079W	Dubious ORF
-1.49261	STS1	Ubiquitin-mediated Degradation
-1.49703	VBA1	Permease
-1.49713	RIB5	Riboflavin Synthase
-1.49913	VMA5	Vacuolar ATPase
-1.49963	YCR085W	Dubious ORF
-1.50359	CCC1	Ion Transporter
-1.51254	ACS2	Acetyl-CoA Synthetase
-1.51294	YIG1	Anaerobic Glycerol Production
-1.51515	HSL7	Methyltransferase
-1.52574	SYF2	Spliceosome
-1.52842	YHL015W-A	Unknown
-1.53114	RNY1	Rnase
-1.53148	ASF1	Nucleosome Assembly Factor
-1.53385	PEX25	Peroxisomal Protein
-1.53657	FYV12	Unknown
-1.53698	YDR524C-B	Unknown
-1.53749	ARO8	Aminotransferase
-1.54235	AFG3	Mitochondrial Protein
-1.54306	RBG1	Ribosome Translation
-1.54696	SEO1	Permease
-1.54733	YPL136W	Dubious ORF
-1.55058	OPI6	Dubious ORF
-1.55764	HTD2	Mitochondrial Protein
-1.56489	YKL131W	Dubious ORF
-1.56566	YCL056C	Unknown
-1.56759	HIT1	Unknown
-1.568	DCS1	mRNA Processing
-1.57555	HCM1	Transcription Factor
-1.57751	MEI5	Meiotic Recombination
-1.58225	SPC19	DAM Complex
-1.58276	ECM1	Unknown
-1.58313	ECM40	Mitochondrial Protein
-1.58655	YMR193C-A	Dubious ORF
-1.59242	RPP0	Ribosomal Protein
-1.5945	YKL123W	Dubious ORF
-1.59512	GRX2	Maintains Redox State
-1.59522	FPR1	Isomerase
-1.5976	DYN1	Dynein
-1.60007	RPS18B	40S Ribosome
-1.60383	YGL217C	Dubious ORF
-1.61017	CTK3	Transcription Machinery
-1.61247	MAP1	Methionine Aminopeptidase
-1.61578	PEX22	Peroxisome

-1.6217	YAL065C	Unknown
-1.63247	HGH1	Unknown
-1.63639	SOL2	tRNA Export
-1.63641	IPI1	rRNA Processing
-1.64469	YAL004W	Dubious ORF
-1.6483	YKL023W	Unknown
-1.64832	DCP1	mRNA Processing
-1.65293	TGS1	Trimethyl Guanosine Synthase
-1.65596	RPS29B	40S Ribosome
-1.66109	VPS69	Dubious ORF
-1.66139	FCF1	18S rRNA Processing
-1.66151	HIS3	Histidine Biosynthesis
-1.66226	RPL37B	60S Ribosome
-1.66515	RPL20A	60S Ribosome
-1.6695	YGR015C	Unknown
-1.66952	ECM33	Unknown
-1.67715	FUI1	Uridine Permease
-1.67746	LAC1	Ceramide Synthase
-1.67762	MCH1	Permease
-1.68651	ACO2	Mitochondrial Protein
-1.68862	STE4	Mating Pathway
-1.68934	INP53	Phosphatidylinositol Phosphatase
-1.69481	HCR1	Translation Factor
-1.70338	YPS5	Aspartic Protease
-1.71246	ERG13	HMG CoA Synthase
-1.71346	SNF5	Chromatin Remodeling
-1.71528	TFP1	Vacuolar ATPase
-1.71611	RPS28B	40S Ribosome
-1.71948	VPH2	Vacuolar ATPase
-1.7195	YKR040C	Dubious ORF
-1.73154	MRPL40	Mitochondrial Large Ribosomal Protein
-1.73226	PTP2	Osmolarity Sensing
-1.73467	PRO3	Proline Biosynthesis
-1.73588	SNO1	Pyridoxine Metabolism
-1.73657	IDP2	Isocitrate Dehygrogenase
-1.74543	RPL37A	60S Ribosome
-1.74753	PFA5	Palmitoyltransferase
-1.74762	CBF5	Pseudouridine Synthase
-1.75415	MSN4	Trancriptional Activator
-1.75785	URM1	Post-Translational Modification
-1.75829	VPS64	Vacuolar Protein Sorting
-1.7663	SPB4	RNA helicase
-1.77412	MUC1	Flocculin
-1.782	TCO89	Nutrient-dependent Growth
-1.7876	SUI2	Translation Factor
-1.78809	CNM67	Spindle Pole Body
-1.7898	AMD1	AMP Deaminase

-1.79277	YMR242W-A	Unknown
-1.79744	RPB9	RNA Polymerase
-1.80256	BEM4	Cell Polarity
-1.80551	BRO1	Vacuolar Protein Sorting
-1.81326	GUT1	Glycerol Kinase
-1.82154	RPL1A	60S Ribosome
-1.82406	YLR184W	Dubious ORF
-1.82767	YGL261C	Unknown
-1.82778	GPD2	Glycerol Dehydrogenase
-1.83716	YKL134C	Mitochondrial Protein
-1.84931	RPS18A	40S Ribosome
-1.85244	PRP46	Spliceosome
-1.85751	NOP15	60S Ribosome
-1.86209	ARX1	60S Ribosome
-1.86603	YLR149C	Unknown
-1.86674	YDR215C	Dubious ORF
-1.86693	TGL1	Steryl Ester Hydrolase
-1.87017	YGR064W	Dubious ORF
-1.88028	SAT4	Protein Kinase
-1.88036	YLR408C	Unknown
-1.88354	RPL42B	60S Ribosome
-1.88581	YBR085C-A	Unknown
-1.89261	MCA1	Cysteine Protease
-1.90057	URE2	Transcriptional Repressor
-1.91848	RPS10B	40S Ribosome
-1.91861	RRP8	Nucleolar Protein
-1.92539	GCD1	Translation Factor
-1.92539	NOP58	18S rRNA Processing
-1.94421	CBC2	Spliceosome
-1.94444	SMY1	Kinesin
-1.94902	GAC1	Heat Shock Pathway
-1.95175	VPS35	CORVET Complex
-1.95309	COX18	Mitochondrial Protein
-1.96464	VPS24	ESCRT-III Complex
-1.96884	MTG1	Mitochondrial GTPase
-1.97368	RPL6A	60S Ribosome
-1.97971	ADK1	Purine Metabolism
-1.98548	TIR3	Cell Wall Mannoprotein
-1.98778	ASC1	GDI
-1.98992	SDT1	Pyrimidine Nucleotidase
-2.00218	EAP1	Translation Factor
-2.00359	YGL230C	Unknown
-2.04118	MSL1	Spliceosome
-2.04536	AIM18	Unknown
-2.04836	ARP8	Actin-related Protein
-2.05299	ARF3	GTPase
-2.05715	CAB4	CoA Synthesis

-2.0587	YDJ1	Protein Chaperone
-2.06887	TMA23	Nucleolar Protein
-2.0775	YDR203W	Dubious ORF
-2.08001	NOB1	Proteasome
-2.08218	URA8	CTP Synthase
-2.08245	FYV6	Unknown
-2.08395	BUD21	Ribosomal Protein
-2.09203	RPS24B	40S Ribosome
-2.09247	YCL007C	Dubious ORF
-2.09296	MGA2	ER Protein
-2.09831	MRT4	Nucleolus
-2.10381	GUP2	Membrane Protein
-2.11128	ARC1	tRNA Catalysis
-2.11803	RPL37B	60S Ribosome
-2.12507	SAS5	Histone Acetylation
-2.14609	TAF14	RNA Polymerase
-2.15203	RRP6	Exosome Complex
-2.1796	YLR232W	Dubious ORF
-2.18277	NAM7	RNA helicase
-2.19235	YOL075C	Putative ABC Transporter
-2.20444	YPR099C	Dubious ORF
-2.22136	VPS15	Vacuolar Protein Sorting
-2.23908	AAT1	Mitochondrial Protein
-2.25589	DOC1	Ubiquitination Factor
-2.26389	ARP5	Actin-related Protein
-2.29159	YGR017W	Unknown
-2.29928	RPL5	60S Ribosome
-2.29965	KIP2	Kinesin
-2.31045	RPS21A	40S Ribosome
-2.31239	IFM1	Mitochondrial Translation Initiation Factor
-2.33281	UBP3	Ubiquitin Protease
-2.33616	AIM41	Unknown
-2.34502	YGR001C	Unknown
-2.35089	FYV7	18S rRNA Processing
-2.3727	YNL226W	Dubious ORF
-2.40087	YPL216W	Unknown
-2.40115	COQ4	Ubiquinone Biosynthesis
-2.41126	RPL27A	60S Ribosome
-2.43812	NUP133	Nuclear Pore Complex
-2.44028	Bud19	Dubious ORF
-2.46638	YFR032C-B	Unknown
-2.4789	YPL205C	Unknown
-2.48574	RSC1	Chromatin Remodeling
-2.48745	EGD2	Protein Sorting
-2.50503	DBP3	RNA helicase
-2.5115	SUA7	Transcription Factor
-2.51327	NUP120	Nuclear Pore Complex

-2.53711	VPS21	GTPase
-2.56072	UTP13	18S rRNA Processing
-2.58675	EST3	Telomerase
-2.61366	SHP1	Ubiquitin Regulation
-2.62556	MSC3	Unknown
-2.63274	RPS16A	40S Ribosome
-2.63808	LRP1	RNA Processing
-2.71631	YOR365C	Unknown
-2.72618	YDR433W	Dubious ORF
-2.78094	RPS0B	40S Ribosome
-2.82229	YKL118W	Dubious ORF
-2.84518	RPL8A	60S Ribosome
-2.86275	YLR062C	Dubious ORF
-2.88677	SNT309	NineTeen Complex
-2.94625	RPL16B	60S Ribosome
-2.96342	YOR331C	Dubious ORF
-2.9956	YGR018C	Dubious ORF
-3.01685	TUL1	Ubiquitin Ligase
-3.02099	RPP2B	Ribosomal Protein
-3.04094	YCL001W-B	Unknown
-3.07248	CCE1	Mitochondrial Endonuclease
-3.19002	LTV1	GSE Complex
-3.19199	SYF1	Spliceosome
-3.25374	DBP7	RNA helicase
-3.29057	RPL39	60S Ribosome
-3.33907	RPS16A	40S Ribosome
-3.35022	RPS7A	40S Ribosome
-3.35387	RAI1	Pre-RNA Processing
-3.37061	YNL296W	Dubious ORF
-3.49984	RPS19B	40S Ribosome
-3.52011	ERG24	Sterol Reductase
-3.54608	POP2	DEDD RNase
-3.5812	STB3	rRNA Processing
-3.73865	IPP1	Pyrophosphatase
-3.8103	OAR1	Mitochondrial Protein
-3.86516	RPL39	60S Ribosome
-4.02146	RPS27B	40S Ribosome
-4.07451	POP2	DEDD RNase
-4.23286	BUD20	Bud site selection
-4.30587	LOC1	mRNA Localization
-4.35852	VPS35	Retromer Complex
-4.88103	YGR204C-A	Unknown
-4.90076	GUP2	Proton Symport
-5.14427	BUD31	U2 snRNP
-5.19034	EFG1	18S rRNA
-5.35664	RPL31A	60S Ribosome
-5.60913	RPL14A	60S Ribosome

REFERENCES

Akhmanova, A., and A.S. Yap. 2008. Organizing junctions at the cell-cell interface. *Cell*. 135:791-793.

Allingham, J.S., L.R. Sproul, I. Rayment, and S.P. Gilbert. 2007. Vik1 modulates microtubule-Kar3 interactions through a motor domain that lacks an active site. *Cell*. 128:1161-1172.

Amaro, I.A., M. Costanzo, C. Boone, and T.C. Huffaker. 2008. The Saccharomyces cerevisiae homolog of p24 is essential for maintaining the association of p150Glued with the dynactin complex. *Genetics*. 178:703-709.

Azimzadeh, J., and W.F. Marshall. 2010. Building the centriole. *Curr Biol*. 20:R816-825.

Blake-Hodek, K.A., L. Cassimeris, and T.C. Huffaker. 2010. Regulation of microtubule dynamics by Bim1 and Bik1, the budding yeast members of the EB1 and CLIP-170 families of plus-end tracking proteins. *Mol Biol Cell*. 21:2013-2023.

Bloom, K. 2001. Nuclear migration: cortical anchors for cytoplasmic dynein. *Curr Biol*. 11:R326-329.

Brachat, A., J.V. Kilmartin, A. Wach, and P. Philippsen. 1998. Saccharomyces cerevisiae cells with defective spindle pole body outer plaques accomplish nuclear migration via half-bridge-organized microtubules. *Mol Biol Cell*. 9:977-991.

Burke, D., P. Gasdaska, and L. Hartwell. 1989. Dominant effects of tubulin overexpression in Saccharomyces cerevisiae. *Mol Cell Biol*. 9:1049-1059.

Burns, R.G. 1991. Alpha-, beta-, and gamma-tubulins: sequence comparisons and structural contraints. *Cell Motif Cytoskeleton*. 20:181-189.

Byers, B., and L. Goetsch. 1975. Behavior of spindles and spindle plaques in the cell cycle and conjugation of Saccharomyces cerevisiae. *J Bacteriol*. 124:511-523.

Carvalho, P., M.L. Gupta, Jr., M.A. Hoyt, and D. Pellman. 2004. Cell cycle control of kinesin-mediated transport of Bik1 (CLIP-170) regulates microtubule stability and dynein activation. *Dev Cell*. 6:815-829.

Cassimeris, L. 1993. Regulation of microtubule dynamic instability. *Cell Motil Cytoskeleton*. 26:275-281.

Caudron, F., A. Andrieux, D. Job, and C. Boscheron. 2008. A new role for kinesin-directed transport of Bik1p (CLIP-170) in Saccharomyces cerevisiae. *J Cell Sci*. 121:1506-1513.

Cheeseman, I.M., C. Brew, M. Wolyniak, A. Desai, S. Anderson, N. Muster, J.R. Yates, T.C. Huffaker, D.G. Drubin, and G. Barnes. 2001. Implication of a novel multiprotein Dam1p complex in outer kinetochore function. *J Cell Biol*. 155:1137-1145.

Cheeseman, I.M., and A. Desai. 2005. A combined approach for the localization and tandem affinity purification of protein complexes from metazoans. *Sci STKE*. 2005:pl1.

Chen, X.P., H. Yin, and T.C. Huffaker. 1998. The yeast spindle pole body component Spc72p interacts with Stu2p and is required for proper microtubule assembly. *J Cell Biol*. 141:1169-1179.

Chu, H.M., M. Yun, D.E. Anderson, H. Sage, H.W. Park, and S.A. Endow. 2005. Kar3 interaction with Cik1 alters motor structure and function. *Embo J*. 24:3214-3223.

Clark, S.W., and M.D. Rose. 2006. Arp10p is a pointed-end-associated component of yeast dynactin. *Mol Biol Cell*. 17:738-748.

Cottingham, F.R., L. Gheber, D.L. Miller, and M.A. Hoyt. 1999. Novel roles for saccharomyces cerevisiae mitotic spindle motors. *J Cell Biol*. 147:335-350.

Dagenbach, E.M., and S.A. Endow. 2004. A new kinesin tree. *J Cell Sci*. 117:3-7.

Desai, A., and T.J. Mitchison. 1997. Microtubule polymerization dynamics. *Annu Rev Cell Dev Biol*. 13:83-117.

DeZwaan, T.M., E. Ellingson, D. Pellman, and D.M. Roof. 1997. Kinesin-related KIP3 of Saccharomyces cerevisiae is required for a distinct step in nuclear migration. *J Cell Biol*. 138:1023-1040.

Dimitrov, A., M. Quesnoit, S. Moutel, I. Cantaloube, C. Pous, and F. Perez. 2008. Detection of GTP-tubulin conformation in vivo reveals a role for GTP remnants in microtubule rescues. *Science*. 322:1353-1356.

Dittmar, G.A., C.R. Wilkinson, P.T. Jedrzejewski, and D. Finley. 2002. Role of a ubiquitin-like modification in polarized morphogenesis. *Science*. 295:2442-2446.

Dohlman, H.G., and J.E. Slessareva. 2006. Pheromone signaling pathways in yeast. *Sci STKE*. 2006:cm6.

Doxsey, S.J., P. Stein, L. Evans, P.D. Calarco, and M. Kirschner. 1994. Pericentrin, a highly conserved centrosome protein involved in microtubule organization. *Cell*. 76:639-650.

Egelman, E.H., A. Orlova, E.C. Garner, V.E. Galkin, J. Heuser, and R.D. Mullins. 2007. The structure of bacterial ParM filaments. *Nat Struct Mol Biol*. 14:921-926.

Erickson, H.P., D.E. Anderson, and M. Osawa. 2010. FtsZ in bacterial cytokinesis: cytoskeleton and force generator all in one. *Microbiol Mol Biol Rev*. 74:504-528.

Errico, A., A. Ballabio, and E.I. Rugarli. 2002. Spastin, the protein mutated in autosomal dominant hereditary spastic paraplegia, is involved in microtubule dynamics. *Hum Mol Genet*. 11:153-163.

Espinet, C., M.A. de la Torre, M. Aldea, and E. Herrero. 1995. An efficient method to isolate yeast genes causing overexpression-mediated growth arrest. *Yeast*. 11:25-32.

Gardner, M.K., D.C. Bouck, L.V. Paliulis, J.B. Meehl, E.T. O'Toole, J. Haase, A. Soubry, A.P. Joglekar, M. Winey, E.D. Salmon, K. Bloom, and D.J. Odde. 2008a. Chromosome congression by Kinesin-5 motor-mediated disassembly of longer kinetochore microtubules. *Cell*. 135:894-906.

Gardner, M.K., J. Haase, K. Mythreye, J.N. Molk, M. Anderson, A.P. Joglekar, E.T. O'Toole, M. Winey, E.D. Salmon, D.J. Odde, and K. Bloom. 2008b. The microtubule-based motor Kar3 and plus end-binding protein Bim1 provide structural support for the anaphase spindle. *J Cell Biol*. 180:91-100.

Ghaemmaghami, S., W.K. Huh, K. Bower, R.W. Howson, A. Belle, N. Dephoure, E.K. O'Shea, and J.S. Weissman. 2003. Global analysis of protein expression in yeast. *Nature*. 425:737-741.

Giaever, G., A.M. Chu, L. Ni, C. Connelly, L. Riles, S. Veronneau, S. Dow, A. Lucau-Danila, K. Anderson, B. Andre, A.P. Arkin, A. Astromoff, M. El-Bakkoury, R. Bangham, R. Benito, S. Brachat, S. Campanaro, M. Curtiss, K. Davis, A. Deutschbauer, K.D. Entian, P. Flaherty, F. Foury, D.J. Garfinkel, M. Gerstein, D. Gotte, U. Guldener, J.H. Hegemann, S. Hempel, Z. Herman, D.F. Jaramillo, D.E. Kelly, S.L. Kelly, P. Kotter, D. LaBonte, D.C. Lamb, N. Lan, H. Liang, H. Liao, L. Liu, C. Luo, M. Lussier, R. Mao, P. Menard, S.L. Ooi, J.L. Revuelta, C.J. Roberts, M. Rose, P. Ross-Macdonald, B. Scherens, G. Schimmack, B. Shafer, D.D. Shoemaker, S. Sookhai-Mahadeo, R.K. Storms, J.N. Strathern, G. Valle, M. Voet, G. Volckaert, C.Y. Wang, T.R. Ward, J. Wilhelmy, E.A. Winzeler, Y. Yang, G. Yen, E. Youngman, K. Yu, H. Bussey, J.D. Boeke, M. Snyder, P. Philippsen, R.W. Davis, and M. Johnston. 2002. Functional profiling of the Saccharomyces cerevisiae genome. *Nature*. 418:387-391.

Gibbons, I.R. 1966. Studies on the adenosine triphosphatase activity of 14 S and 30 S dynein from cilia of Tetrahymena. *J Biol Chem*. 241:5590-5596.

Gordon-Weeks, P.R. 2004. Microtubules and growth cone function. *J Neurobiol*. 58:70-83.

Gruneberg, U., K. Campbell, C. Simpson, J. Grindlay, and E. Schiebel. 2000. Nud1p links astral microtubule organization and the control of exit from mitosis. *Embo J*. 19:6475-6488.

Gupta, M.L., Jr., P. Carvalho, D.M. Roof, and D. Pellman. 2006. Plus end-specific depolymerase activity of Kip3, a kinesin-8 protein, explains its role in positioning the yeast mitotic spindle. *Nat Cell Biol*. 8:913-923.

Heil-Chapdelaine, R.A., J.R. Oberle, and J.A. Cooper. 2000. The cortical protein Num1p is essential for dynein-dependent interactions of microtubules with the cortex. *J Cell Biol*. 151:1337-1344.

Hildebrandt, E.R., and M.A. Hoyt. 2000. Mitotic motors in Saccharomyces cerevisiae. *Biochim Biophys Acta*. 1496:99-116.

Hochstrasser, M. 1998. There's the rub: a novel ubiquitin-like modification linked to cell cycle regulation. *Genes Dev*. 12:901-907.

Hochstrasser, M. 2000. Evolution and function of ubiquitin-like protein-conjugation systems. *Nat Cell Biol*. 2:E153-157.

Hoepfner, D., A. Brachat, and P. Philippsen. 2000. Time-lapse video microscopy analysis reveals astral microtubule detachment in the yeast spindle pole mutant cnm67. *Mol Biol Cell*. 11:1197-1211.

Hoepfner, D., F. Schaerer, A. Brachat, A. Wach, and P. Philippsen. 2002. Reorientation of mispositioned spindles in short astral microtubule mutant spc72Delta is dependent on spindle pole body outer plaque and Kar3 motor protein. *Mol Biol Cell*. 13:1366-1380.

Holzbaur, E.L., J.A. Hammarback, B.M. Paschal, N.G. Kravit, K.K. Pfister, and R.B. Vallee. 1991. Homology of a 150K cytoplasmic dynein-associated polypeptide with the Drosophila gene Glued. *Nature*. 351:579-583.

Hoyt, M.A., L. He, K.K. Loo, and W.S. Saunders. 1992. Two Saccharomyces cerevisiae kinesin-related gene products required for mitotic spindle assembly. *J Cell Biol*. 118:109-120.

Hoyt, M.A., L. He, L. Totis, and W.S. Saunders. 1993. Loss of function of Saccharomyces cerevisiae kinesin-related CIN8 and KIP1 is suppressed by KAR3 motor domain mutations. *Genetics*. 135:35-44.

Huh, W.K., J.V. Falvo, L.C. Gerke, A.S. Carroll, R.W. Howson, J.S. Weissman, and E.K. O'Shea. 2003. Global analysis of protein localization in budding yeast. *Nature*. 425:686-691.

Huyett, A., J. Kahana, P. Silver, X. Zeng, and W.S. Saunders. 1998. The Kar3p and Kip2p motors function antagonistically at the spindle poles to influence cytoplasmic microtubule numbers. *J Cell Sci*. 111 (Pt 3):295-301.

Hwang, E., J. Kusch, Y. Barral, and T.C. Huffaker. 2003. Spindle orientation in Saccharomyces cerevisiae depends on the transport of microtubule ends along polarized actin cables. *J Cell Biol*. 161:483-488.

Hyman, A.A., S. Salser, D.N. Drechsel, N. Unwin, and T.J. Mitchison. 1992. Role of GTP hydrolysis in microtubule dynamics: information from a slowly hydrolyzable analogue, GMPCPP. *Mol Biol Cell*. 3:1155-1167.

Iwatsuki, H., and M. Suda. 2010. Seven kinds of intermediate filament networks in the cytoplasm of polarized cells: structure and function. *Acta Histochem Cytochem*. 43:19-31.

Jaspersen, S.L., B.J. Huneycutt, T.H. Giddings, Jr., K.A. Resing, N.G. Ahn, and M. Winey. 2004. Cdc28/Cdk1 regulates spindle pole body duplication through phosphorylation of Spc42 and Mps1. *Dev Cell*. 7:263-274.

Jaspersen, S.L., and M. Winey. 2004. The budding yeast spindle pole body: structure, duplication, and function. *Annu Rev Cell Dev Biol*. 20:1-28.

Joglekar, A.P., D.C. Bouck, J.N. Molk, K.S. Bloom, and E.D. Salmon. 2006. Molecular architecture of a kinetochore-microtubule attachment site. *Nat Cell Biol*. 8:581-585.

Jones, M.H., J.B. Bachant, A.R. Castillo, T.H. Giddings, Jr., and M. Winey. 1999. Yeast Dam1p is required to maintain spindle integrity during mitosis and interacts with the Mps1p kinase. *Mol Biol Cell*. 10:2377-2391.

Kahana, J.A., G. Schlenstedt, D.M. Evanchuk, J.R. Geiser, M.A. Hoyt, and P.A. Silver. 1998. The yeast dynactin complex is involved in partitioning the mitotic spindle between mother and daughter cells during anaphase B. *Mol Biol Cell*. 9:1741-1756.

Kardon, J.R., S.L. Reck-Peterson, and R.D. Vale. 2009. Regulation of the processivity and intracellular localization of Saccharomyces cerevisiae dynein by dynactin. *Proc Natl Acad Sci U S A*. 106:5669-5674.

Katz, W., B. Weinstein, and F. Solomon. 1990. Regulation of tubulin levels and microtubule assembly in Saccharomyces cerevisiae: consequences of altered tubulin gene copy number. *Mol Cell Biol*. 10:5286-5294.

Kikkawa, M., T. Ishikawa, T. Nakata, T. Wakabayashi, and N. Hirokawa. 1994. Direct visualization of the microtubule lattice seam both in vitro and in vivo. *J Cell Biol*. 127:1965-1971.

King, S.M., R.S. Patel-King, C.G. Wilkerson, and G.B. Witman. 1995. The 78,000-M(r) intermediate chain of Chlamydomonas outer arm dynein is a microtubule-binding protein. *J Cell Biol*. 131:399-409.

Kline-Smith, S.L., S. Sandall, and A. Desai. 2005. Kinetochore-spindle microtubule interactions during mitosis. *Curr Opin Cell Biol*. 17:35-46.

Knaus, M., E. Cameroni, I. Pedruzzi, K. Tatchell, C. De Virgilio, and M. Peter. 2005. The Bud14p-Glc7p complex functions as a cortical regulator of dynein in budding yeast. *Embo J*. 24:3000-3011.

Knop, M., G. Pereira, S. Geissler, K. Grein, and E. Schiebel. 1997. The spindle pole body component Spc97p interacts with the gamma-tubulin of Saccharomyces cerevisiae and functions in microtubule organization and spindle pole body duplication. *Embo J*. 16:1550-1564.

Knop, M., and E. Schiebel. 1997. Spc98p and Spc97p of the yeast gamma-tubulin complex mediate binding to the spindle pole body via their interaction with Spc110p. *Embo J*. 16:6985-6995.

Knop, M., and E. Schiebel. 1998. Receptors determine the cellular localization of a gamma-tubulin complex and thereby the site of microtubule formation. *Embo J*. 17:3952-3967.

Kollman, J.M., J.K. Polka, A. Zelter, T.N. Davis, and D.A. Agard. 2010. Microtubule nucleating gamma-TuSC assembles structures with 13-fold microtubule-like symmetry. *Nature*. 466:879-882.

Kollman, J.M., A. Zelter, E.G. Muller, B. Fox, L.M. Rice, T.N. Davis, and D.A. Agard. 2008. The structure of the gamma-tubulin small complex: implications of its architecture and flexibility for microtubule nucleation. *Mol Biol Cell*. 19:207-215.

Komarova, Y., C.O. De Groot, I. Grigoriev, S.M. Gouveia, E.L. Munteanu, J.M. Schober, S. Honnappa, R.M. Buey, C.C. Hoogenraad, M. Dogterom, G.G. Borisy, M.O.

Steinmetz, and A. Akhmanova. 2009. Mammalian end binding proteins control persistent microtubule growth. *J Cell Biol*. 184:691-706.

Kops, G.J., A.T. Saurin, and P. Meraldi. 2010. Finding the middle ground: how kinetochores power chromosome congression. *Cell Mol Life Sci*. 67:2145-2161.

Korinek, W.S., M.J. Copeland, A. Chaudhuri, and J. Chant. 2000. Molecular linkage underlying microtubule orientation toward cortical sites in yeast. *Science*. 287:2257-2259.

Kuznetsov, S.A., V.I. Rodionov, V.I. Gelfand, and V.A. Rosenblat. 1978. Purification of a thermostable high molecular weight factor promoting tubulin polymerization. *FEBS Lett*. 95:339-342.

Lansbergen, G., and A. Akhmanova. 2006. Microtubule plus end: a hub of cellular activities. *Traffic*. 7:499-507.

Li, Y.Y., E. Yeh, T. Hays, and K. Bloom. 1993. Disruption of mitotic spindle orientation in a yeast dynein mutant. *Proc Natl Acad Sci U S A*. 90:10096-10100.

Liakopoulos, D., J. Kusch, S. Grava, J. Vogel, and Y. Barral. 2003. Asymmetric loading of Kar9 onto spindle poles and microtubules ensures proper spindle alignment. *Cell*. 112:561-574.

Lillie, S.H., and S.S. Brown. 1994. Immunofluorescence localization of the unconventional myosin, Myo2p, and the putative kinesin-related protein, Smy1p, to the same regions of polarized growth in Saccharomyces cerevisiae. *J Cell Biol*. 125:825-842.

Ma, L., J. McQueen, L. Cuschieri, J. Vogel, and V. Measday. 2007. Spc24 and Stu2 promote spindle integrity when DNA replication is stalled. *Mol Biol Cell*. 18:2805-2816.

Maddox, P., E. Chin, A. Mallavarapu, E. Yeh, E.D. Salmon, and K. Bloom. 1999. Microtubule dynamics from mating through the first zygotic division in the budding yeast Saccharomyces cerevisiae. *J Cell Biol*. 144:977-987.

Maddox, P.S., J.K. Stemple, L. Satterwhite, E.D. Salmon, and K. Bloom. 2003. The minus end-directed motor Kar3 is required for coupling dynamic microtubule plus ends to the cortical shmoo tip in budding yeast. *Curr Biol*. 13:1423-1428.

Manning, B.D., J.G. Barrett, J.A. Wallace, H. Granok, and M. Snyder. 1999. Differential regulation of the Kar3p kinesin-related protein by two associated proteins, Cik1p and Vik1p. *J Cell Biol*. 144:1219-1233.

Markus, S.M., and W.L. Lee. 2011. Regulated offloading of cytoplasmic dynein from microtubule plus ends to the cortex. *Dev Cell*. 20:639-651.

Markus, S.M., K.M. Plevock, B.J. St Germain, J.J. Punch, C.W. Meaden, and W.L. Lee. 2011. Quantitative analysis of Pac1/LIS1-mediated dynein targeting: Implications for regulation of dynein activity in budding yeast. *Cytoskeleton (Hoboken)*. 68:157-174.

Markus, S.M., J.J. Punch, and W.L. Lee. 2009. Motor- and tail-dependent targeting of dynein to microtubule plus ends and the cell cortex. *Curr Biol*. 19:196-205.

McMillan, J.N., and K. Tatchell. 1994. The JNM1 gene in the yeast Saccharomyces cerevisiae is required for nuclear migration and spindle orientation during the mitotic cell cycle. *J Cell Biol*. 125:143-158.

McNally, F.J., and R.D. Vale. 1993. Identification of katanin, an ATPase that severs and disassembles stable microtubules. *Cell*. 75:419-429.

Miller, R.K., S.C. Cheng, and M.D. Rose. 2000. Bim1p/Yeb1p mediates the Kar9p-dependent cortical attachment of cytoplasmic microtubules. *Mol Biol Cell*. 11:2949-2959.

Miller, R.K., K.K. Heller, L. Frisen, D.L. Wallack, D. Loayza, A.E. Gammie, and M.D. Rose. 1998. The kinesin-related proteins, Kip2p and Kip3p, function differently in nuclear migration in yeast. *Mol Biol Cell*. 9:2051-2068.

Mitchison, T., and M. Kirschner. 1984. Dynamic instability of microtubule growth. *Nature*. 312:237-242.

Molk, J.N., and K. Bloom. 2006. Microtubule dynamics in the budding yeast mating pathway. *J Cell Sci*. 119:3485-3490.

Molk, J.N., E.D. Salmon, and K. Bloom. 2006. Nuclear congression is driven by cytoplasmic microtubule plus end interactions in S. cerevisiae. *J Cell Biol*. 172:27-39.

Moore, J.K., S. D'Silva, and R.K. Miller. 2006. The CLIP-170 homologue Bik1p promotes the phosphorylation and asymmetric localization of Kar9p. *Mol Biol Cell*. 17:178-191.

Moore, J.K., and R.K. Miller. 2007. The cyclin-dependent kinase Cdc28p regulates multiple aspects of Kar9p function in yeast. *Mol Biol Cell*. 18:1187-1202.

Moore, J.K., M.D. Stuchell-Brereton, and J.A. Cooper. 2009. Function of dynein in budding yeast: mitotic spindle positioning in a polarized cell. *Cell Motil Cytoskeleton*. 66:546-555.

Muhua, L., T.S. Karpova, and J.A. Cooper. 1994. A yeast actin-related protein homologous to that in vertebrate dynactin complex is important for spindle orientation and nuclear migration. *Cell*. 78:669-679.

Muller, E.G., B.E. Snydsman, I. Novik, D.W. Hailey, D.R. Gestaut, C.A. Niemann, E.T. O'Toole, T.H. Giddings, Jr., B.A. Sundin, and T.N. Davis. 2005. The organization of the core proteins of the yeast spindle pole body. *Mol Biol Cell*. 16:3341-3352.

Nguyen, T., D.B. Vinh, D.K. Crawford, and T.N. Davis. 1998. A genetic analysis of interactions with Spc110p reveals distinct functions of Spc97p and Spc98p, components of the yeast gamma-tubulin complex. *Mol Biol Cell*. 9:2201-2216.

Oakely, C.E., & Oakely, B. R. 1989. Identification of g-tubulin, a new member of the tubulin superfamily encoded by mipA gene of *Aspergillus nidulans*. *Nature*. 338:662-664.

Ortiz, J., C. Funk, A. Schafer, and J. Lechner. 2009. Stu1 inversely regulates kinetochore capture and spindle stability. *Genes Dev*. 23:2778-2791.

Page, B.D., L.L. Satterwhite, M.D. Rose, and M. Snyder. 1994. Localization of the Kar3 kinesin heavy chain-related protein requires the Cik1 interacting protein. *J Cell Biol*. 124:507-519.

Pasqualone, D., and T.C. Huffaker. 1994. STU1, a suppressor of a beta-tubulin mutation, encodes a novel and essential component of the yeast mitotic spindle. *J Cell Biol*. 127:1973-1984.

Pauleau, A.L., and S. Erhardt. 2011. Centromere regulation: New players, new rules, new questions. *Eur J Cell Biol*.

Pedrioli, P.G., S. Leidel, and K. Hofmann. 2008. Urm1 at the crossroad of modifications. 'Protein Modifications: Beyond the Usual Suspects' Review Series. *EMBO Rep*. 9:1196-1202.

Pereira, G., U. Grueneberg, M. Knop, and E. Schiebel. 1999. Interaction of the yeast gamma-tubulin complex-binding protein Spc72p with Kar1p is essential for microtubule function during karyogamy. *Embo J*. 18:4180-4195.

Pruyne, D., A. Legesse-Miller, L. Gao, Y. Dong, and A. Bretscher. 2004. Mechanisms of polarized growth and organelle segregation in yeast. *Annu Rev Cell Dev Biol*. 20:559-591.

Roof, D.M., P.B. Meluh, and M.D. Rose. 1992. Kinesin-related proteins required for assembly of the mitotic spindle. *J Cell Biol*. 118:95-108.

Sandblad, L., K.E. Busch, P. Tittmann, H. Gross, D. Brunner, and A. Hoenger. 2006. The Schizosaccharomyces pombe EB1 homolog Mal3p binds and stabilizes the microtubule lattice seam. *Cell*. 127:1415-1424.

Saunders, W.S., and M.A. Hoyt. 1992. Kinesin-related proteins required for structural integrity of the mitotic spindle. *Cell*. 70:451-458.

Schaerer, F., G. Morgan, M. Winey, and P. Philippsen. 2001. Cnm67p is a spacer protein of the Saccharomyces cerevisiae spindle pole body outer plaque. *Mol Biol Cell*. 12:2519-2533.

Schatz, P.J., L. Pillus, P. Grisafi, F. Solomon, and D. Botstein. 1986. Two functional alpha-tubulin genes of the yeast Saccharomyces cerevisiae encode divergent proteins. *Mol Cell Biol*. 6:3711-3721.

Schramm, C., S. Elliott, A. Shevchenko, and E. Schiebel. 2000. The Bbp1p-Mps2p complex connects the SPB to the nuclear envelope and is essential for SPB duplication. *Embo J*. 19:421-433.

Schroer, T.A. 2004. Dynactin. *Annu Rev Cell Dev Biol*. 20:759-779.

Schuyler, S.C., and D. Pellman. 2001. Microtubule "plus-end-tracking proteins": The end is just the beginning. *Cell*. 105:421-424.

Severin, F., B. Habermann, T. Huffaker, and T. Hyman. 2001. Stu2 promotes mitotic spindle elongation in anaphase. *J Cell Biol*. 153:435-442.

Shang, C., T.R. Hazbun, I.M. Cheeseman, J. Aranda, S. Fields, D.G. Drubin, and G. Barnes. 2003. Kinetochore protein interactions and their regulation by the Aurora kinase Ipl1p. *Mol Biol Cell*. 14:3342-3355.

Sherman, F. 2002. Getting started with yeast. *Methods Enzymol*. 350:3-41.

Siller, K.H., and C.Q. Doe. 2009. Spindle orientation during asymmetric cell division. *Nat Cell Biol*. 11:365-374.

Sopko, R., D. Huang, N. Preston, G. Chua, B. Papp, K. Kafadar, M. Snyder, S.G. Oliver, M. Cyert, T.R. Hughes, C. Boone, and B. Andrews. 2006. Mapping pathways and phenotypes by systematic gene overexpression. *Mol Cell*. 21:319-330.

Spang, A., I. Courtney, U. Fackler, M. Matzner, and E. Schiebel. 1993. The calcium-binding protein cell division cycle 31 of Saccharomyces cerevisiae is a component of the half bridge of the spindle pole body. *J Cell Biol*. 123:405-416.

Spang, A., I. Courtney, K. Grein, M. Matzner, and E. Schiebel. 1995. The Cdc31p-binding protein Kar1p is a component of the half bridge of the yeast spindle pole body. *J Cell Biol*. 128:863-877.

Spang, A., S. Geissler, K. Grein, and E. Schiebel. 1996. gamma-Tubulin-like Tub4p of Saccharomyces cerevisiae is associated with the spindle pole body substructures that organize microtubules and is required for mitotic spindle formation. *J Cell Biol*. 134:429-441.

Sproul, L.R., D.J. Anderson, A.T. Mackey, W.S. Saunders, and S.P. Gilbert. 2005. Cik1 targets the minus-end kinesin depolymerase kar3 to microtubule plus ends. *Curr Biol*. 15:1420-1427.

Stearns, T., L. Evans, and M. Kirschner. 1991. Gamma-tubulin is a highly conserved component of the centrosome. *Cell*. 65:825-836.

Su, L.K., M. Burrell, D.E. Hill, J. Gyuris, R. Brent, R. Wiltshire, J. Trent, B. Vogelstein, and K.W. Kinzler. 1995. APC binds to the novel protein EB1. *Cancer Res*. 55:2972-2977.

Sundberg, H.A., L. Goetsch, B. Byers, and T.N. Davis. 1996. Role of calmodulin and Spc110p interaction in the proper assembly of spindle pole body compenents. *J Cell Biol*. 133:111-124.

Tanaka, K., E. Kitamura, Y. Kitamura, and T.U. Tanaka. 2007. Molecular mechanisms of microtubule-dependent kinetochore transport toward spindle poles. *J Cell Biol*. 178:269-281.

Tanaka, K., N. Mukae, H. Dewar, M. van Breugel, E.K. James, A.R. Prescott, C. Antony, and T.U. Tanaka. 2005. Molecular mechanisms of kinetochore capture by spindle microtubules. *Nature*. 434:987-994.

Thompson, W.C., L. Wilson, and D.L. Purich. 1981. Taxol induces microtubule assembly at low temperature. *Cell Motil*. 1:445-454.

Tong, A.H., M. Evangelista, A.B. Parsons, H. Xu, G.D. Bader, N. Page, M. Robinson, S. Raghibizadeh, C.W. Hogue, H. Bussey, B. Andrews, M. Tyers, and C. Boone. 2001. Systematic genetic analysis with ordered arrays of yeast deletion mutants. *Science*. 294:2364-2368.

Tournebize, R., A. Popov, K. Kinoshita, A.J. Ashford, S. Rybina, A. Pozniakovsky, T.U. Mayer, C.E. Walczak, E. Karsenti, and A.A. Hyman. 2000. Control of microtubule dynamics by the antagonistic activities of XMAP215 and XKCM1 in Xenopus egg extracts. *Nat Cell Biol*. 2:13-19.

Tusher, V.G., R. Tibshirani, and G. Chu. 2001. Significance analysis of microarrays applied to the ionizing radiation response. *Proc Natl Acad Sci U S A*. 98:5116-5121.

Tytell, J.D., and P.K. Sorger. 2006. Analysis of kinesin motor function at budding yeast kinetochores. *J Cell Biol*. 172:861-874.

Usui, T., H. Maekawa, G. Pereira, and E. Schiebel. 2003. The XMAP215 homologue Stu2 at yeast spindle pole bodies regulates microtubule dynamics and anchorage. *Embo J*. 22:4779-4793.

Vale, R.D., T.S. Reese, and M.P. Sheetz. 1985. Identification of a novel force-generating protein, kinesin, involved in microtubule-based motility. *Cell*. 42:39-50.

Vallee, R.B., K.T. Vaughan, and C.J. Echeverri. 1995. Targeting of cytoplasmic dynein to membranous organelles and kinetochores via dynactin. *Cold Spring Harb Symp Quant Biol*. 60:803-811.

Vallen, E.A., M.A. Hiller, T.Y. Scherson, and M.D. Rose. 1992. Separate domains of KAR1 mediate distinct functions in mitosis and nuclear fusion. *J Cell Biol*. 117:1277-1287.

Varga, V., J. Helenius, K. Tanaka, A.A. Hyman, T.U. Tanaka, and J. Howard. 2006. Yeast kinesin-8 depolymerizes microtubules in a length-dependent manner. *Nat Cell Biol*. 8:957-962.

Varga, V., C. Leduc, V. Bormuth, S. Diez, and J. Howard. 2009. Kinesin-8 motors act cooperatively to mediate length-dependent microtubule depolymerization. *Cell*. 138:1174-1183.

Wade, R.H. 2009. On and around microtubules: an overview. *Mol Biotechnol*. 43:177-191.

Walker, R.A., E.T. O'Brien, N.K. Pryer, M.F. Soboeiro, W.A. Voter, H.P. Erickson, and E.D. Salmon. 1988. Dynamic instability of individual microtubules analyzed by video light microscopy: rate constants and transition frequencies. *J Cell Biol*. 107:1437-1448.

Wang, H.W., S. Long, C. Ciferri, S. Westermann, D. Drubin, G. Barnes, and E. Nogales. 2008. Architecture and flexibility of the yeast Ndc80 kinetochore complex. *J Mol Biol*. 383:894-903.

Wang, H.W., and E. Nogales. 2005. Nucleotide-dependent bending flexibility of tubulin regulates microtubule assembly. *Nature*. 435:911-915.

Wang, H.W., V.H. Ramey, S. Westermann, A.E. Leschziner, J.P. Welburn, Y. Nakajima, D.G. Drubin, G. Barnes, and E. Nogales. 2007. Architecture of the Dam1 kinetochore ring complex and implications for microtubule-driven assembly and force-coupling mechanisms. *Nat Struct Mol Biol*. 14:721-726.

Wang, P.J., and T.C. Huffaker. 1997. Stu2p: A microtubule-binding protein that is an essential component of the yeast spindle pole body. *J Cell Biol*. 139:1271-1280.

Waterman-Storer, C.M., and E.D. Salmon. 1997. Actomyosin-based retrograde flow of microtubules in the lamella of migrating epithelial cells influences microtubule dynamic instability and turnover and is associated with microtubule breakage and treadmilling. *J Cell Biol*. 139:417-434.

Weinstein, B., and F. Solomon. 1990. Phenotypic consequences of tubulin overproduction in Saccharomyces cerevisiae: differences between alpha-tubulin and beta-tubulin. *Mol Cell Biol*. 10:5295-5304.

Westermann, S., D.G. Drubin, and G. Barnes. 2007. Structures and functions of yeast kinetochore complexes. *Annu Rev Biochem*. 76:563-591.

Westermann, S., H.W. Wang, A. Avila-Sakar, D.G. Drubin, E. Nogales, and G. Barnes. 2006. The Dam1 kinetochore ring complex moves processively on depolymerizing microtubule ends. *Nature*. 440:565-569.

Wolyniak, M.J., K. Blake-Hodek, K. Kosco, E. Hwang, L. You, and T.C. Huffaker. 2006. The regulation of microtubule dynamics in Saccharomyces cerevisiae by three interacting plus-end tracking proteins. *Mol Biol Cell*. 17:2789-2798.

Wong, J., Y. Nakajima, S. Westermann, C. Shang, J.S. Kang, C. Goodner, P. Houshmand, S. Fields, C.S. Chan, D. Drubin, G. Barnes, and T. Hazbun. 2007. A protein interaction map of the mitotic spindle. *Mol Biol Cell*. 18:3800-3809.

Woodruff, J.B., D.G. Drubin, and G. Barnes. 2009. Dynein-driven mitotic spindle positioning restricted to anaphase by She1p inhibition of dynactin recruitment. *Mol Biol Cell*. 20:3003-3011.

Woodruff, J.B., D.G. Drubin, and G. Barnes. 2010. Mitotic spindle disassembly occurs via distinct subprocesses driven by the anaphase-promoting complex, Aurora B kinase, and kinesin-8. *J Cell Biol*. 191:795-808.

Wordeman, L., and T.J. Mitchison. 1995. Identification and partial characterization of mitotic centromere-associated kinesin, a kinesin-related protein that associates with centromeres during mitosis. *J Cell Biol*. 128:95-104.

Yeh, E., R.V. Skibbens, J.W. Cheng, E.D. Salmon, and K. Bloom. 1995. Spindle dynamics and cell cycle regulation of dynein in the budding yeast, Saccharomyces cerevisiae. *J Cell Biol*. 130:687-700.

Yeh, E., C. Yang, E. Chin, P. Maddox, E.D. Salmon, D.J. Lew, and K. Bloom. 2000. Dynamic positioning of mitotic spindles in yeast: role of microtubule motors and cortical determinants. *Mol Biol Cell*. 11:3949-3961.

Yildiz, A., J.N. Forkey, S.A. McKinney, T. Ha, Y.E. Goldman, and P.R. Selvin. 2003. Myosin V walks hand-over-hand: single fluorophore imaging with 1.5-nm localization. *Science*. 300:2061-2065.

Yildiz, A., M. Tomishige, R.D. Vale, and P.R. Selvin. 2004. Kinesin walks hand-over-hand. *Science*. 303:676-678.

Yin, H., D. Pruyne, T.C. Huffaker, and A. Bretscher. 2000. Myosin V orientates the mitotic spindle in yeast. *Nature*. 406:1013-1015.

Yin, H., L. You, D. Pasqualone, K.M. Kopski, and T.C. Huffaker. 2002. Stu1p is physically associated with beta-tubulin and is required for structural integrity of the mitotic spindle. *Mol Biol Cell*. 13:1881-1892.

Yu, J.W., J.M. Mendrola, A. Audhya, S. Singh, D. Keleti, D.B. DeWald, D. Murray, S.D. Emr, and M.A. Lemmon. 2004. Genome-wide analysis of membrane targeting by S. cerevisiae pleckstrin homology domains. *Mol Cell*. 13:677-688.